

ANALYSIS OF LOW LEVEL MOISTURE TRANSPORT OVER SOUTH ASIA

A dissertation submitted to the Department of Physics,
Bangladesh University of Engineering and Technology (BUET), Dhaka in partial
fulfillment of the requirements for the degree of

MASTER OF SCIENCE IN PHYSICS

Submitted by

Nazmoon Naher

Roll No.: 1014142502F

Session: October/2014



DEPARTMENT OF PHYSICS

BANGLADESH UNIVERSITY OF ENGINEERING AND TECHNOLOGY

(BUET) DHAKA-1000, BANGLADESH

September, 2016

CANDIDATE'S DECLARATION

It is hereby declared that this thesis or any part of it has not been submitted elsewhere for the award of any degree or diploma.

Signature of the Candidate

Nazmoon Naher

Nazmoon Naher

Roll No.: 1014142502F

Session: October/2014

BANGLADESH UNIVERSITY OF ENGINEERING AND TECHNOLOGY




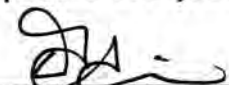
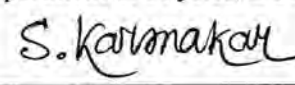
DEPARTMENT OF PHYSICS, DHAKA-1000



Certification of Thesis work

The thesis titled “ANALYSIS OF LOW LEVEL MOISTURE TRANSPORT OVER SOUTH ASIA”, submitted by NAZMOON NAHER, Roll No: 1014142502F Session: October/2014, has been accepted as satisfactory in partial fulfillment of the requirement for the degree of Master of Science (M.Sc.) in Physics on 06 September, 2016.

BOARD OF EXAMINERS

1. 
Dr. Nasreen Akter **Chairman**
Associate Professor
Department of Physics, BUET, Dhaka.
(Supervisor)
2. 
Prof. Fahima Khanam **Member (Ex-Officio)**
Head
Department of Physics, BUET, Dhaka.
3. 
Dr. Afia Begum **Member**
Professor
Department of Physics, BUET, Dhaka
4. 
Dr. Md. Rafi Uddin **Member**
Professor
Department of Physics, BUET, Dhaka
5. 
Dr. Samarendra Karmakar **Member (External)**
Former Director
Bangladesh Meteorological Department and SMRC.

Dedicated To
My Beloved Parents
And
All of My Friends

CONTENTS

	Page No.
List of Tables	viii
List of Figures	ix
Acknowledgement	xiv
Abstract	xv
CHAPTER 1: INTRODUCTION	1-4
1.1 Prelude	1
1.2 Objective of the present study	3
CHPATER 2: LITERATURE REVIEW	5-23
2.1 Previous work	5
2.2 Overview of the study	7
2.2.1 Moisture	7
2.2.2 Dew Point Temperature	9
2.2.3 Mixing ratio	10
2.2.4 Specific humidity	11
2.2.5 Relative Humidity	12
2.2.6 Moisture flux	14
2.2.7 Vertically integrated moisture flux and its convergence	14
2.2.8 Atmospheric Parameters	16
2.2.9 Precipitation	16
2.2.10 Evaporation	18
2.3 Geographical description of South-Asia and Bay of Bengal	19
2.3.1 South-West region (5°N-18°N & 70°E-82°E)	21
2.3.2 Bay of Bengal (BoB) (5°N-18°N & 82°E-95°E)	21
2.3.3. South-East region (5°N-18°N & 95°E-105°E)	21
2.3.4. North-East region (18°N-27°N & 95°E-105°E)	22
2.3.5. Bangladesh and surrounding (18°N-27°N & 82°E-95°E)	22

2.3.6. North-West region (18°N-27°N & 70°E-82°E)	23
CHAPTER 3: DATA AND METHODS	24-30
3.1 DATA used	24
3.2 Study Area	25
3.3 Study Method	27
3.3.1 Calculation for vertically integrated moisture flux (VIMF)	27
3.3.2 Calculation of precipitation	27
3.3.3 The Grid Analysis and Display System (GrADS)	29
CHAPTER 4: RESULTS AND DISCUSSION	31-94
4.1 Vertically Integrated Moisture Flux (VIMF) for study area	31
4.1.1 Spatial distribution of annual VIMF	31
4.1.2 Annual variation of VIMF	32
4.1.3 Spatial distribution of seasonal VIMF	33
4.1.4 Seasonal variation of VIMF	36
4.1.5 Spatial distribution of monthly VIMF	38
4.1.6 Monthly variation of VIMF	41
4.2 Moisture flux for individual domain	41
4.3 Annual variation of Moisture Flux for six domains	42
4.3.1 South-West domain (SW)	42
4.3.2 Bay of Bengal (BoB)	44
4.3.3 South-East domain (SE)	45
4.3.4 North-West domain (NW)	46
4.3.5 Bangladesh & surrounding (BAN)	48
4.3.6 North-East domain (NE)	49
4.4 Seasonal variation of VIMF for six domains	51
4.5 Monthly variation of VIMF for six domains	54
4.5.1 South-West domain (SW)	55
4.5.2 Bay of Bengal (BoB)	56
4.5.3 South-East domain (SE)	56

4.5.4 North-West domain (NW)	57
4.5.5 North-West domain (NW)	58
4.5.6 North-East domain (NE)	58
4.6 Region to Region variation	59
4.6.1 Annual variation of VIMF for six domains	59
4.6.2 Seasonally variation of VIMF for six domains	61
4.6.3 Monthly variation of VIMF for six domains	62
4.7 Variability of Precipitation	63
4.7.1 Spatial distribution of precipitation for study area	63
4.7.2 Seasonal variation of precipitation for 6 domains	64
4.7.3 Monthly variation of precipitation for 6 domains	65
4.8 Variability of Evaporation	66
4.8.1 Spatial distribution of evaporation for study area	66
4.8.2 Seasonal variation of evaporation for 6 domains	67
4.8.3 Monthly variation of evaporation for 6 domains	68
4.9 Causes of precipitation	70
4.9.1 Relation between moisture flux and precipitation for study area.	70
4.9.2 Relation between evaporation and precipitation for study area.	71
4.9.3 Relation between moisture flux and precipitation for six domains.	73
4.9.4 Relation between evaporation and precipitation for six domains.	74
4.10 Components of precipitation	76
4.11 Verification of P_a and P_m	88
CHAPTER 5: CONCLUSIONS	95-98
REFERENCES	99-102

List of Tables

No.	Captions	Page No.
Table-1:	Seasonal average increase of VIMF for total domain (1979-2015).	37
Table-2:	Seasonal variation of VIMF for six domains (1979- 2015).	53-54
Table-3:	Average increase of VIMF for six domains (1979- 2015).	60
Table-4:	Percentage of seasonal VIMF for six domains (1979-2015).	61
Table-5:	Monthly variation of VIMF for six domains (1979-2015).	62
Table-6:	Seasonal variation of precipitation for six domains (1979-2015).	65
Table-7:	Monthly variation of precipitation for six domains (1979-2015).	66
Table-8:	Seasonal variation of evaporation for six domains (1979-2015).	68
Table-9:	Monthly variation of evaporation for six domains (1979-2015).	69
Table-10:	R ² value between VIMF and evaporation with precipitation for six domains.	74
Table-11:	Value of VIMF, E, P, P_a and P_m for six domains.	87
Table-12:	Monthly average R ² value and r value for six domains (1979-2015).	94

List of Figures

No.	Captions	Page No.
Fig. 2.1.	Natural forms of moisture in the atmosphere.	8
Fig. 2.2.	Saturated mixing ratio.	11
Fig. 2.3.	Vapour capacity graph shows how warm air can hold more water than cold air.	12
Fig. 2.4.	Relative humidity with temperature.	13
Fig. 2.5.	Average south Asia and south-east Asia precipitation (mm/day) since 1978 to 2002.	17
Fig. 2.6.	Average global evaporation in a year for the Month of January and May since 1985 to 1999.	19
Fig. 2.7.	Regional map showing the coverage area of 5°N-27°N, 70 °E-105°E. Gray shading indicates the topography.	20
Fig. 3.1.	Study area with topography.	26
Fig. 3.2.	Schematic for the processes considered in recycling of moisture.	27
Fig. 3.3.	GrADS example output.	30
Fig. 4.1.	Spatial distribution of average VIMF ($\text{kg m}^{-1} \text{s}^{-1}$) and average wind velocity (m s^{-1}) from 1000 hPa to 850 hPa for study area during 1979-2015.	31
Fig. 4.2.	Yearly variation of average VIMF (green line) for the study area. Red line indicates the 5-years running mean from 1979 to 2015.	32
Fig. 4.3.	Spatial distribution of average VIMF (shading; $\text{kg m}^{-1} \text{s}^{-1}$) and average wind velocity (m s^{-1}) for 1000-850 hPa in the pre-monsoon and monsoon season during 1979-2015.	34

Fig. 4.4.	Spatial distribution of average VIMF (shading; $\text{kg m}^{-1} \text{s}^{-1}$) and average wind velocity (m s^{-1}) for 1000-850 hPa in the post-monsoon and winter season during 1979-2015.	35
Fig. 4.5.	Seasonal variation of average VIMF during 1979-2015.	36
Fig. 4.6.	Annual variation of 5-years running mean value of seasonal average VIMF during 1979-2015.	37
Fig. 4.7.	Spatial distribution of monthly (Jan-Jun) average VIMF (shading; $\text{kg m}^{-1} \text{s}^{-1}$) and average wind velocity (m s^{-1}) for 1000-850 hPa during 1979-2015.	39
Fig. 4.8.	Spatial distribution of monthly (Jul-Dec) average VIMF (shading; $\text{kg m}^{-1} \text{s}^{-1}$) and average wind velocity (m s^{-1}) for 1000-850 hPa during 1979-2015.	40
Fig. 4.9.	Monthly variation of average VIMF for total domain during 1979-2015.	41
Fig. 4.10.	Yearly variation of VIMF for six domains during 1979-2015.	42
Fig. 4.11.	Yearly variation of average VIMF and 5-years running mean (red line) for the South-West domain during 1979-2015.	43
Fig. 4.12.	5-years running mean value of seasonal average VIMF for the South-West domain during 1979-2015.	43
Fig. 4.13.	Yearly variation of average VIMF and 5-years running mean (red line) for the Bay of Bengal during 1979-2015.	44
Fig. 4.14.	5-years running mean value of seasonal average VIMF for the Bay of Bengal domain during 1979-2015.	45
Fig. 4.15.	Yearly variation of average VIMF and 5-years running mean (red line) for the South-East domain during 1979-2015.	45
Fig. 4.16.	5-years running mean value of seasonal average VIMF for the South-East domain during 1979-2015.	46

Fig. 4.17.	Yearly variation of average VIMF and 5-years running mean (red line) for the North-West domain during 1979-2015.	47
Fig. 4.18.	5-years running mean value of seasonal average VIMF for the North-West domain during 1979-2015.	47
Fig. 4.19.	Yearly variation of average VIMF and 5-years running mean (red line) for the Bangladesh & surrounding domain during 1979-2015.	48
Fig. 4.20.	5-years running mean value of seasonal average VIMF for the Bangladesh and surrounding domain during 1979-2015.	49
Fig. 4.21.	Yearly variation of average VIMF and 5-years running mean (red line) for the North-East domain during 1979 to 2015.	49
Fig. 4.22.	5-years running mean value of seasonal average VIMF for the North-East domain during 1979-2015.	50
Fig. 4.23.	Seasonal variation of average VIMF for the South-West, Bay of Bengal and the South-East domains during 1979-2015.	51
Fig. 4.24.	Seasonal variation of average VIMF for the North-West, Bangladesh and surrounding and the North-East domains during 1979-2015.	52
Fig. 4.25.	Monthly variation of average VIMF for six domains during 1979-2015.	55
Fig. 4.26.	Monthly variation of average VIMF for the South-West domain during 1979-2015.	55
Fig. 4.27.	Monthly variation of average VIMF for the Bay of Bengal domain during 1979- 2015.	56
Fig. 4.28.	Monthly variation of average VIMF for the South-East domain during 1979-2015.	57
Fig. 4.29.	Monthly variation of average VIMF for the North-West domain during 1979-2015.	57

Fig. 4.30.	Monthly variation of average VIMF for the Bangladesh and surrounding domain during 1979-2015.	58
Fig. 4.31.	Monthly variation of average VIMF for the North-East domain during 1979-2015.	59
Fig. 4.32.	5-years running mean value of average VIMF for six domains during 1979-2015.	60
Fig. 4.33.	Seasonal variation of average VIMF for six domains during 1979-2015.	61
Fig. 4.34.	Monthly variation of average VIMF for six domains during 1979-2015.	62
Fig. 4.35.	Spatial distribution of average precipitation (shading; mm/day) during 1979-2015.	63
Fig. 4.36.	Seasonal variation of 37-years averaged precipitation (mm/day) for six domains during 1979-2015.	64
Fig. 4.37.	Monthly variation of 37-years averaged precipitation (mm/day) for six domains during 1979-2015.	65
Fig. 4.38.	Spatial distribution of average evaporation (shading; mm/day) during 1979-2015.	67
Fig. 4.39.	Seasonal variation of 37-years averaged evaporation (mm/day) for six domains during 1979-2015.	68
Fig. 4.40.	Monthly variation of 37-years averaged evaporation (mm/day) for six domains during 1979-2015.	69
Fig. 4.41.	Relation between moisture flux and precipitation for the study area.	70
Fig. 4.42.	Scatter plot between moisture flux and precipitation for the study area during 1979-2015.	71
Fig. 4.43.	Relation between evaporation and precipitation for the study area.	72

Fig. 4.44.	Scatter plot between evaporation and precipitation and for the study area during 1979-2015.	72
Fig. 4.45.	Scatter plot between precipitation and moisture flux for six domains during 1979-2015.	73
Fig. 4.46.	Scatter plot between precipitation and evaporation for six domains during 1979-2015.	75
Fig. 4.47.	The 37-years averaged VIMF (shading; kg m ⁻¹ s ⁻¹) and average wind velocity (m s ⁻¹) in January for the South-West domain during 1979-2015.	77
Fig. 4.48.	The 37-years averaged VIMF (shading; kg m ⁻¹ s ⁻¹) and average wind velocity (m s ⁻¹) in January for the BoB domain during 1979-2015.	79
Fig. 4.49.	The 37-years averaged VIMF (shading; kg m ⁻¹ s ⁻¹) and average wind velocity (m s ⁻¹) in January for the South-East domain during 1979-2015.	80
Fig. 4.50.	The 37-years averaged VIMF (shading; kg m ⁻¹ s ⁻¹) and average wind velocity (m s ⁻¹) in January for the North-West domain during 1979-2015.	82
Fig. 4.51.	The 37-years averaged VIMF (shading; kg m ⁻¹ s ⁻¹) and average wind velocity (m s ⁻¹) in January for Bangladesh and surrounding during 1979-2015.	84
Fig. 4.52.	The 37-years averaged VIMF (shading; kg m ⁻¹ s ⁻¹) and average wind velocity (m s ⁻¹) in January for the North-East domain during 1979-2015.	86
Fig. 4.53.	Percentage of the advective component of precipitation (P^a) and precipitation arising from local evaporation (P^m) for six domains.	87
Fig. 4.54.	Variation of monthly average VIMF and P^a for SW domain.	88

Fig. 4.55.	Variation of monthly average evaporation and P_m for BoB domain.	88
Fig. 4.56.	Variation of monthly average VIMF and P_a for BoB domain.	89
Fig. 4.57.	Variation of monthly average evaporation and P_m for BoB domain.	89
Fig. 4.58.	Variation of monthly average VIMF and P_a for SE domain.	90
Fig. 4.59.	Variation of monthly average evaporation and P_m for SE domain.	90
Fig. 4.60.	Variation of monthly average VIMF and P_a for NW domain.	91
Fig. 4.61.	Variation of monthly average evaporation and P_m for NW domain.	91
Fig. 4.62.	Variation of monthly average VIMF and P_a for BAN domain.	92
Fig. 4.63.	Variation of monthly average evaporation and P_m for BAN domain.	92
Fig. 4.64.	Variation of monthly average VIMF and P_a for NE domain.	93
Fig. 4.65.	Variation of monthly average evaporation and P_m for NE domain.	93

Acknowledgment

All praises are due to the Almighty God who has enabled me to complete this thesis for the M.Sc degree.

I would like to express my gratitude and appreciation to my supervisor Dr. Nasreen Akter, Associate Professor, Department of Physics, Bangladesh University of Engineering and Technology (BUET) for her guidance and fruitful criticism throughout the entire period of research works and during preparation of the manuscript of this thesis.

I am grateful to Professor Fahima Khanam, Head, Department of Physics, Bangladesh University of Engineering and Technology (BUET) to support and to allow me to do this research. I am very much thankful to Dr. Md. Rafi Uddin, Professor, Department of Physics (BUET) for his kind cooperation for improving my research related computer skill and valuable suggestions about my research.

I would also like to thank A.T.M. Shafiul Azam, Assistant Professor, Department of Physics, Bangladesh University of Engineering and Technology (BUET), for his valuable teaching efforts and suggestions that helped quite a great extent in writing of this thesis. I would like to thank Atmospheric Laboratory, Department of Physics (BUET) to provide the facilities for the study.

I express my cordial thanks to my friends and all well-wishers especially each and every members of Atmospheric Lab. (BUET), including the entire faculty member in BUET for their help and suggestions during the study period.

Lastly but not the least, I express my profound gratitude to my beloved parents and my elder sister and all relatives for their inspiration, encouragement and endless love to complete my study.

The Author

ABSTRACT

This study investigates long-term variation of low-level vertically integrated moisture flux (VIMF) for 37-year from 1979 to 2015 and its contributions to the total rainfall over South Asia (SA), which includes also the Bay of Bengal and the eastern part of Arabian Sea. For this purpose wind, specific humidity, precipitation and evaporation data are collected from ERA-Interim reanalysis data generated by European Centre for Medium-Range Weather Forecasts (ECMWF) having horizontal resolution of approximately 80 km. The region is further sub divided into six areas i.e. South-West (SW), Bay of Bengal (BoB), South-East (SE), North-West (NW), Bangladesh and surrounding (BAN) and North-East (NE) for understanding details of spatial and temporal characteristics of low-level moisture flux and its effect on precipitation. SW, BoB and SE domains are considered as Southern part and NW, BAN and NE domains are considered as Northern part. The averaged VIMF is found to be $113.71 \text{ kg m}^{-1} \text{ s}^{-1}$ for the total study area. The annual variation of VIMF remains almost constant for 37 years over SA with average increasing rate of only 0.14% per year. Southern parts of the study area (SW, BoB and SE) acquire 67% of the total flux, whereas, 33% of the total moisture flux is observed over the Northern parts (NW, BAN and NE), which are mainly the land area. According to season, about 41% of the total VIMF is found to be advected in the monsoon season, whereas, only 17% of the total VIMF is found in the winter season. The monthly value of VIMF ($191.74 \text{ kg m}^{-1} \text{ s}^{-1}$) is highest in July over SA which is 33% more than the minimum value in March. For six individual domains, highest amount of VIMF (27% of the total VIMF) is found over the BoB whereas only 6% of the total VIMF is found over the NE domain. The SW, SE, NW and BAN regions receive 21%, 19%, 13% and 14% of the total flux, respectively. Annual variation of VIMF for individual domain is also found constant except in the NE domain where VIMF is increased significantly with coefficient of determinant (R^2) value of 0.54. However, the NE region has the lowest amount of VIMF ($35.01 \text{ kg m}^{-1} \text{ s}^{-1}$). Seasonal variation in the domains indicates that the Southern parts of the study area have two times higher VIMF than the Northern parts during the the monsoon season. The lowest amount of VIMF approximately $29.73 \text{ kg m}^{-1} \text{ s}^{-1}$ is observed in January for the Northern region and for the Southern region the lowest value of approximately $76.78 \text{ kg m}^{-1} \text{ s}^{-1}$ is found in March.

The relation between VIMF and total precipitation (P) over SA is analyzed which shows the R^2 value of 0.77. It indicates that 77% of the total variation of precipitation can be explained by the relationship between VIMF and precipitation. The contribution of VIMF and evaporation in the total precipitation studied in details. Following the procedure, the total precipitation over SA is separated into two components i.e. the advective component of precipitation (P_a) and the precipitation arising from local evaporation (P_m). It is found that about 3.65 mm/day of precipitation comes from the advected part and 1.44 mm/day of precipitation arises from local evaporation. The R^2 value and correlation coefficient (r) between VIMF and P_a are 0.871 and 0.933 respectively, whereas, the value between evaporation (E) and P_m are 0.456 and 0.675, respectively. Similarly, precipitation components of P_a and P_m are separately calculated for all domains which show that the SW, BoB, SE, NW, BAN and NE domains receive 83%, 81%, 75%, 93%, 86%, 63% precipitation from P_a and 17%, 19%, 25%, 7%, 14%, 37% precipitation from P_m , respectively. Therefore, low-level moisture transport is the main reason of precipitation which contributes approximately 75%, on the average, to the total precipitation over the study area.

CHAPTER-1

INTRODUCTION

1.1 Prelude

The variability of available water is one of the most important parameters for sustaining life, agriculture, and economic development in the South Asian countries. Among the various climatic parameters which influence the growth of crops in South Asia, the most important parameter is considered to be precipitation. Precipitation is the condensation of water vapour in the form of water droplets that falls to the Earth's surface. It plays an important role in the economy and economical growth of South Asia directly or indirectly [1]. The success of crop production also mainly depends on the amount of rainfall or precipitation.

The yearly variations of the long term seasonal mean precipitation over the Indian region is strongly correlated with food production. About 70%-80% of the precipitation is used by plants as soil moisture [1]. Therefore, precipitation is the most important atmospheric variable which depends on water vapour. Water vapour is the primary form of atmospheric moisture which define as the gaseous phase of water and helps to regulate the Earth's temperature by reflecting and scattering radiation from the Sun and by absorbing the Earth's infrared radiation.

Water vapour transported by atmospheric circulation is one of the most important processes in the hydrologic cycle and plays a vital role in determining rainfall distribution [2]. Water vapor for precipitation comes from both local evapo-transpiration (ET) and remote moisture transport or moisture flux [3, 4]. Heavy rainfall can be occurred only if water vapor is continuously transported into a sink region from outside [2]. Water vapour present in rain-bearing clouds which are responsible for all kinds of precipitation, and the amount of water vapour present in a given volume of air indicates the atmosphere's potential capacity for precipitation. The amount of water vapour also decides the quantity of latent energy stored up in the atmosphere for development of storms and cyclones. Therefore, measurement and

knowledge of atmospheric water vapor is essential for the prediction of weather elements like cloud, fog, temperature, humidity and precipitation.

Most of the rainfall is produced from convective cloud systems in which rainfall intensity varies through the life time of the cloud system. Mesoscale convective systems (MCSs) are the largest of the convective storms. They account for a large proportion of precipitation in both the tropics and warmer midlatitudes. For the occurrence of rainfall, enough moisture and upward motion is necessary. At first tiny water droplets must condense on even tinier dust, salt, or smoke particles, which act as a nucleus. Water droplets may grow as a result of additional condensation of water vapor when the particles collide. If enough collisions occur to produce a droplet with a fall velocity which exceeds the cloud updraft speed, precipitation falls from convective clouds (those with strong upward vertical motion) such as cumulonimbus (thunder clouds). The formation and longevity of convective system mainly depends on the amount of moisture availability at low level. As a result, low level moisture flux or moisture flux convergence is considered as a useful tool in prediction of convection as well as precipitation [5, 6].

Moisture flux is the horizontal transport of water vapour by the wind. The variability in atmospheric moisture flux plays a crucial role in the terrestrial hydrologic response and their fluctuations can relate directly to droughts and floods [7]. Early estimates of atmospheric moisture fluxes helped to highlight both the importance of the low level (planetary boundary layer) winds for determining the moisture transport, and obtaining accurate estimates of water vapour flux convergence [8-10]. Many previous studies have used vertically integrated moisture flux (VIMF) to estimate the moisture sources and transport for the precipitation [11-13] which is defined as humidity with horizontal wind integrated from the surface to a specified pressure level [5,6]. The unit of vertically integrated moisture flux is $\text{kg m}^{-1} \text{s}^{-1}$.

In South Asia, the atmospheric moisture transport from North Indian Ocean (NIO) to land is largely associated with the Indian summer monsoon which is the most prominent in the world's monsoon systems. It is characterized with a distinct seasonal reversal of wind and clear partition between dry and wet season in the annual cycle, which is related with the seasonal reversal of the large-scale atmospheric

heating and steady circulation features [14-16]. The southeast monsoon brings large amounts of rainfall to the region during June and July which depends on moisture-laden air from the NIO (North Indian Ocean). The summer monsoons are especially useful for India, Bangladesh and Myanmar and bringing a large portion of their water supply and providing valuable water for subsistence farmers. The economy of these countries largely depends on the success of this season. The Indian summer monsoon provides about 80% of annual rainfall to around a billion people in South Asia and variations in its timing, intensity and duration have a dramatic impact on society.

Therefore an overall understanding and proper quantification of annual moisture balance over South Asia is vital to know seasonal distribution of the hydro-climate processes over this region. Such an analysis contributes to understand the processes responsible for the variability of rainfall and hence the occurrence of drought or flood.

Very few studies have investigated the moisture transport over South Asia (SA) using reanalysis data and modeling [21-23]. They mainly analyzed moisture flux associated with the Indian monsoon rainfall. However, to our knowledge no study has been done for the low-level VIMF and its long-term variability over SA including the Bay of Bengal. Therefore, it is essential to know the distribution of low-level VIMF in synoptic scale and associated rainfall over South Asia and the Bay of Bengal.

1.2 Objective of the present study

The objectives of this research work are:

- To calculate low level vertically integrated moisture flux (VIMF) for South Asia including the Bay of Bengal.
- To analyze long-term annual variability of VIMF.
- To examine the monthly and seasonal variation of VIMF.
- To differentiate the rainfall coming from moisture transport and evaporation process.

- To find out the amount of precipitation that occurred by low level VIMF.

The primary purpose of this paper is to develop a phenomenological description of the seasonal modes of moisture transport anomalies that will help to better understand the relations between large-scale atmospheric circulation, atmospheric moisture availability and precipitation over South Asia. The results of this research will give valuable information about spatial and temporal characteristics of low-level total moisture flux and its effect on rainfall over South Asia. It will also help to improve the climate model for focusing the convective system and its physical processes.

CHAPTER-2

LITERATURE REVIEW

2.1 Previous work

The works that have already done over moisture flux and its convergence effect are explained below:

Trenberth *et al.* [3] found that the global average precipitation rate from global precipitation estimates (Huffman *et al.* 1997; Xie and Arkin 1997) is about 2.8 mm/day. Hence, this is also the global evaporation rate, as the imbalance is tiny. Moreover, evaporation is continuous, subject to availability of moisture from the surface (which is not a limitation over the oceans), and increases to about 5 mm/day in summer (Trenberth and Guillemot 1998). So, the moisture supply for moderate or heavy precipitation locally does not come directly from evaporation. Instead it has to come from transport, and thus from convergence of low-level moisture elsewhere in the atmosphere.

Lele *et al.* [5] reported that vertically integrated atmospheric water vapor flux for the surface to 850 hPa is calculated to account for total low-level moisture flux contribution to rainfall over West Africa (WA). The zonal component is the largest contributor to mean moisture transport into the Sahel, while the meridional transport contributes the most over the Guinea coast. The correlations between components of moisture transport and rainfall confirm the strong association between the zonal moisture transport and Sahelian precipitation.

Banacos, P.C., and Schultz, D. M. [6] showed that surface moisture flux convergence (MFC) is directly proportional to the horizontal mass convergence field, allowing MFC to be highly effective in highlighting mesoscale boundaries between different air masses near the earth's surface. The effectiveness of boundaries in generating deep moist convection is influenced by the depth of the vertical circulation along the boundary and the presence of convective available potential energy (CAPE) and convective inhibition (CIN) near the boundary.

Wei *et al.* [17] investigated the influence of atmospheric moisture fluxes and land surface soil moisture on local precipitation. Experiments showed that the variation of moisture flux convergence (MFC) is more important than that of soil moisture for precipitation variation over the southern U.S. MFC affects precipitation both directly through changing moisture inflow (wet areas) and indirectly by changing the precipitation efficiency (transitional zones). MFC is more important for the probability of heavier rainfall over most regions.

Min, W., and Schubert, S. D. [18] investigated the main moisture flux anomalies associated with extreme climate (drought and flood) events during the period 1985-93. The correspondence is strongest over the Great Plains and weakest over the Indian monsoon region reflecting differences in the observational coverage. For the reanalysis products, the uncertainties in the lower tropospheric winds are by far the dominant source of the discrepancies in the moisture flux anomalies in the middle latitude regions. Only in the Indian Monsoon region, the moisture bias plays a substantial role.

Trenberth K. E. [19] investigated how much moisture that precipitates out comes from local evaporation versus horizontal transport. Results showed that often the intensity of the hydrological cycle is not greatest at times of highest precipitation because moisture transport into the region are maximum, especially in the monsoonal regions. Over the Amazon, strong advection of moisture dominates the supply of atmospheric moisture over much of the river basin but local evaporation is much more prominent over the southern parts and for the annual cycle as a whole, about 34% of the moisture is recycled.

Cadet and Nnoli [20] used one summer (1979) of the European Centre for Medium-Range Weather Forecasts (ECMWF) data to study the water vapor transport over Africa. They analyzed biweekly fields of water vapor flux between the surface and 850 hPa and showed that the Gulf of Guinea and central Africa supply most of the moisture for rainfall over WA (West Africa).

Very few studies are found about moisture flux over South Asia which is described below:

Huang Y. and Cui X. [21] observed moisture sources and transport and quantification of the contribution from moisture sources by using the Lagrangian method. They calculated vertically integrated moisture flux from the surface to 700 hPa by the given equation,

$$-\frac{1}{g} \int_{p_s}^{700} qV dp$$

The vast majority of target particles influencing the precipitation originated from the relatively lower atmospheric layers south of the precipitation region and can be traced back to the Bay of Bengal, the Arabian Sea, and the Somali Peninsula. The total moisture from the source regions accounts for more than 80% of the precipitation; moisture originating from the India Peninsula–Bay of Bengal–Indo-China Peninsula region had the highest contribution.

Jiang *et al.* [22] reported that the southward retreat of meridional water vapor flux and weakening of zonal water vapor flux over North China could be responsible for the southward retreat of atmospheric column water vapor transport. Meridional water vapor transport depends on water vapor carried by the southwesterly wind of Asian summer monsoon.

Karmakar [23] showed that vertically integrated tropospheric moisture, dry static energy, latent energy and total energy over Bangladesh have a tendency to decrease at the formation stages of the cyclones in the Bay of Bengal and then the same shows a significant increase as the cyclones move northwards for ultimate landfall.

2.2 Overview of the study

2.2.1 Moisture

Moisture is the amount of water vapour present in the air. Moisture is related to the content of water (water in liquid state). Measurement and knowledge of atmospheric water vapour, or “moisture”, is crucial in the prediction of all weather elements, especially clouds, fog, temperature, humidity thermal comfort indices and

precipitation. Moisture that condenses as rainfall may experience evaporation, condensation, and re-evaporation on its path before reaching the sink region. Therefore, based on water vapour flux, we showed only the moisture transport routine in the atmosphere, but not its actual source region. In the past few decades, a number of studies have tried to discover where the moisture ultimately originated. A direct way to detect the actual rainfall origin is to incorporate “tagged” water into general circulation models (GCMs) by tagging the moisture at its origins and following it through the atmospheric process until it has precipitated from the atmosphere. Moisture in the atmosphere can appear in three states--solid, liquid, and a gaseous vapour that shows in Fig. 2.1. It is very rare when the air does not contain some water vapour. When the air is cooled to its saturation point, condensation occurs in the form of clouds and perhaps precipitation. Water vapour in the air comes almost entirely from three sources:

- Evaporation from any moist surface or body of water
- Evaporation from soil and
- Transpiration from plants.

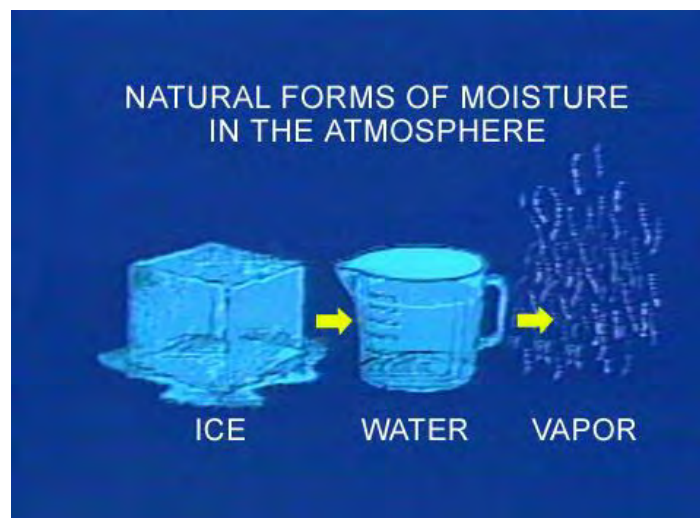


Fig. 2.1: Natural forms of moisture in the atmosphere.

Some water vapour results from combustion. Because the oceans cover more than three-fourths of the earth's surface, they are the most important moisture source, but land sources can also be important locally. Atmospheric moisture within a region can

be advected from external sources, or can come from local evapo-transpiration within the region [24].

Moisture Transfer = Evaporation - Precipitation

The transfer happens in where vapour pressure difference and radiation imbalances between different places. More moisture is transferred in southern hemisphere. Two types of transfer are happened. They are:

a) Vertical transfer:

Surface to atmosphere happens through evapo-transpiration, condensation and precipitation.

b) Horizontal transfer:

- Tropics have the moisture deficit in the atmosphere.
- Desert has the moisture surplus in the atmosphere.
- Moisture is transferred poleward and equatorward from 30°.

Moisture and temperature interact, and one controls the other. Relative humidity and dew point both give us an idea of the amount of moisture in the atmosphere.

2.2.2 Dew Point Temperature

Dew points indicate the amount moisture in the air. The higher the dew points, the higher the moisture content of the air at a given temperature. Dew point is a better indicator of humidity than relative humidity because it is not a percentage dependent on temperature. A state of saturation exists when the air is holding the maximum amount of water vapour possible at the existing temperature and pressure. When the dew point temperature and air temperature are equal, the air is said to be saturated and the relative humidity is 100%. Dew point temperature is never greater than the air temperature. Therefore, if the air cools, moisture must be removed from the air and this is accomplished through condensation. This process results in the formation of tiny water droplets that can lead to the development of fog, frost, clouds, or even

precipitation. Hygrometers are used to measure dew point over a wide range of temperatures.

The dew point can be either lower than (if the air is not saturated) or equal to (if the air is saturated) the actual temperature. The bigger the difference between the actual air temperature and the dew point, the drier the air is. Relative Humidity can be inferred from dew point values. When air temperature and dew point temperatures are very close, the air has a high relative humidity. The opposite is true when there is a large difference between air and dew point temperatures, which indicates air with lower relative humidity. Weather conditions at locations with high dew point temperatures (65 or greater) are likely to be uncomfortably humid. For example, a relative humidity of 100% means dew point is the same as air temp. For 90% RH, dew point is 3 degrees Fahrenheit lower than air temp. For every 10 percent lower, dew point drops 3°F [25].

2.2.3 Mixing ratio

Mixing ratio (w) is the amount of water vapour that is in the air. w is the grams of vapour per kg of dry air. w is an absolute measure of the amount of water vapour in the air. It differs from specific humidity only in that it is related to the mass of dry air instead of to the total dry air plus water vapour. It is very nearly equal numerically to specific humidity, but it is always slightly greater. It is non conservative for changes involving a gain or loss of water vapour. The mixing ratio has the same characteristic properties as the specific humidity. Mixing ratio is calculated by the given formula:

$$w = 621.97 \times \frac{e}{p_{sta} - e}$$

Here,

e = Actual vapor pressure,

p_{sta} = Station pressure,

w = Actual Mixing ratio

In meteorology the mixing ratio is useful for tracing the properties of vast air masses as they rise or fall in the atmosphere. This is the most common way to indicate air humidity in scientific applications. At the Earth's surface, mixing ratio varies from ~18 gm/kg in the tropics to less than 2 gm/kg near the poles. The maximum mixing ratio is determined by temperature alone, as shown in the temperature/vapour pressure graph. At 40° C, the maximum amount of water that can occur in vapour form = 40 g kg⁻¹, whereas at 0° C, the maximum possible mixing ratio = 4 g kg⁻¹ [26].

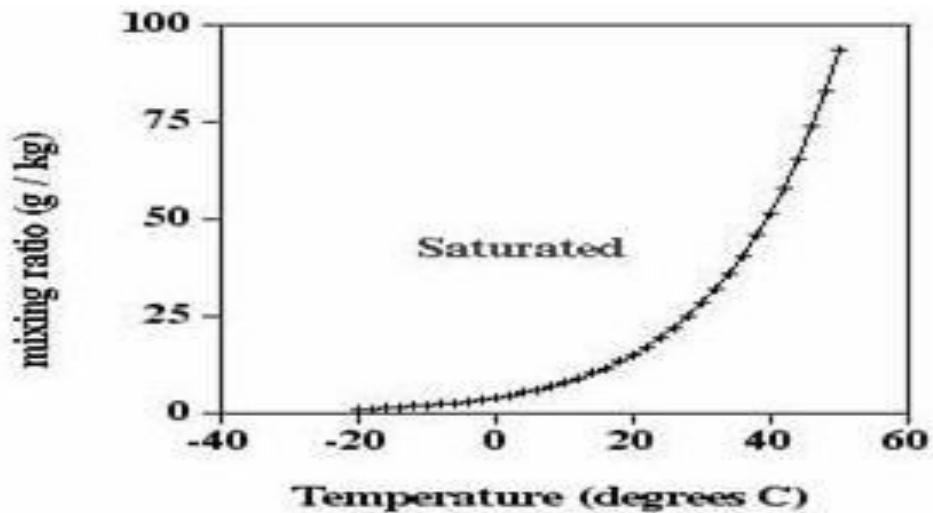


Fig. 2.2: Saturated mixing ratio.

2.2.4 Specific humidity

Mass of water vapour in a unit mass of moist air is called specific humidity. It is expressed as grams of vapour per kilograms of air. The mass of water vapour m_v in a unit mass of air (dry air plus water vapour) is called the specific humidity q , that is

$$q \equiv \frac{m_v}{m_v + m_d} = \frac{w}{1 + w}$$

The specific humidity is an extremely useful quantity in meteorology. The rate of evaporation of water from any surface is directly proportional to the specific humidity difference between the surface and the adjoining air. Specific humidity is measured by hygrometer. Knowing the specific humidity, without knowledge of the

temperature, does not enable one to determine the probability of cloud formation or precipitation. Specific humidity does not vary as the temperature or pressure of a body of air changes, as long as moisture is not added to or taken away from it. Specific humidity can be expressed in other ways including [27]:

$$SH = \frac{0.622 \times p_{H_2O}}{p_{(dry\ air)}} \times \frac{MM_{H_2O}}{MM_{(dry\ air)}}$$

or:

$$SH = \frac{0.622 \times p_{H_2O}}{p - 0.378 \times p_{H_2O}}$$

Specific humidity is not affected by pressure but the condition of saturation depends both upon atmospheric moisture content and temperature is shown in Fig.2.3.

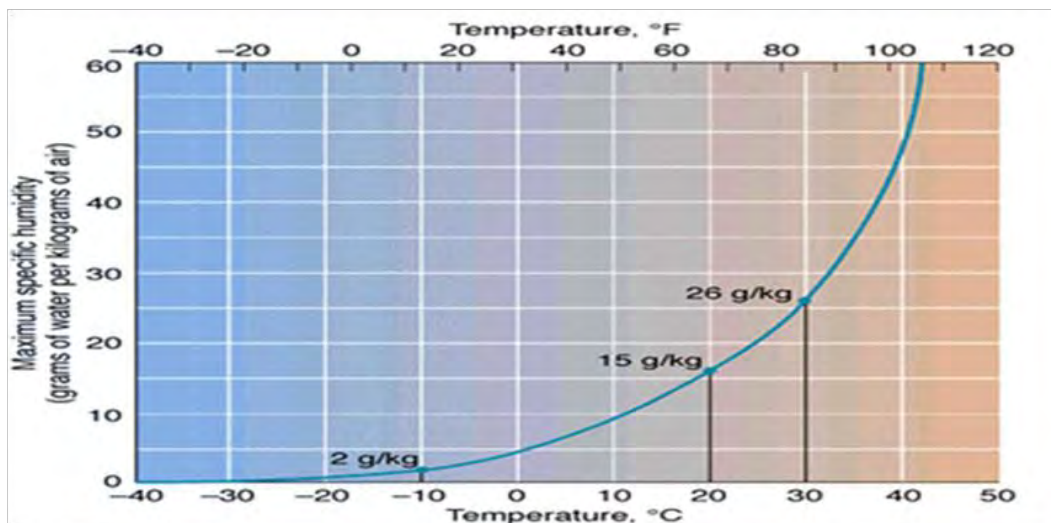


Fig. 2.3: Vapour capacity graph shows how warm air can hold more water than cold air.

2.2.5 Relative Humidity

Relative humidity is a measure of how much water vapour the air actually could hold at a certain temperature. The relative humidity represents how close the air is to saturation. Saturated air will have an RH of 100%. Locations with high relative

humidity indicate that the air is nearly saturated with moisture; clouds and precipitation are therefore quite possible. Relative humidity may be defined as:

$$\text{Relative Humidity (RH)} = \frac{\text{(Actual Vapor Density)}}{\text{(Saturation Vapor Density)}} \times 100\%$$

Relative humidity is also approximately the ratio of the actual to the saturation vapor pressure.

$$\text{RH} = \frac{\text{(Actual Vapor Pressure)}}{\text{(Saturation Vapor Pressure)}} \times 100\%$$

Actual vapour pressure is a measurement of the amount of water vapour in a volume of air and increases as the amount of water vapour increases. Air that attains its saturation vapour pressure has established equilibrium with a flat surface of water. That means, an equal number of water molecules are evaporating from the surface of the water into the air as are condensing from the air back into the water. Relative humidity varies with temperature. Since warm air will hold more moisture than cold air, the percentage of relative humidity must change with changes in air temperature that shown in Fig. 2.4.

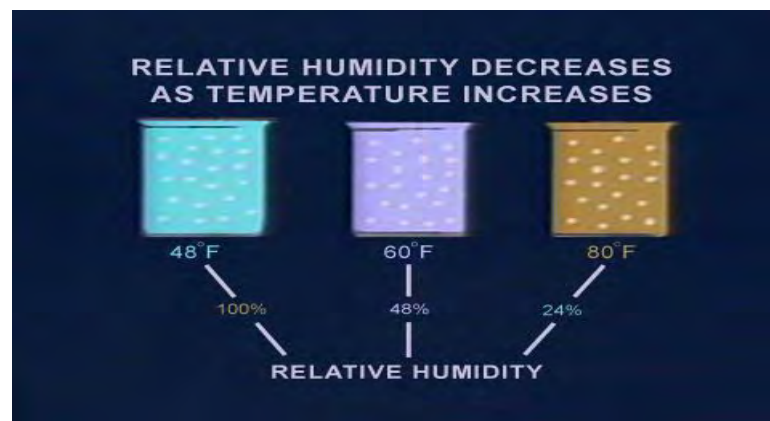


Fig. 2.4: Relative humidity with temperature.

The number of water vapour molecules is the same in each container. At 40° air temperature, the parcel is saturated and will hold no more molecules of water vapour. The relative humidity is 100 percent. If the temperature of that air parcel is raised by 20°, it will hold about twice as many water molecules to reach saturation. Thus, the

new relative humidity is now 48 percent. If the temperature is raised another 20°, it will again double its capacity to hold water vapour molecules. The relative humidity is only 24 percent. The importance of air temperature to moisture is obvious. At 80°, the air has a relatively low humidity and is relatively dry. As it cools, the humidity increases, reaching its saturation point at 40° [24]. The dew point of the air is 40° in all three containers in the illustration. During day, relative humidity and temperature have inverse relationship. Relative humidity is measured by Sling Psychrometer (hygrometer).

2.2.6 Moisture flux

Moisture flux is the horizontal transport of water vapour by the wind. It plays a very important role in the development of precipitation. The variability in atmospheric moisture flux plays a crucial role in the terrestrial hydrologic response and their fluctuations can relate directly to droughts and floods. In terms of mixing ratio, horizontal transport/advection can be represented in terms of moisture flux:

$$f = qV$$

Here q is the mixing ratio. Zonal and meridional moisture flux unit is $m\ s^{-1}$. Early estimates of atmospheric moisture fluxes helped to highlight both the importance of the low level (planetary boundary layer) winds for determining the moisture transport, and the inadequacy of the rawinsonde network for obtaining accurate estimates of water vapour flux convergence [28].

2.2.7 Vertically integrated moisture flux and its convergence

The formation and longevity of convective system mainly depends on the amount of moisture availability at low level. As a result, low level vertically integrated moisture flux (VIMF) or moisture flux convergence is considered as a useful tool in prediction of convection or precipitation. The VIMF is defined as [5, 6]

$$\frac{1}{g} \int_{p_s}^p qV dp$$

Where V is the horizontal wind, g is the gravitational acceleration and q is the specific humidity. The column pressure extends from the surface p_s to a specific pressure level

p . The unit of VIMF is $\text{kg m}^{-1} \text{s}^{-1}$. Moisture flux convergence (MFC) is a term in the conservation of water vapour equation and was first calculated in the 1950s and 1960s as a vertically integrated quantity to predict rainfall associated with synoptic-scale systems. A scale analysis shows that surface MFC is directly proportional to the horizontal mass convergence field, allowing MFC to be highly effective in highlighting mesoscale boundaries between different air masses near the Earth's surface. The expression for MFC can be derived from the conservation of water vapour in pressure (p) coordinates:

$$\frac{dq}{dt} = S, \quad (1)$$

where

$$\frac{d}{dt} = \frac{\partial}{\partial t} + u \frac{\partial}{\partial x} + v \frac{\partial}{\partial y} + \omega \frac{\partial}{\partial p},$$

u , v , and ω represent the standard three-dimensional wind components in pressure coordinates, and q is the specific humidity; S represents the storage of water vapour, which is the difference between the sources and sinks of water vapour following air parcel motion. Here S typically takes the form $E-C$, where E (C) is the evaporation (condensation) rate into the air parcel. Studies employing (1) often assume that all the condensed water immediately precipitates out (P), so that $S = E - P$ [29]. Further, the mass continuity equation, $\partial u/\partial x + \partial v/\partial y + \partial \omega/\partial p = 0$, allows (1) to be expanded and rewritten in flux form by effectively adding zero to both sides of (1):

$$\begin{aligned} \frac{\partial q}{\partial t} + u \frac{\partial q}{\partial x} + v \frac{\partial q}{\partial y} + \omega \frac{\partial q}{\partial p} + q \left(\frac{\partial u}{\partial x} + \frac{\partial v}{\partial y} + \frac{\partial \omega}{\partial p} \right) \\ = E - P. \end{aligned} \quad (2)$$

$$\frac{\partial q}{\partial t} + \frac{\partial}{\partial x} (qu) + \frac{\partial}{\partial y} (qv) + \frac{\partial}{\partial p} (q\omega) = E - P.$$

$$\underbrace{\frac{\partial q}{\partial t}}_{\text{local rate of change of } q} + \underbrace{\nabla \cdot (q\mathbf{V}_h)}_{\text{-horizontal MFC}} + \underbrace{\frac{\partial}{\partial p} (q\omega)}_{\text{-vertical MFC}} = \underbrace{E - P}_{\text{sources and sinks}}, \quad (3)$$

where $\nabla = \hat{\mathbf{i}}(\partial/\partial x) + \hat{\mathbf{j}}(\partial/\partial y)$ and $\mathbf{V}_h = (u, v)$. Specifically, (3) expresses the moisture budget for an air parcel, where the terms consist of the local rate of change of q , horizontal moisture flux divergence (the negative of horizontal MFC), the vertical moisture flux divergence (the negative of vertical MFC), and source and sink terms of moisture (specifically, evaporation and precipitation rates) [30, 31]. By vector identity, horizontal MFC can be written as

$$\text{MFC} = -\nabla \cdot (q\mathbf{V}_h) = -\mathbf{V}_h \cdot \nabla q - q\nabla \cdot \mathbf{V}_h, \quad (4)$$

$$\text{MFC} = \underbrace{-u \frac{\partial q}{\partial x} - v \frac{\partial q}{\partial y}}_{\text{advection term}} - \underbrace{q \left(\frac{\partial u}{\partial x} + \frac{\partial v}{\partial y} \right)}_{\text{convergence term}}. \quad (5)$$

In (5), the advection term represents the horizontal advection of specific humidity, whereas the convergence term denotes the product of the specific humidity and horizontal mass convergence. Vertically Integrated Moisture Flux Convergence (VIMFC) alone and in combination with the lifted stability index of the most unstable layer (SMUL) is evaluated as a thunderstorm predictor.

2.2.8 Atmospheric Parameters

Atmospheric parameters such as precipitation, evaporation, specific humidity were used in the study. Specific humidity was discussed in the section 2.2.4. In this section precipitation and evaporation are discussed.

2.2.9 Precipitation

Precipitation is the water that falls, solid or liquid, from the clouds. It is a major component of the water cycle, and is responsible for depositing the fresh water on the planet. Precipitation occurs when a portion of the atmosphere becomes saturated with water vapour, so that the water condenses and "precipitates". Moisture overriding associated with weather fronts is an overall major method of precipitation production. If enough moisture and upward motion is present, precipitation falls from convective clouds such as cumulonimbus and can organize into narrow rain bands.

Precipitation is measured with a pluviometer. It is expressed in millimeters or in liters per square meter.

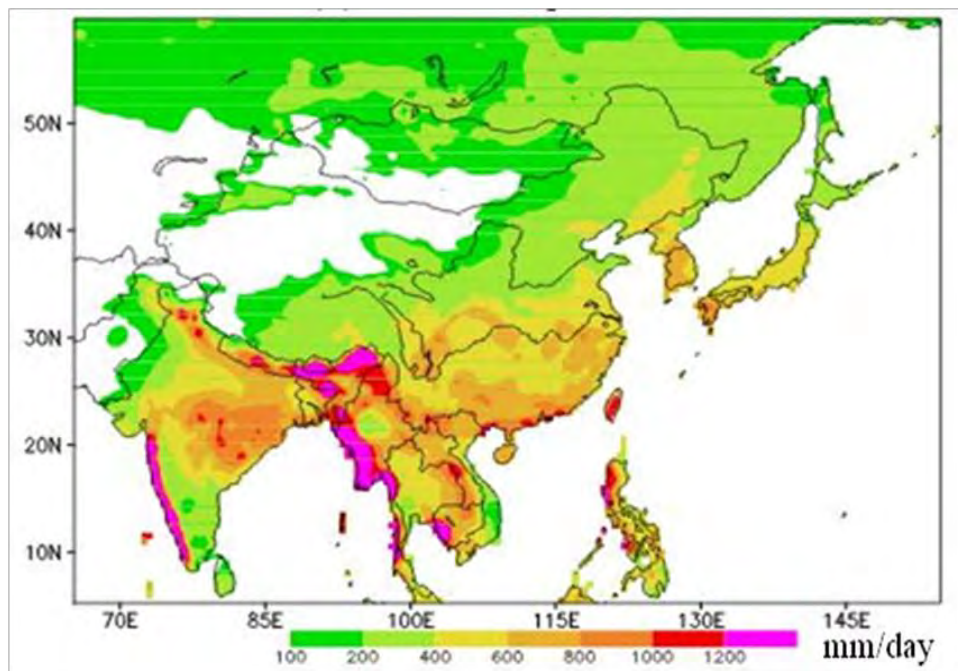


Fig. 2.5: Average south Asia and south-east Asia precipitation (mm/day) since 1978 to 2002.

The global average precipitation rate from global precipitation estimates is about 2.8 mm/day [32, 33]. Mechanisms of producing precipitation include convective, stratiform, and orographic rainfall. Two main mechanisms have been identified to explain the growth of water droplets to form precipitation:

- Activated nuclei, or the growth of droplets by condensation from surrounding vapour.
- Collision or the growth of droplets by the combination of two colliding particles.

There are many reasons for changes in precipitation. The leading cause is a change in temperature. Many scientists believe an increase in temperature could lead to a more intense water cycle. The rates of evaporation from soils and water, as well as transpiration from plants, could increase. The amount of precipitation could also increase. Precipitation over land is composed of a mixture of oceanic, as well as terrestrial, sources of moisture. South Asian Monsoon affects the Indian subcontinent

and surrounding regions. Rainfall around the continent is favored across its southern portion from India east and northeast across the Philippines and southern China into Japan due to the monsoon advecting moisture primarily from the Indian Ocean into the region. The Indian summer monsoon provides about 80% of annual rainfall to around a billion people in South Asia and variations in its timing, intensity and duration have a dramatic impact on society [34].

2.2.10 Evaporation

Evaporation is an essential part of the water cycle. Whenever a water molecule leaves a surface and diffuses into a surrounding gas, it is said to have evaporated. Evaporation of water occurs when the surface of the liquid is exposed, allowing molecules to escape and form water vapour; this vapour can then rise up and form clouds. The sun (solar energy) drives evaporation of water from oceans, lakes, moisture in the soil, and other sources of water. In hydrology, evaporation and transpiration (which involves evaporation within plant stomata) are collectively termed evapo-transpiration. The rate of evaporation depends upon:

- Wind speed: the higher the wind speed, the more evaporation
- Temperature: the higher the temperature, the more evaporation
- Humidity: the lower the humidity, the more evaporation

The tropics drive the global energy and water cycle since the oceans, which comprise most of the tropical surface, receive a surplus of radiative heating. While evaporation over land is less than that over the ocean, its distribution plays a vital role in the initiation and evolution of convective weather systems. The rate of evaporation near the Equator is greater due to the temperature increase.

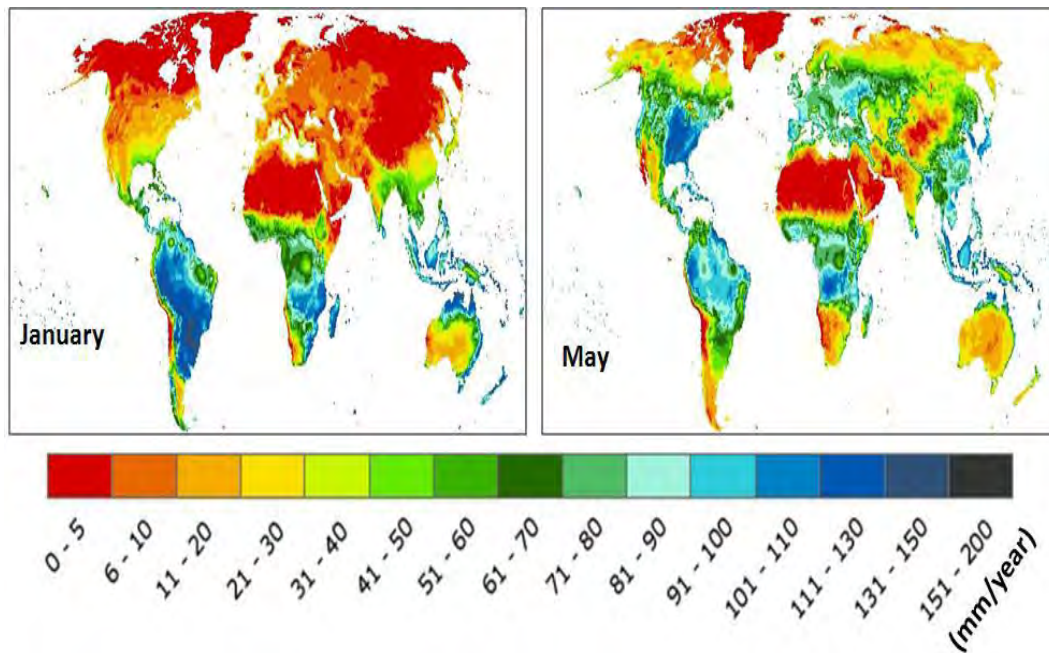


Fig. 2.6: Average global evaporation in a year for the month of January and May since 1985 to 1999.

Approximately 80% of all evaporation is from the oceans, with the remaining 20% coming from inland water and vegetation. Winds transport the evaporated water around the globe, influencing the humidity of the air throughout the world. It is computed that, on average, 40% of the terrestrial precipitation originates from land evaporation and that 57% of all terrestrial evaporation returns as precipitation over land [35, 36]. Evaporation can be measured using eddy correlation or eddy covariance techniques and relative humidity sensors that record changes on highly turbulent scales (sometimes less than 1 second). Evaporation rates are also estimated from satellite microwave sensors, which detect radiation emitted by water vapor.

2.3 Geographical description of South-Asia and Bay of Bengal

Study area will be selected for South Asia including the Bay of Bengal (5°N-27°N & 70°E-105°E) and eastern part of the Arabian Sea. South Asia is the southern region of the Asian continent. Topographically, it is dominated by the Indian Plate, which rises above sea level as Nepal and northern parts of India situated south of the Himalayas and the Hindu Kush. It is surrounded by three water bodies - the Bay of Bengal, the Indian Ocean and the Arabian Sea. These water bodies help moisture accumulate in the winds during the hot season. The Bay of Bengal, the largest bay in the world, forms the northeastern part of the Indian Ocean [37]. It is triangular in

shape and bordered mostly by India and Sri Lanka to the west, Bangladesh to the north, Myanmar and the Andaman and Nicobar Islands to the east. It contributes a significant amount of moistures resulting intense precipitation in the eastern parts of India and the neighboring countries. The Bay of Bengal possesses certain unique characteristics which are believed to play an important role in moisture generation and transport process. The Bay of Bengal acts as a major sink of water vapour during the summer months (May to Sep) as precipitation (P) far exceeds the evaporation (E) but provides vapour to atmosphere during the rest of the year.

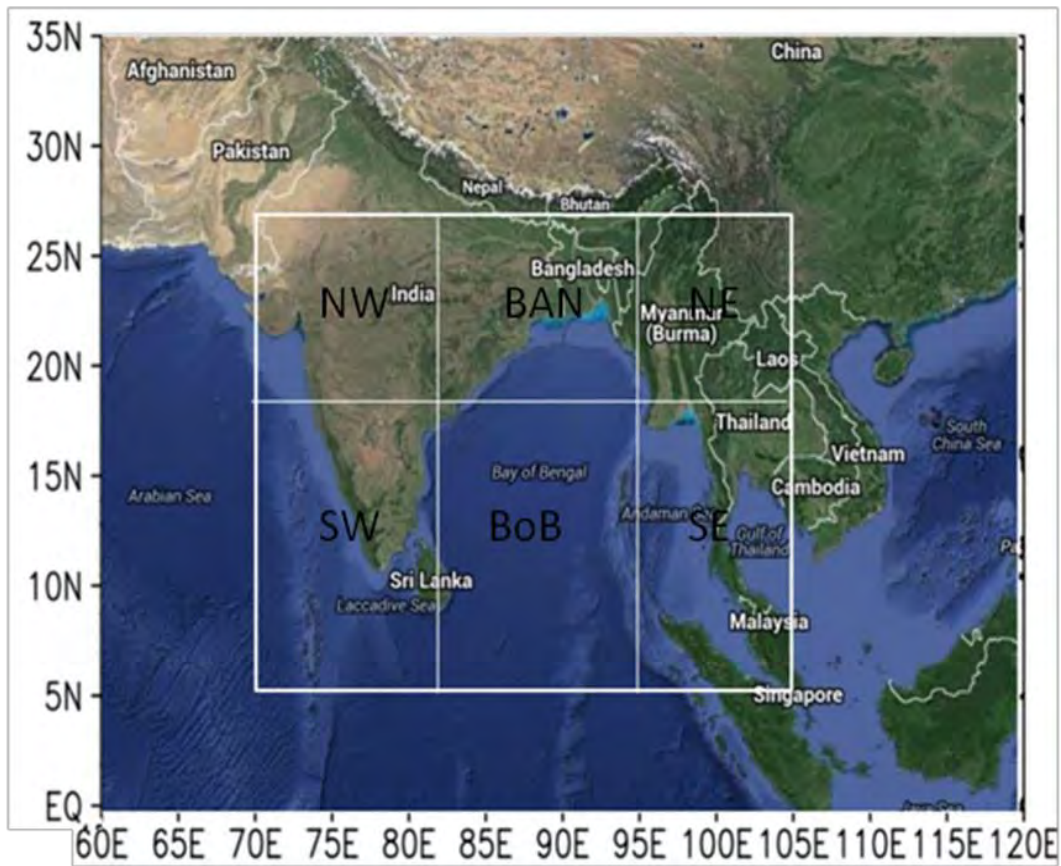


Fig. 2.7: Regional map showing the coverage area of 5°N-27°N, 70°E-105°E. Gray shading indicates the topography.

For understanding spatial and temporal characteristics of moisture flux and its effect on precipitation in different regions the area is sub divided into six regions i.e.

2.3.1 South-West region (5°N-18°N & 70°E-82°E)

This region covers Sri Lanka, some part of India (Andhra Pradesh, Karnataka, and Tamil Nadu), Laccadive Sea, and Lakshadweep islands. Sri Lanka lies in the Indian Ocean southwest of the Bay of Bengal, between latitudes 5° and 10°N, and longitudes 79° and 82°E. Sri Lanka climate is tropical and consists of distinct wet and dry seasons. The Yala monsoon brings abundant rainfall to the western and southern regions from May to September. The Maha monsoon affects northern and eastern Sri Lanka weather and often lasts from October to January. India lies on the Indian Plate, the northern portion of the Indo-Australian Plate, whose continental crust forms the Indian subcontinent [38]. The country is situated north of the equator between 8°4' and 37°6' north latitude and 68°7' and 97°25' east longitude.

2.3.2 Bay of Bengal (BoB) (5°N-18°N & 82°E-95°E)

The Bay of Bengal, the largest bay in the world, forms the northeastern part of the Indian Ocean. It lies roughly between latitudes 5° and 22° N and longitudes 80° and 90° E. It is bordered by Sri Lanka and India to the west, Bangladesh to the north, and Myanmar (Burma) and the northern part of the Malay Peninsula to the east. Weather conditions are often brutal in the Bay of Bengal as the area is ravished by heavy monsoon rains, both summer and winter. The Bay of Bengal strongly responds to Intra seasonal oscillation (ISO) and it is believed that it plays a crucial role in modulating this process [37]. The Bay of Bengal is also characterized by low pressure systems (LPS) that cause extreme rainfall events especially in the coastal regions of India, Bangladesh, Myanmar, Sri Lanka etc.

2.3.3. South-East region (5°N-18°N & 95°E-105°E)

This region covers Thailand, some parts of Malaysia (AlorSetar, Butterworth, Kota Baharu, Putih, Kuala Terengganu), Cambodia (Phumi Samraong, Preah Vihear, Sisophon, Battambang, Siemreab, Sihanoukville, Kampong Chhnang, KrongKaoh Kong, Kampong Spce, Kampot), Myanmar (Pegu, Yangon, Thanlyin, Mawlamyine, Kwanhlar, Ye, Dawei, Palaw, Myeik, Tenasserim, Manoron, Maliwun), Gulf of Thailand and some parts of the Andaman sea. Thailand is situated in the south eastern part of Asia between 15° 00' North latitude and 100° 00' East longitude. Thailand

climate is controlled by tropical monsoons and the weather in Thailand is generally hot and humid throughout the year. Malaysia, in the south east part of Asia, has a geographic coordinate that reads 2° 30' North latitude and 112° 30' East longitude. Malaysia has tropical weather, influenced by monsoonal climate because of its latitude and longitude. Summer monsoon brings lots of downpour in Malaysia. Winter monsoon does not cause that much rain and is generally dry. The geographic alignments of the country of Cambodia indicates 13° 00' N and 105° 00' E latitude and longitude respectively. The climatic condition of Cambodia is considered as tropic. Two main seasons dominate Cambodia as semiarid season and rainy season.

2.3.4. North-West region (18°N-27°N & 70°E-82°E)

This region covers India (Pune, Mumbai, Raipur, Nagpur, Daman, Surat, Rajkot, Vadodara, Ahmadabad, Bhopal, Jodhpur, Jaipur, Gurgaon, Agra, Gwalior, Kanpur, Allahbad, Lucknow) and little part of the Arabian sea. For the country of India the latitude of 22° 00' N and longitude of 77° 00' E denote its geographical alignment. The specific latitude of India suggests its position in Northern Hemisphere. The terra firma of India is bounded by the Bay of Bengal, Arabian Sea, Pakistan, Bangladesh, Myanmar, Nepal, Bhutan and China. The diversity of the climatic condition in India is featured by tropic rainy season in the southern region while the northern part is temperate. The Arabian Sea is located in the northwestern part of the Indian Ocean, situated between the Arabian Peninsula and the Indian subcontinent. The presence of abundant water bodies of the Arabian Sea helps moisture accumulate in the winds during the hot season.

2.3.5. Bangladesh and surrounding (18°N-27°N & 82°E-95°E)

This region covers Bangladesh and some part of India (West Bengal, Bihar and Meghalaya). Bangladesh, one of the major neighboring countries of India, sits in between 24° 00' North latitude and 90° 00' East longitude. Geographically Bangladesh is in the highly disasterprone area of deltaic origin of Ganges-Brahmaputra Basin. The land of Bangladesh is very flat: elevation is about 1-10 m above sea level except small portions in the southeast (elevation ~200 m), which is border with Myanmar, and in the northeast (elevation ~100 m), which is border with Shillong hill of India. The Bay of Bengal is located in the south of Bangladesh with a complex coastal configuration

and the highly elevated Himalayas and Tibetan Plateau in the north. Bangladesh is situated within such a latitude and longitude that it has got a weather that is tropical in nature. These geographical features are very favorable for the development of convection as the water vapour transported by the monsoonal winds from the Bay of Bengal and blocked by the highly elevated regions cause development of convection in Bangladesh. During summer season the climate is very hot and humid. In fact Bangladesh has got a very wet type of weather. In winter the climate is cold with and dry. Bangladesh receives a very high amount of precipitation each year that amounts to more than 1,500 mm. But this country is also subject to the devastation of cyclone many times a year.

2.3.6. North-East region (18°N-27°N & 95°E-105°E)

Most of the parts of Myanmar and some parts of Laos (Phongsali, Louangnamtha, Xay, XamNua, Muang Hongsa, Louangphabang, Muang Soum) are situated in this domain. Myanmar (also known as Burma) is the northwestern-most country on the mainland of Southeast Asia. Myanmar's latitude and longitude is 22° 00' N and 98° 00' E. It is characterized by strong monsoon influences, has a considerable amount of sun, a high rate of rainfall, and high humidity that makes it sometimes feel quite uncomfortable. The summers are hot and humid and even during the winter rainfall continues and the temperature remains mild and pleasant. The Lao People's Democratic Republic is situated at the South Asia between 18°00'N latitude and 105°00'E longitude. The geographic latitude and longitude of the region is responsible for Laos's humid tropical weather and high temperatures. Monsoons last between the months of May to November and the Dry season lasts from December to April [39].

CHAPTER-3

DATA AND METHODS

3.1 Data used

Global atmospheric 6-hourly reanalysis data product ERA-Interim generated by European Centre for Medium-Range Weather Forecasts (ECMWF) [6] were used in this study for 37 years from 1979 to 2015. As satellite soundings were not available before the year of 1979, the study was focused on the period from 1979 to 2015, where the data are most reliable. The horizontal resolution of data is approximately 80 km with 60 vertical levels from the surface up to 0.1 hPa. Data for meridional and zonal wind component and specific humidity at different pressure levels were utilized for analyzing low level vertically integrated moisture flux (VIMF) calculated from the equation mention below in section 3.3.1. Here, vertical integration was calculated from surface to 850 hPa pressure level. Furthermore, we used daily mean precipitation and evaporation data for knowing the consequences of moisture flux on annual rainfall.

ERA-Interim is the latest global atmospheric reanalysis from 1979, continuously updated in real time produced by the European Centre for Medium-Range Weather Forecasts (ECMWF). ERA-Interim is a global reanalysis of recorded climate observations over the past 3.5 decades. It is presented as a gridded data set at approximately 0.7 degrees spatial resolution, and 37 atmospheric levels. Gridded data products include a large variety of 3-hourly surface parameters, describing weather as well as ocean-wave and land-surface conditions, and 6-hourly upper-air parameters covering the troposphere and stratosphere. Vertical integrals of atmospheric fluxes, monthly averages for many of the parameters, and other derived fields have also been produced. The data assimilation system used to produce ERA-Interim is based on a 2006 release of the IFS (Cy31r2). The system includes a 4-dimensional variational analysis (4D-Var) with a 12-hour analysis window. The spatial resolution of the data set is approximately 80 km (T255 spectral) on 60 vertical levels from the surface up to 0.1 hPa.

Temporal Coverage:

- 4 times daily, January 1979 to at present.

Spatial Coverage:

- Global grid, 0.7 degrees approximate resolution.
- 89.5S - 89.5N, 0E - 359.3E.
- Grid dimensions are 256 latitudes x 512 longitudes.
- Grid type: N128 Gaussian grid. Equal spacing on longitudes.

Levels:

- All 37 original pressure levels, 1 to 1000 hPa, quasi-logarithmic.
- Pressure levels: 1, 2, 3, 5, 7, 10, 20, 30, 50, 70, 100, 125, 150, 175, 200, 225, 250, 300, 350, 400, 450, 500, 550, 600, 650, 700, 750, 775, 800, 825, 850, 875, 900, 925, 950, 975, 1000 hPa.
- All 15 original isentropic (theta) levels, 265 to 850 Kelvin.
- Theta levels: 265, 275, 285, 300, 315, 330, 350, 370, 395, 430, 475, 530, 600, 700, 850 Kelvin.

ERA-Interim also provided an opportunity to improve the technical infrastructure for reanalysis production at ECMWF. This includes the handling of input observations, procedures for quality control and bias correction of the observations, and tools for monitoring the data assimilation system and its overall performance. An advantage of using reanalysis for climate change assessment is that the data provide a global view that encompasses many essential climate variables in a physically consistent framework, with only a short time delay. Most of the meteorological input data are taken from the ERA-Interim reanalysis. One of the main objectives of the ERA-Interim project was to improve the representation of the hydrological cycle [40].

3.2 Study Area

In this study, South Asia including the Bay of Bengal (BoB) and eastern part of the Arabian Sea (5°N-27°N & 70°E-105°E) are selected that is shown in Fig. 3.1.

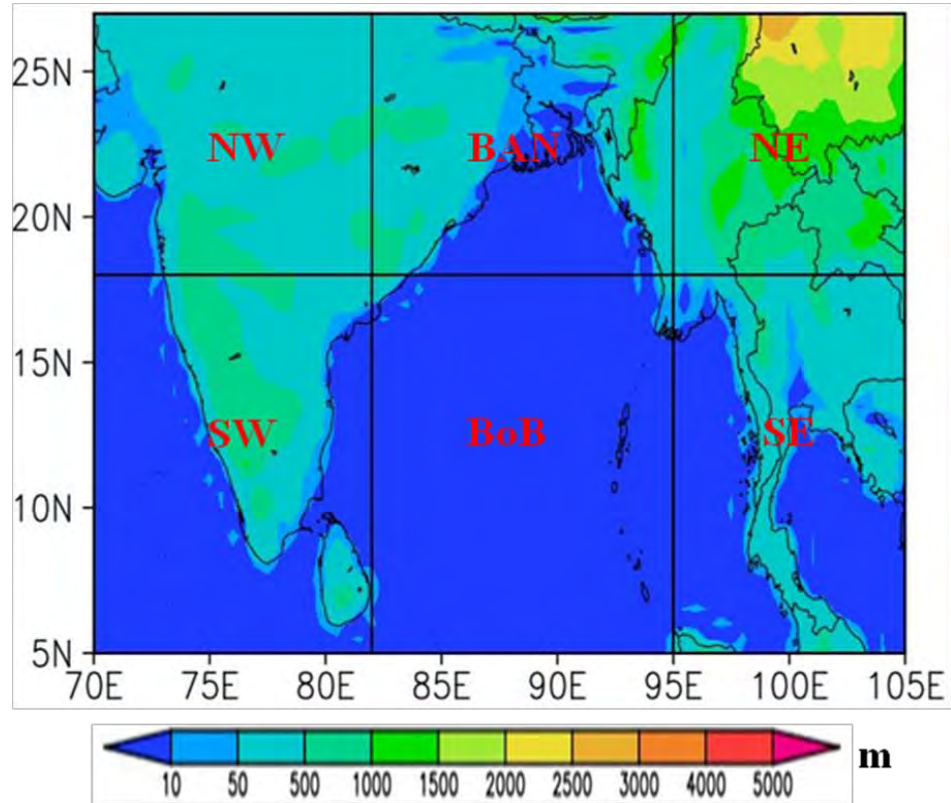


Fig. 3.1: Study area with topography.

For understanding spatial and temporal characteristics of moisture flux and its consequence effect on precipitation in different regions, the total study area is further sub divided into six regions i.e.

1. South-West region (5°N-18°N & 70°E-82°E)
2. Bay of Bengal region (5°N-18°N & 82°E-95°E)
3. South-East region (5°N-18°N & 95°E-105°E)
4. North-East region (18°N-27°N & 95°E-105°E)
5. Bangladesh and surrounding region (18°N-27°N & 82°E-95°E)
6. North-West region (18°N-27°N & 70°E-82°E)

Here, BoB is the main source of moisture flux, which is transported to the surrounding land including Bangladesh. Therefore, six domains are divided by centering the BoB. The details geographical description of the study area is discussed in the previous section [2.3].

3.3 Study Method

3.3.1 Calculation for vertically integrated moisture flux (VIMF)

The VIMF is defined as [5]

$$\frac{1}{g} \int_{p_s}^p q \mathbf{V} dp$$

Where \mathbf{V} is the horizontal wind, g is the gravitational acceleration and q is the specific humidity. The column pressure extends from the surface p_s to a specific pressure level p . The unit of VIMF is $\text{kg m}^{-1} \text{s}^{-1}$. For the purpose of this work, VIMF is calculated from the above mention equation for the pressure levels of 1000 hPa to 850 hPa.

3.3.2 Calculation of precipitation

The amount of precipitation over any region depends on moisture flux that is advected from the ocean or local evaporation rate (Trenberth, 1999) proposed a simple method for differentiation precipitation by the moisture advection and local evaporated moisture [19]. This method is used in this study for differentiating precipitation coming from moisture flux and evaporation Details procedure is described below:

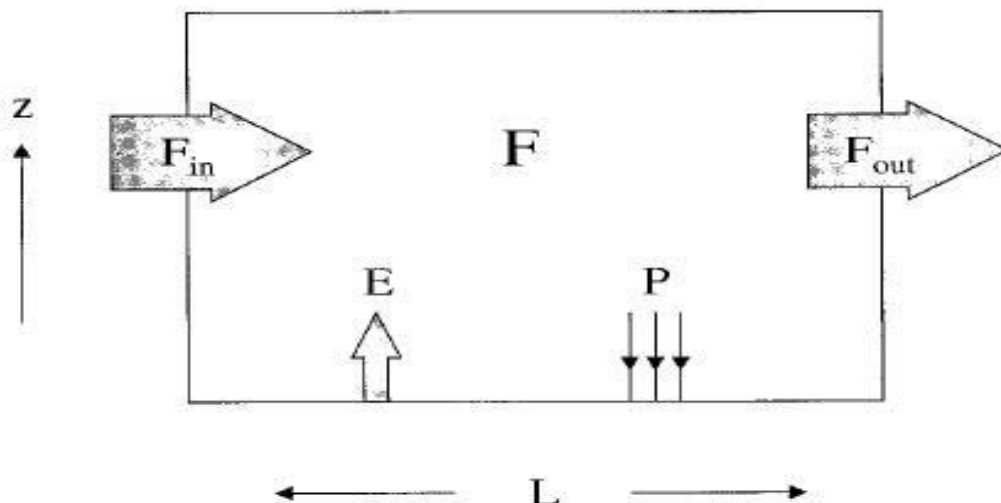


Fig. 3.2: Schematic for the processes considered in recycling of moisture. [Source: Trenberth, 1999]

In Fig. 3.2, a domain of length L aligned along the trajectory of the air with a flux of moisture into the box of F_{in} and a flux out of F_{out} and a total evaporation (E) and precipitation (P) in the box; then

$$F_{out} = F_{in} + (E - P) \quad (1)$$

and the average horizontal moisture flux through the box is

$$F = 0.5(F_{in} + F_{out}) = F_{in} + 0.5(E - P)L \quad (2)$$

If $P = P_a + P_m$, where P_a is the advective component and P_m is the component of precipitation arising from local evaporation, then the average horizontal flux of advected moisture over the region is $F_{in} - 0.5P_aL$, and the average horizontal flux of locally evaporated moisture is $0.5(E - P_m)L$. An important assumption is that the atmosphere is well mixed so that the ratio of precipitation that falls arising from advection versus local evaporation is equal to the ratio of average advected to evaporated moisture in the air. Thus,

$$\frac{P_a}{P_m} = \frac{F_{in} - 0.5P_aL}{0.5(E - P_m)L} \quad (3)$$

$$\text{Or, } \frac{P_a}{P_m} = 2F_{in}/EL \quad (4)$$

From (4) the ratio of P_m and P is written as,

$$\begin{aligned} \frac{P_m}{P} &= \frac{P_m}{P_m + P_a} \\ &= \frac{P_m/P_a}{P_m/P_a + 1} \\ &= \frac{EL/2F_{in}}{EL/2F_{in} + 1} \quad [\text{using equation 4}] \end{aligned} \quad (5)$$

Precipitation by evaporation,

$$P_m = \frac{EL}{EL + 2F_{in}} \times P \quad (6)$$

Precipitation by advection,

$$P_a = P - P_m = \left(1 - \frac{EL}{EL + 2F_{in}}\right)P \quad (7)$$

Equations (6) and (7) are used for calculating precipitation produced by local evaporation and moisture transport.

The graphical display of data, extract and average of the atmospheric parameters for spatial and temporal cases have been done using The Grid Analysis and Display System (GrADS) software that are discussed in 3.3.3.

3.3.3 The Grid Analysis and Display System (GrADS)

The Grid Analysis and Display System (GrADS) produced by Center for Ocean-Land-Atmosphere Studies, Institute of Global Environment and Society, George Mason University in 1988, is an interactive desktop tool that is used for easy access, manipulation, and visualization of earth science data. GrADS operating systems are Linux, Mac OS X, Microsoft Windows, Solaris, IBM AIX, DEC Alpha, IRIX. The format of the data may be either binary, GRIB, NetCDF, or HDF-SDS (Scientific Data Sets). GrADS will typically be used for operations such as:

- Plotting a variable from a file on a shaded plot and overlaying contours from a second variable.
- Aggregating multiple files into one control file so that slices of data can be read in across multiple files.
- Differencing 2 different datasets.
- Calculating departures from a climatology from a dataset.
- Regridding a dataset.

- Calculating the statistical data from variables.

Fig.3.3 shows a GrADS plot and the command-line interface running on a Linux operating system.

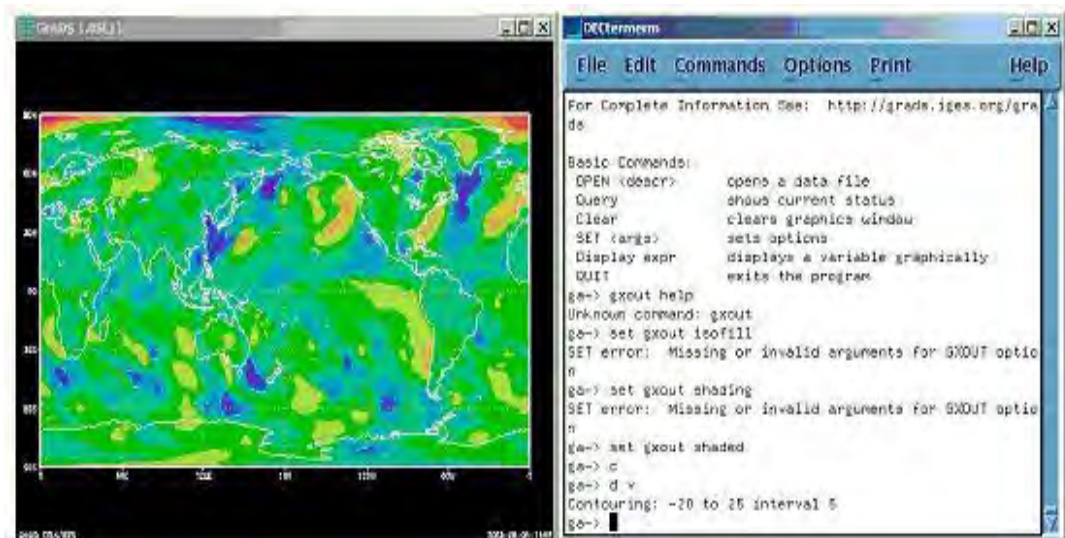


Fig. 3.3: GrADS example output.

GrADS uses a 4-Dimensional data environment: longitude, latitude, vertical level, and time. Data sets are placed within the 4-D space by use of a data descriptor file. GrADS interprets station data as well as gridded data, and the grids may be regular, non-linearly spaced, Gaussian, or of variable resolution. Data from different data sets may be graphically overlaid, with correct spatial and time registration. Data may be displayed using a variety of graphical techniques: line and bar graphs, scatter plots, smoothed contours, shaded contours, streamlines, wind vectors, grid boxes, shaded grid boxes, and station model plots. Graphics may be output in PostScript or image formats. GrADS provides geophysical intuitive defaults, but the user has the option to control all aspects of graphics output [41].

CHAPTER-4

RESULTS AND DISCUSSION

4.1 Vertically integrated moisture flux (VIMF) for study area

Annual, seasonal and monthly distribution of average vertically integrated moisture flux over the study areas is discussed in the following sections. The study area includes South Asian land; Bay of Bengal (BoB) and eastern part of Arabian Sea (AS) are shown in Fig. 3.1. Here, total domain (5°N-27°N & 70°E-105°E) is considered as South Asia (SA).

4.1.1 Spatial distribution of annual VIMF

Spatial distribution of 37-year averaged VIMF and horizontal wind from ECMWF

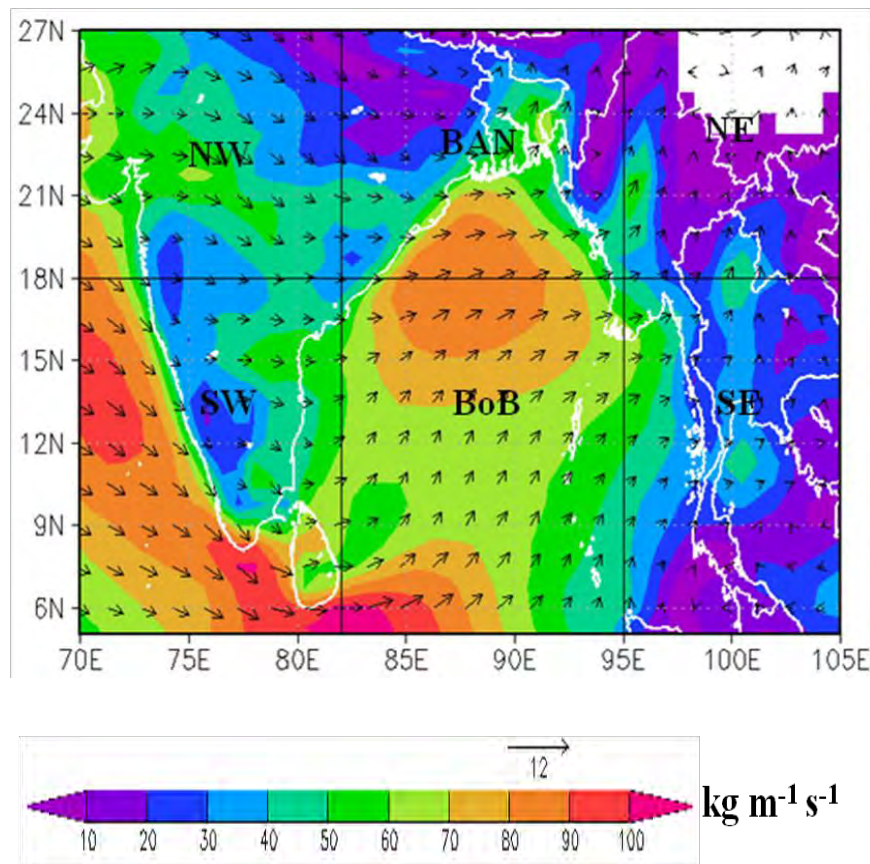


Fig. 4.1: Spatial distribution of average VIMF (shading; $\text{kg m}^{-1} \text{s}^{-1}$) and average wind velocity (m s^{-1}) from 1000 hPa to 850 hPa for the study area during 1979-2015.

data is analyzed for the study area during 1979-2015 as shown in Fig. 4.1. VIMF is calculated by the product of specific humidity with horizontal wind integrated from the surface to 850 hPa pressure level that is described in section 3.3.1. Total VIMF over the region is calculated to be $113.71 \text{ kg m}^{-1} \text{ s}^{-1}$. Highest amount of moisture is found over the Bay of Bengal (BoB) and the eastern part of Arabian Sea (AS), mainly the Ocean place which contributes a significant amount of moisture to the considerable area. About 47% of the total moisture flux is found over this watery area. Maximum value of VIMF is found above $100 \text{ kg m}^{-1} \text{ s}^{-1}$ over the BoB and above $90 \text{ kg m}^{-1} \text{ s}^{-1}$ for the South-West part of the study area. More than $70 \text{ kg m}^{-1} \text{ s}^{-1}$ VIMF is observed over the South-East domain. The value of VIMF over Bangladesh and the North-West part is above $70 \text{ kg m}^{-1} \text{ s}^{-1}$ and $75 \text{ kg m}^{-1} \text{ s}^{-1}$ respectively. Lowest amount of moisture flux is found over the North-East part and it's only $20 \text{ kg m}^{-1} \text{ s}^{-1}$.

4.1.2 Annual variation of VIMF

Yearly variations of average low level VIMF from 1000 hPa to 850 hPa for SA during 1979-2015 are examined in this section. The 37-year averaged VIMF for the total study area has little fluctuation from year to year (1979 to 2015) as shown in Fig. 4.2. Here, green line indicates the value of VIMF and dark red line indicates 5-year running mean value.

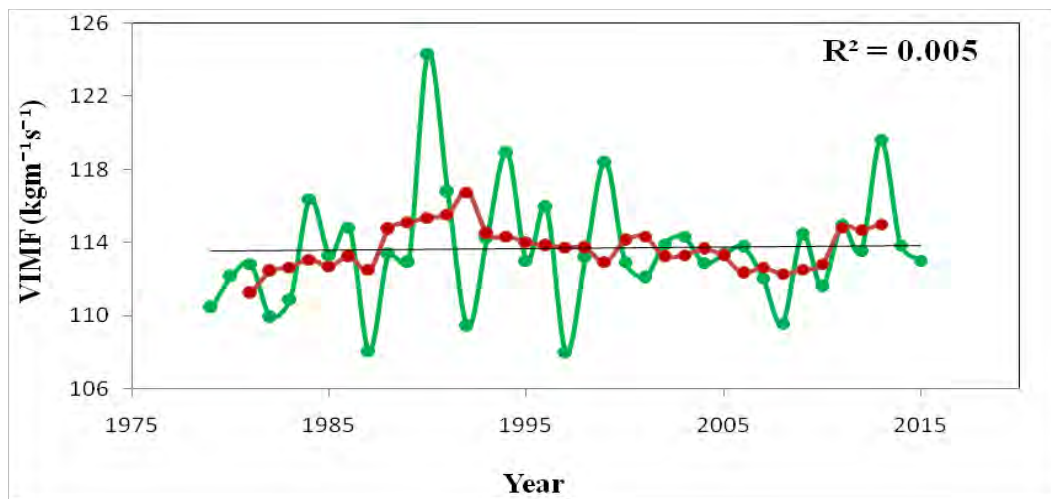


Fig. 4.2: Yearly variation of average VIMF (green line) for the study area. Red line indicates the 5-year running mean from 1979 to 2015.

Maximum value of moisture flux is observed to be $124.33 \text{ kg m}^{-1} \text{ s}^{-1}$ in 1990 and minimum value is observed to be $107.99 \text{ kg m}^{-1} \text{ s}^{-1}$ in 1997. Though there is little variation from year to year but the annual variation of VIMF remains constant for 37 years over SA. The co-efficient of determinant (R^2 value) shows the value of 0.005.

4.1.3 Spatial distribution of seasonal VIMF

According to Indian Meteorological Department (IMD), four seasons are considered to describe the phenomena of the seasonal modes of moisture transport over the study area. They are

- Pre-monsoon (March, April, May)
- Monsoon (June, July, August, September)
- Post-monsoon (October, November, December)
- Winter (January, February)

Spatial distribution of 37-years averaged low-level vertically integrated moisture flux from 1000 hPa to 850 hPa for the pre-monsoon, monsoon, post-monsoon and winter seasons are shown in Figs. 4.3-4.4. Amount of moisture fluxes in the pre-monsoon and post-monsoon seasons are relatively less than that in the monsoon season. In the monsoon season, huge amount of moisture is carried by the strong southwesterly monsoonal wind. Wind helps to propagate moisture north-northeastward in the pre-monsoon, while in the summer monsoon strong southwesterly winds transport moisture from southwest to northeast. The wind intensity in summer monsoon is much stronger than the winter monsoon. Wind intensity reaches its peak in July-August and fades away in October-November. Wind direction is completely reverse in the post-monsoon and the winter season which carries less moisture from the land to ocean. However strong easterly winds convergence near Borneo and carry moisture to the BoB are consistent with Akter & Tsuboki (2012) [42].

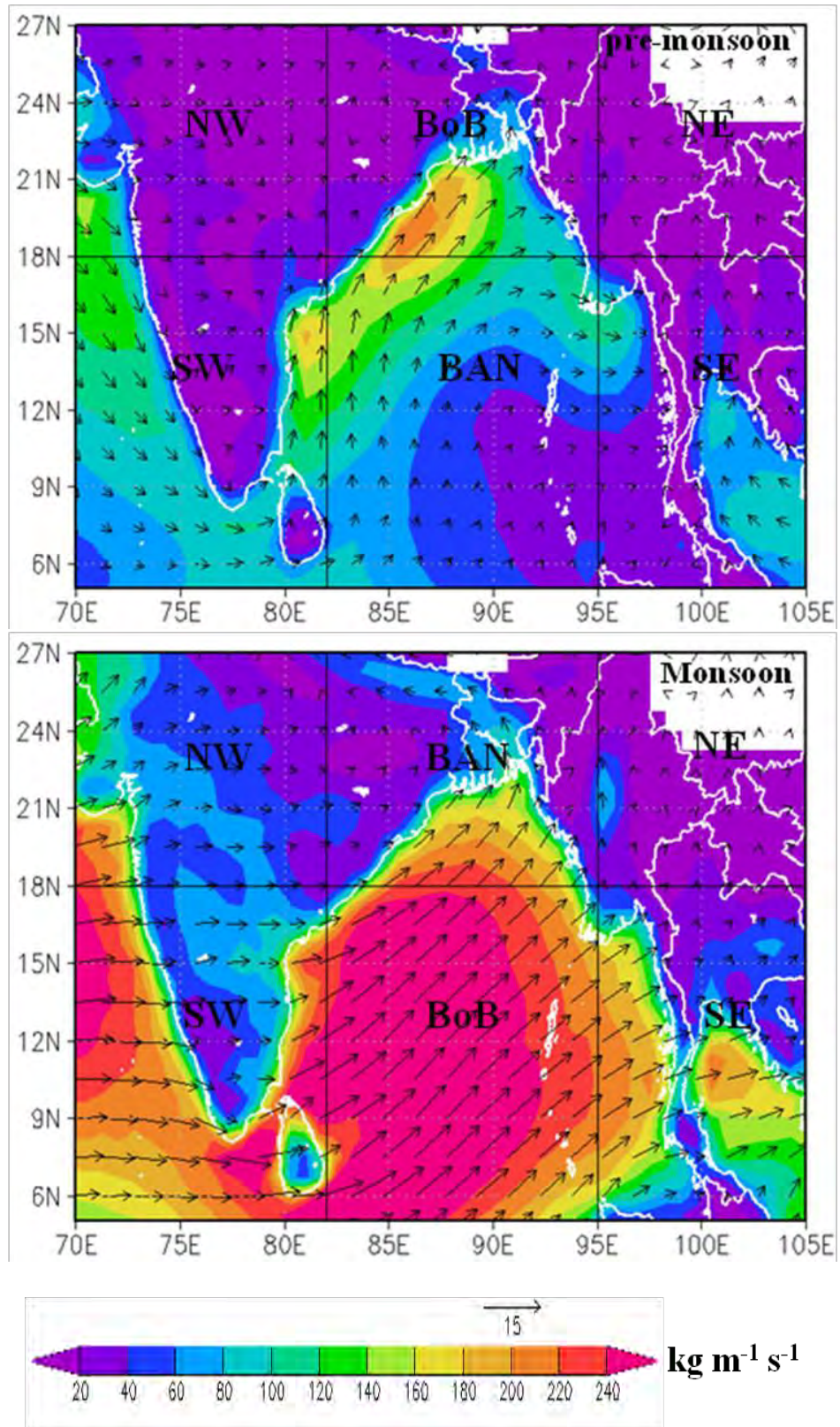


Fig. 4.3: Spatial distribution of average VIMF (shading; $\text{kg m}^{-1} \text{s}^{-1}$) and average wind velocity (m s^{-1}) for 1000-850 hPa in the pre-monsoon and monsoon season during 1979-2015.

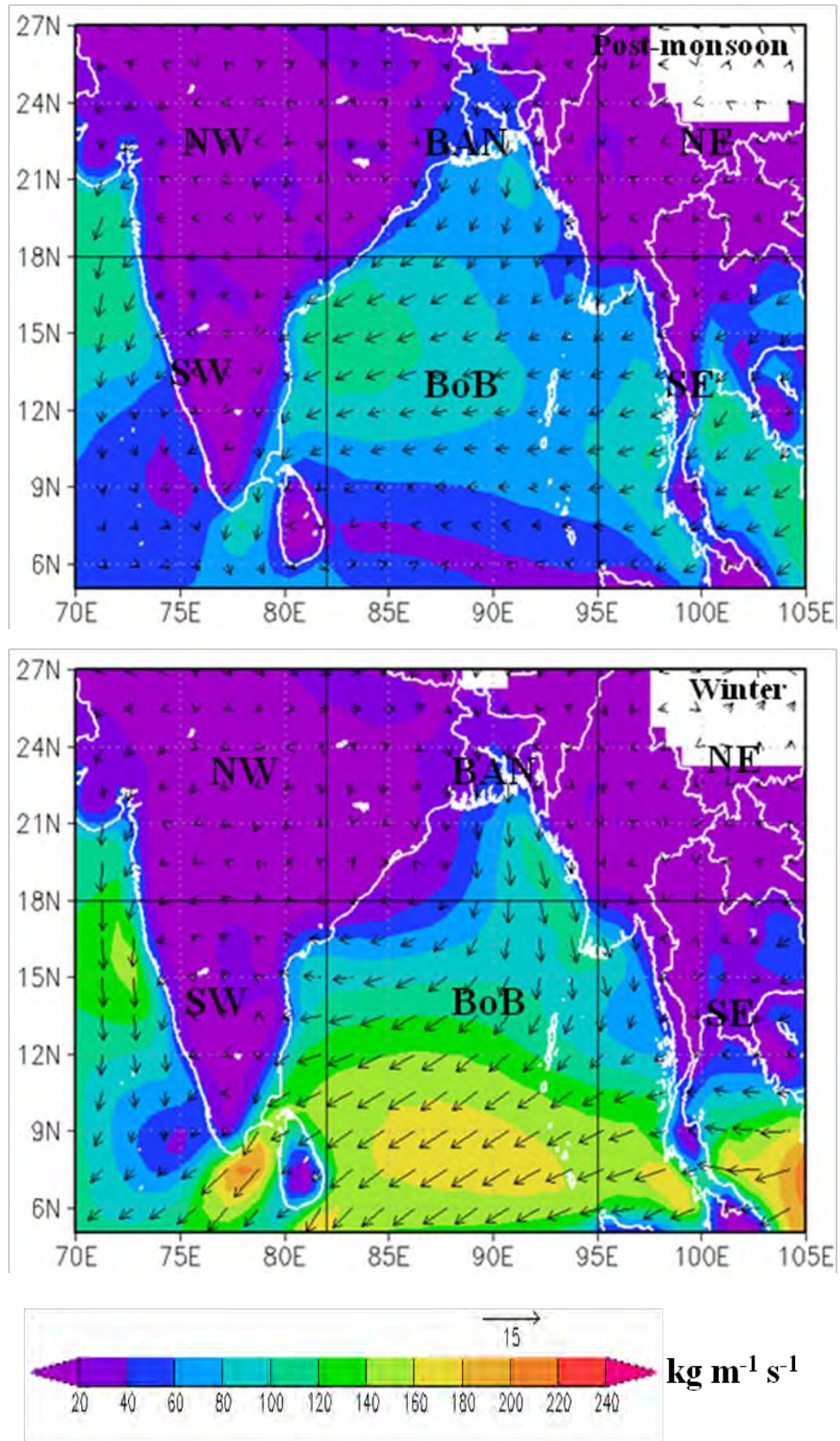


Fig. 4.4: Spatial distribution of average VIMF (shading; $\text{kg m}^{-1} \text{s}^{-1}$) and average wind velocity (m s^{-1}) for 1000-850 hPa in the post-monsoon and winter season during 1979-2015.

4.1.4 Seasonal variation of VIMF

Seasonal average of low-level vertically integrated moisture flux between 1000 hPa to 850 hPa for SA region during 1979-2015 are calculated and shown in Fig. 4.5. The Figure clearly shows that average VIMF is highest in the monsoon season. Approximately 41% of the total moisture flux is found to be advected in the monsoon season. For the monsoon season, maximum value of VIMF is observed to be $187.08 \text{ kg m}^{-1} \text{ s}^{-1}$ in 1994 and minimum value is observed to be $154.65 \text{ kg m}^{-1} \text{ s}^{-1}$ in 2010. For the pre-monsoon season maximum value of VIMF of $102.89 \text{ kg m}^{-1} \text{ s}^{-1}$ is observed in 1996 and minimum value of $73.68 \text{ kg m}^{-1} \text{ s}^{-1}$ is found in 1987. About 21% of the total moisture flux is observed in the pre-monsoon season that is approximately same as the post-monsoon season. In the post-monsoon season, maximum value of VIMF is observed to be $103.07 \text{ kg m}^{-1} \text{ s}^{-1}$ in 1990 and minimum value is found to be $77.73 \text{ kg m}^{-1} \text{ s}^{-1}$ in 1982. Only 17% of the total VIMF is observed in the winter season. For the winter season, maximum value of $80.77 \text{ kg m}^{-1} \text{ s}^{-1}$ is observed in 1994 and minimum value of $62.03 \text{ kg m}^{-1} \text{ s}^{-1}$ is found in 2001.

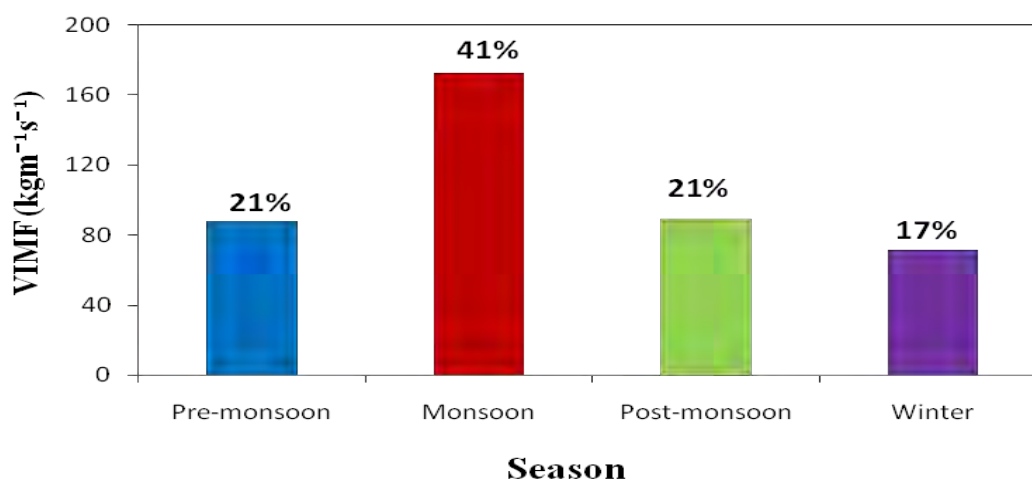


Fig. 4.5: Seasonal variation of average VIMF during 1979-2015.

The line diagram in Fig. 4.6 shows the annual variation of 5-years running mean value of low level seasonal average vertically integrated moisture flux for the total domain. Annual variation of averaged vertically integrated moisture flux is remaining almost constant for 37-years in the pre-monsoon, monsoon, post-monsoon

and winter season. But the fluxes are highest in the monsoon season and lowest in winter season.

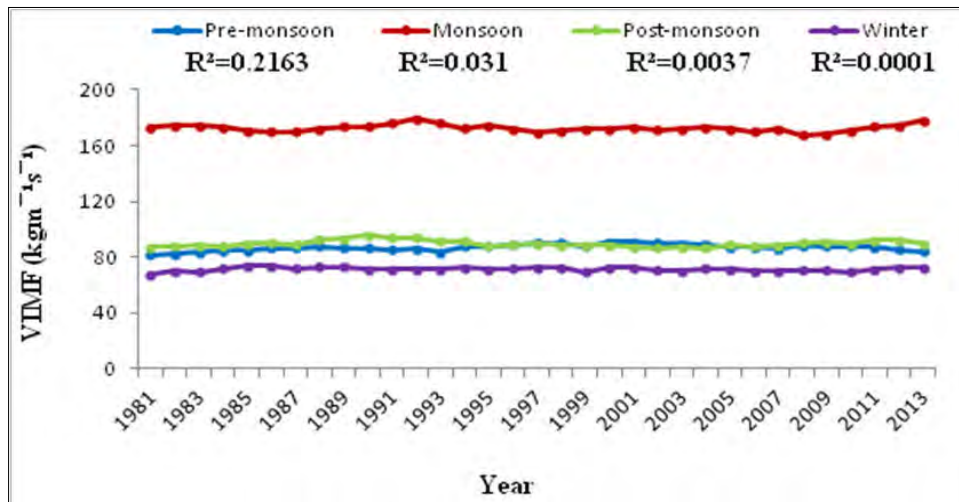


Fig. 4.6: Annual variation of 5-years running mean value of seasonal average VIMF during 1979-2015.

Table-1 shows that the average increasing rate of vertically integrated moisture flux per year is approximately 0.5% in the pre-monsoon and winter season but for the monsoon and post-monsoon seasons, these amounts are 0.31% and 0.33%, respectively, which are almost constant. The pre-monsoon and post-monsoon seasons have the constant value of average VIMF of approximately $88 \text{ kg m}^{-1} \text{ s}^{-1}$, whereas the winter season has almost $71.63 \text{ kg m}^{-1} \text{ s}^{-1}$ over SA. In the monsoon season, VIMF maintains the nearly constant value of $172.54 \text{ kg m}^{-1} \text{ s}^{-1}$ which is more than double values than that of the other seasons.

Table-1: Seasonal average increase of VIMF for total domain (1979-2015).

Season	Average increases in moisture flux (%) per year
Pre-monsoon	0.58
Monsoon	0.31
Post-monsoon	0.33
Winter	0.55

4.1.5 Spatial distribution of monthly VIMF

Spatial distributions of monthly average low-level vertically integrated moisture flux for the total study area are shown in Fig. 4.7 and 4.8. In January, moisture flux is highest over the Bay of Bengal (BoB), South-West and the South-East parts of the selected area and lowest amount of moisture is observed over the land. Wind carries moisture from land to sea in this month and wind direction is northeasterly. Average value of vertically integrated moisture flux in January is about $76.49 \text{ kg m}^{-1} \text{ s}^{-1}$. February and March show the lowest amount of vertically integrated moisture flux and the values are about $66.15 \text{ kg m}^{-1} \text{ s}^{-1}$ and $63.75 \text{ kg m}^{-1} \text{ s}^{-1}$, respectively. In February, wind direction is quite similar as January but in March, direction of wind is cyclonic and rotates clockwise to make a centre at the middle of the BoB that shown in Fig. 4.7. Significant amount of moisture ($74.72 \text{ kg m}^{-1} \text{ s}^{-1}$) is found over the BoB near Bangladesh in the month of April. The low-level southerly wind transports moisture from the BoB to Bangladesh and its surrounding. At the end of April and the beginning of May, amount of moisture is increased gradually over the BoB and wind carries it towards land surface. Huge amount of moisture cover the sea surface in the monsoon months and the value is $121.64 \text{ kg m}^{-1} \text{ s}^{-1}$, $185.06 \text{ kg m}^{-1} \text{ s}^{-1}$ and $191.74 \text{ kg m}^{-1} \text{ s}^{-1}$ in June, July and August, respectively. In those months, the low-level southwesterly or southerly wind carries highest amount of moisture from the BoB and propagates toward southeast ward. At the end of the monsoon, amount of moisture over the Arabian Sea and the Bay of Bengal is decreased. About $134.45 \text{ kg m}^{-1} \text{ s}^{-1}$ of vertically integrated moisture flux is found in the month of September. In October, the value of VIMF is $91.44 \text{ kg m}^{-1} \text{ s}^{-1}$. Moisture flux is northeasterly in the months of November and December. The values of vertically integrated moisture flux in November and December are $89.63 \text{ kg m}^{-1} \text{ s}^{-1}$ and $88.07 \text{ kg m}^{-1} \text{ s}^{-1}$, respectively.

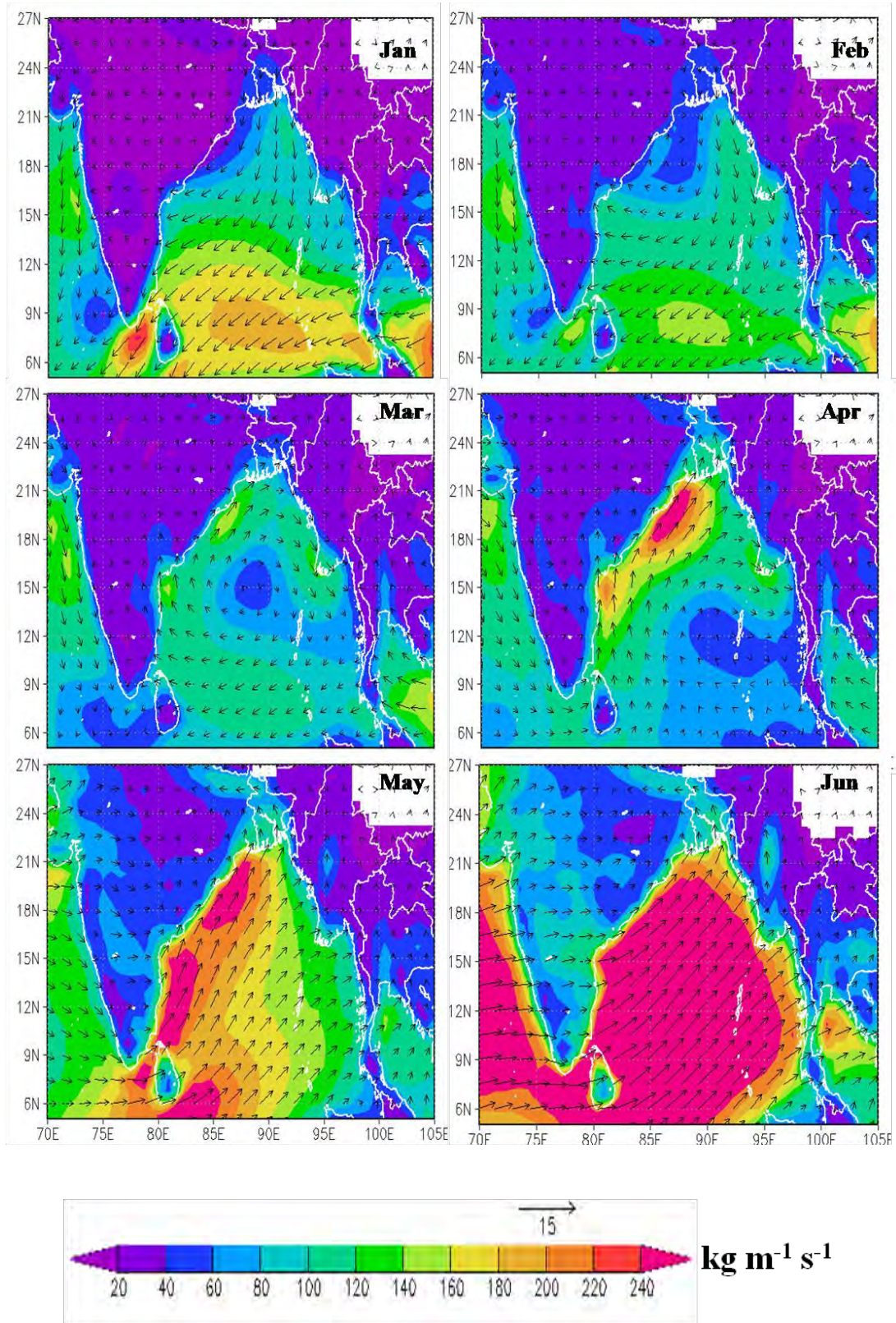


Fig. 4.7: Spatial distribution of monthly (Jan-Jun) average VIMF (shading; $\text{kg m}^{-1} \text{s}^{-1}$) and average wind velocity (m s^{-1}) for 1000-850 hPa during 1979-2015.

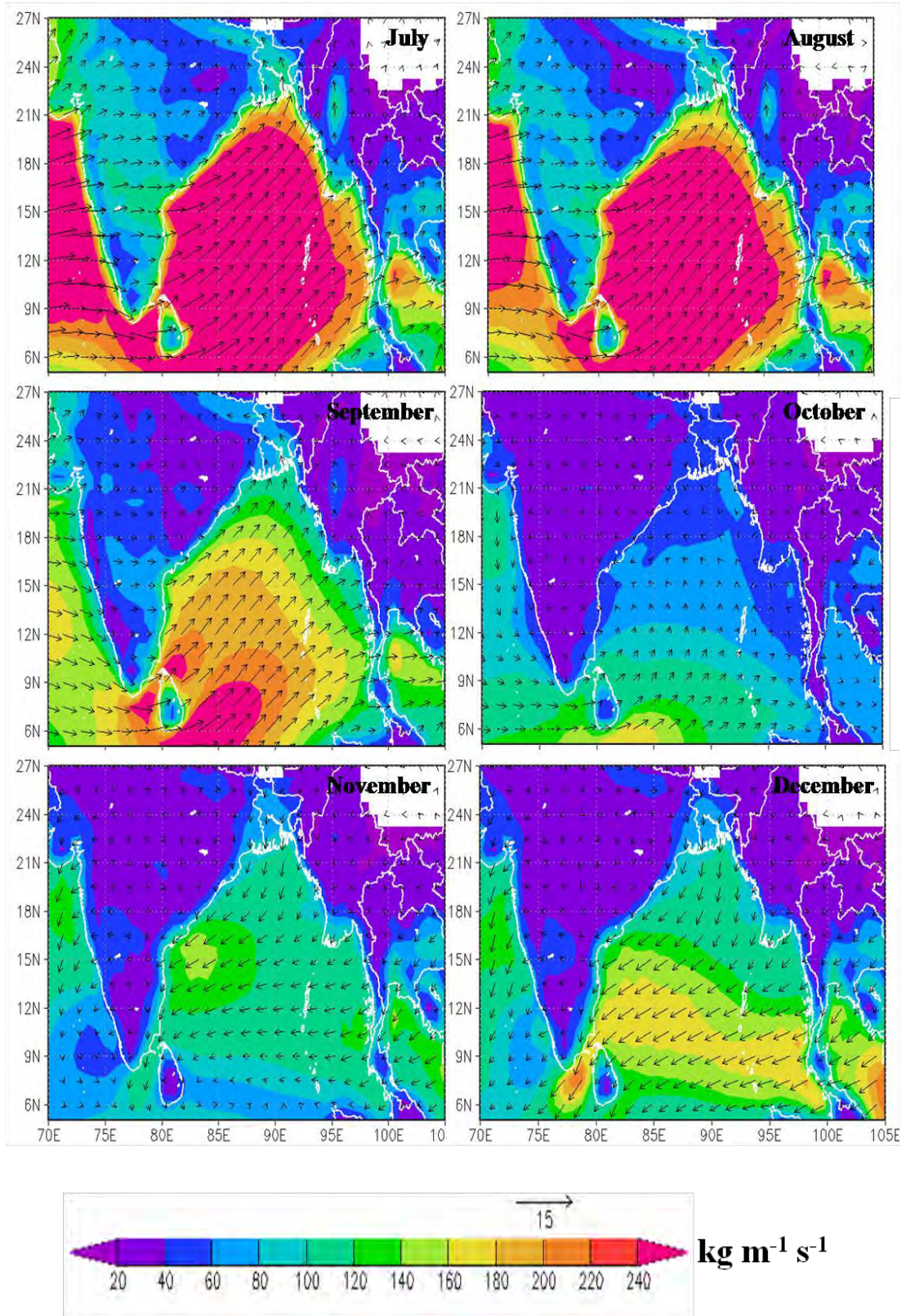


Fig. 4.8: Spatial distribution of monthly (Jul-Dec) average VIMF (shading; $\text{kg m}^{-1} \text{s}^{-1}$) and average wind velocity (m s^{-1}) for 1000-850 hPa during 1979-2015.

4.1.6 Monthly variation of VIMF

Monthly variation of low-level average vertically integrated moisture flux between 1000 hPa to 850 hPa for South Asian region is calculated and shown in Fig. 4.9. Maximum value of VIMF is observed $191.74 \text{ kg m}^{-1} \text{ s}^{-1}$ in July and minimum value is found $63.74 \text{ kg m}^{-1} \text{ s}^{-1}$ in March which is 33% less than the maximum value. Amount of moisture flux in January is higher than February and March but lower than April to December. At the beginning of April, moisture flux is increasing, peak in July and then decreasing gradually from October to December and these three months show quite similar values of moisture flux. Mainly a large amount of moisture flux is found in June, July, August and September over the study area.

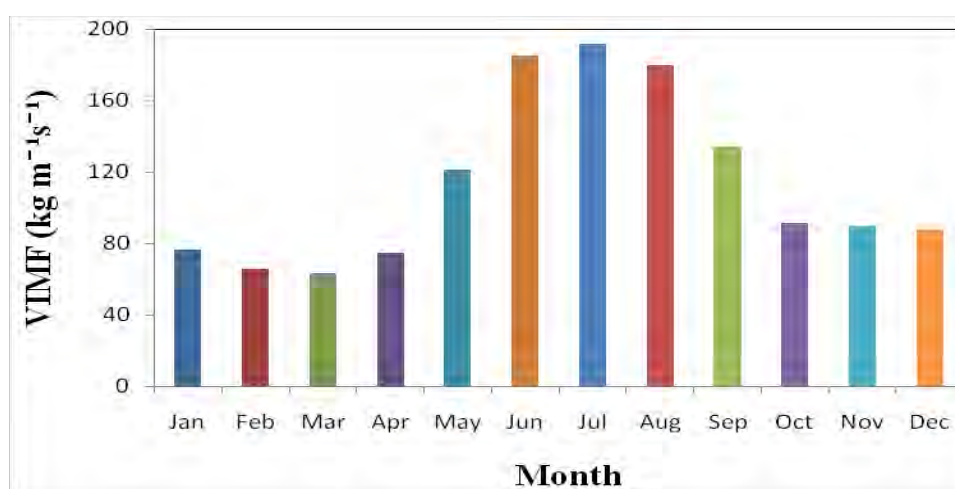


Fig. 4.9: Monthly variation of average VIMF for total domain during 1979-2015.

4.2 Moisture flux for individual domain

The 37-year averaged vertically integrated moisture flux for six domains are discussed in this section. The yearly average vertically integrated moisture flux for six domains are calculated and plotted in Fig.4.10. The figure clearly shows that VIMF is highest over the BoB. About 27% of the total moisture flux is found to be advected over this domain. The South-West and the South-East domains of the study area are found to be advected 21% and 19% of the total moisture flux. The North-East domain shows lowest amount of vertically integrated moisture flux. Only 6% of the total VIMF is observed over this region. About 13% and 14% vertically integrated moisture flux are found over the North-West domain and Bangladesh and

surrounding. VIMF over the Bangladesh and surrounding region is 5.5% greater than the North-West region. About 67% of the total moisture flux is advected over the Southern part whereas only 33% of the total moisture flux is advected over the Northern part [Fig. 4.10]. In the southern region 39% moisture is transported to the BoB, whereas the Northern region moisture transports more i.e. 42% to Bangladesh and surrounding.

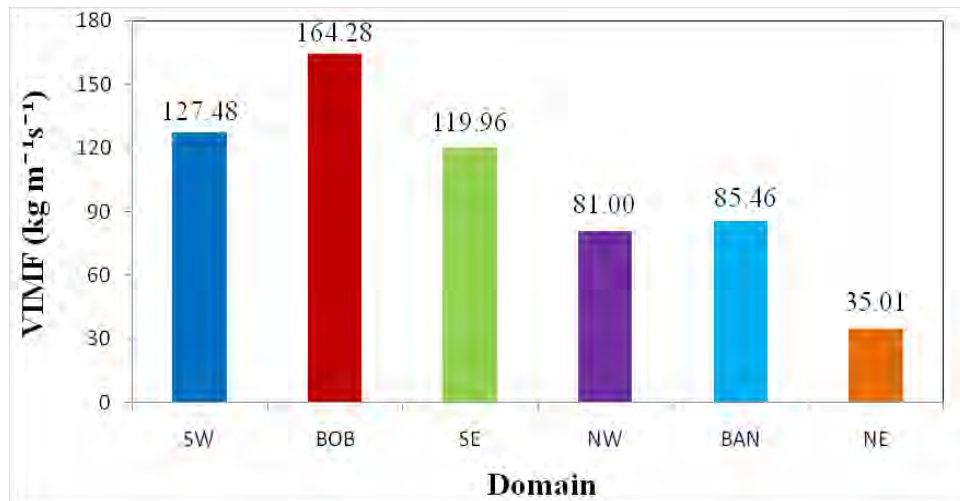


Fig. 4.10: Yearly variation of average VIMF for six domains during 1979-2015.

4.3 Annual variation of moisture flux for six domains

Yearly variation of average low-level vertically integrated moisture flux for 1000 hPa to 850 hPa during 1979-2015 for six domains are calculated and discussed in the following sub-sections.

4.3.1 South-West domain (SW)

Yearly variation of average low-level vertically integrated moisture flux (VIMF) between 1000 hPa to 850 hPa for the South-West region of the study area is examined. Fig. 4.11 shows the 37-year VIMF averaged for the South-West domain. Maximum value of moisture flux is observed to be 140.49 kg m⁻¹ s⁻¹ in 1990 and minimum value is 115.23 kg m⁻¹ s⁻¹ in 1997. Here, blue line indicates the value of VIMF and dark red line indicates the 5-year running mean value. The co-efficient of determination (R² value) shows the value of 0.0207 which means that the long-term annual variations of moisture flux for the South-West domain is almost constant.

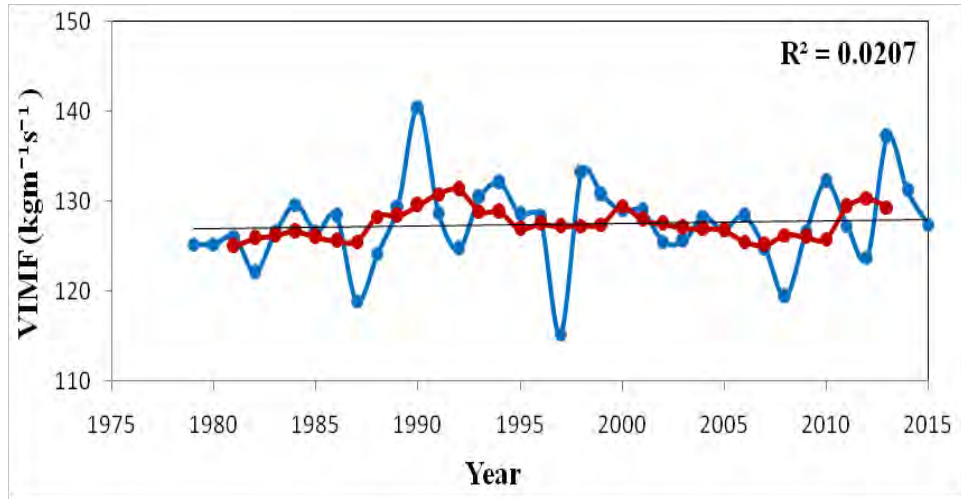


Fig. 4.11: Yearly variation of average VIMF and 5-year running mean (red line) for the South-West domain during 1979-2015.

Annual variation of seasonal average vertically integrated moisture flux (VIMF) for the South-West domain is shown in Fig. 4.12. In the pre-monsoon and the monsoon season, VIMF is not significantly increased over the South-West domain with R^2 of 0.110 and 0.217. The value of VIMF in the post-monsoon and the winter season is remaining constant for 37 years over this domain. Maximum value of VIMF is observed to be $119.09 \text{ kg m}^{-1} \text{ s}^{-1}$ in the monsoon season and minimum value of VIMF is $77.57 \text{ kg m}^{-1} \text{ s}^{-1}$ in the winter season. The post-monsoon season has higher flux ($99.11 \text{ kg m}^{-1} \text{ s}^{-1}$) than the moisture flux ($91.63 \text{ kg m}^{-1} \text{ s}^{-1}$) of the pre-monsoon season.

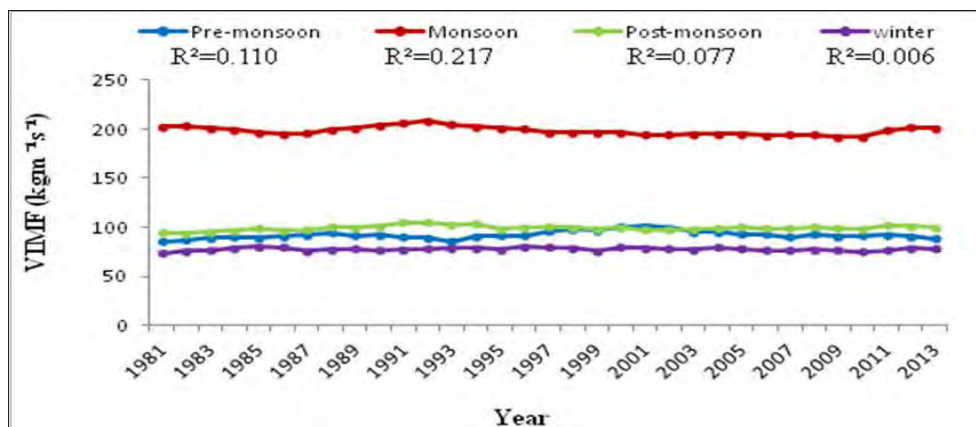


Fig. 4.12: 5-year running mean value of seasonal average VIMF for the South-West domain during 1979-2015.

4.3.2 Bay of Bengal (BoB)

Fig. 4.13 shows the yearly variation of 37-year averaged low-level VIMF for 1000 hPa to 850 hPa for the Bay of Bengal. Maximum value of moisture flux is observed to be $179.99 \text{ kg m}^{-1} \text{ s}^{-1}$ in 1990 and minimum value is observed to be $151.41 \text{ kg m}^{-1} \text{ s}^{-1}$ in 1997. Here, dark red line indicates the 5-year running mean value. The co-efficient of determination (R^2 value) shows the value of 0.0854. That means the annual variation of VIMF is found almost constant over the Bay of Bengal for this period.

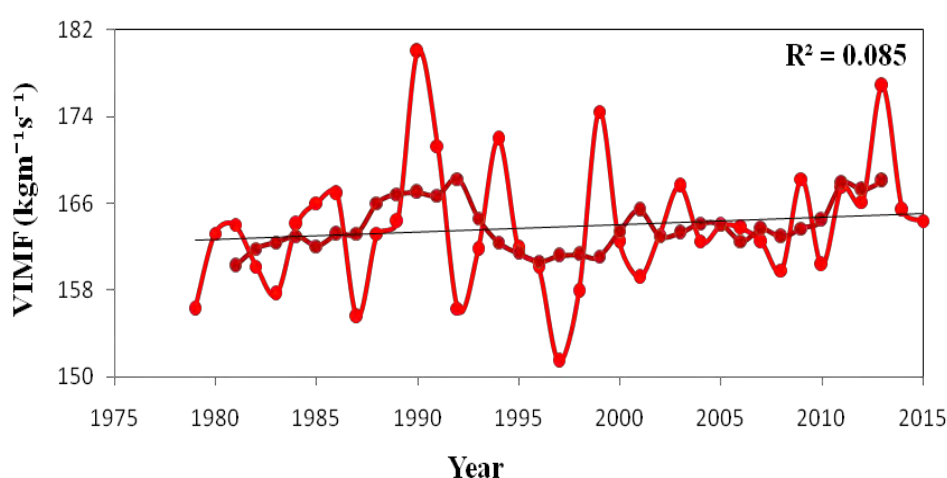


Fig. 4.13: Yearly variation of average VIMF and 5-year running mean (red line) for the Bay of Bengal during 1979-2015.

Annual variation of seasonal average VIMF for the BoB domain is shown in Fig. 4.14. VIMF is increased over the South-West domain in the pre-monsoon with R^2 of 0.433 which is significant statistically. The value of VIMF in the monsoon, post-monsoon and the winter season is remaining constant for 37 years over this domain. Maximum value of VIMF is observed to be $248.66 \text{ kg m}^{-1} \text{ s}^{-1}$ in the monsoon season and minimum value of VIMF is $108.93 \text{ kg m}^{-1} \text{ s}^{-1}$ in the winter season. The post-monsoon season has higher moisture flux ($135.45 \text{ kg m}^{-1} \text{ s}^{-1}$) than the pre-monsoon season ($115.66 \text{ kg m}^{-1} \text{ s}^{-1}$).

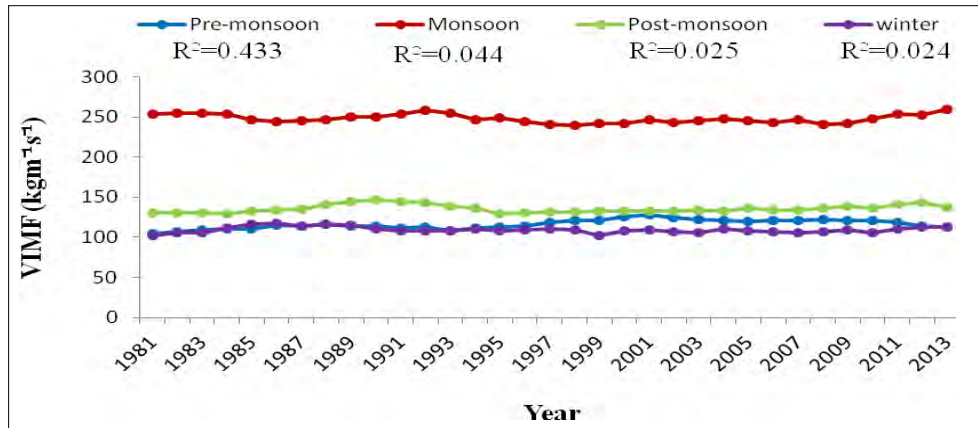


Fig. 4.14: 5-year running mean value of seasonal average VIMF for the Bay of Bengal domain during 1979-2015.

4.3.3 South-East domain (SE)

Yearly variations of average low-level VIMF between 1000 hPa to 850 hPa for the South-East region is analyzed here. Fig. 4.15 shows the 37-year averaged VIMF for the South-East domain. Maximum value of moisture flux is observed $133.54 \text{ kg m}^{-1} \text{ s}^{-1}$ in 1991 and minimum value is observed $111.47 \text{ kg m}^{-1} \text{ s}^{-1}$ in 1998. The co-efficient of determination (R^2 value) shows the value of 0.0216. It indicates that the annual variation of averaged VIMF is statistically insignificant.

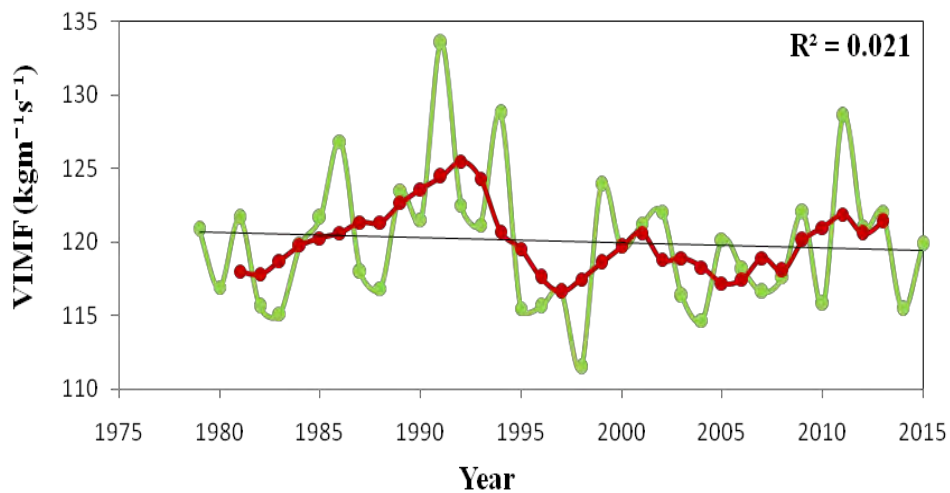


Fig. 4.15: Yearly variation of average VIMF and 5-year running mean (red line) for the South-East domain during 1979-2015.

Annual variation of seasonal average VIMF for the South-East domain is shown in Fig. 4.16. VIMF is not significantly increased over the South-East domain in the monsoon and the winter season with R^2 of 0.249 and 0.276. Increasing rate of VIMF for both seasons is quite similar. The value of VIMF in the pre-monsoon and post-monsoon season is remaining constant for 37 years over this domain. Maximum value of VIMF is observed $150.46 \text{ kg m}^{-1} \text{ s}^{-1}$ in the monsoon season and minimum value of VIMF is $95.87 \text{ kg m}^{-1} \text{ s}^{-1}$ in the pre-monsoon season. The post-monsoon season has higher flux ($117.38 \text{ kg m}^{-1} \text{ s}^{-1}$) than the pre-monsoon season. The value of VIMF is $96.74 \text{ kg m}^{-1} \text{ s}^{-1}$ in winter season over the South-East domain.

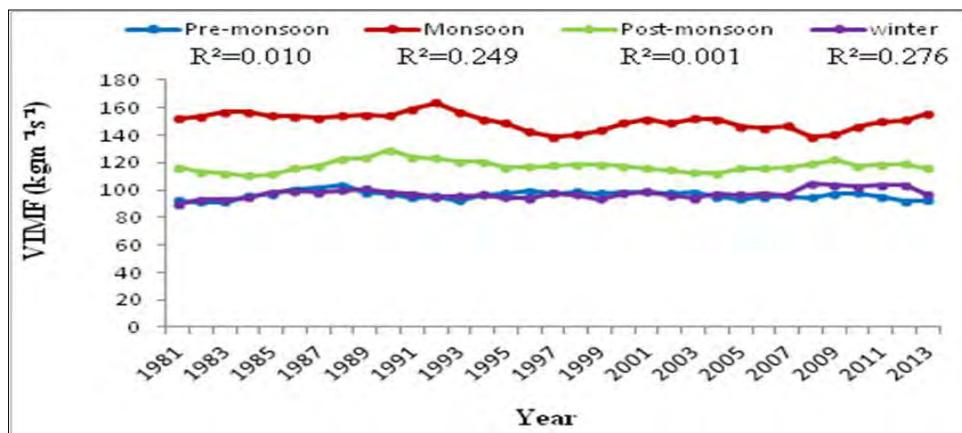


Fig. 4.16: 5-year running mean value of seasonal average VIMF for the South-East domain during 1979-2015.

4.3.4 North-West domain (NW)

Fig. 4.17 shows the 37-year averaged VIMF for the North-West domain. Maximum value of moisture flux is observed $91.77 \text{ kg m}^{-1} \text{ s}^{-1}$ in 1990 and minimum value is observed $73.95 \text{ kg m}^{-1} \text{ s}^{-1}$ in 2010. Here, purple line indicates the value of VIMF and dark red line indicates 5-year running mean value. The co-efficient of determination (R^2 value) shows the value of 0.0173 which means that the long-term annual variations of moisture flux for the North-West domain is constant and the rate is not significant.

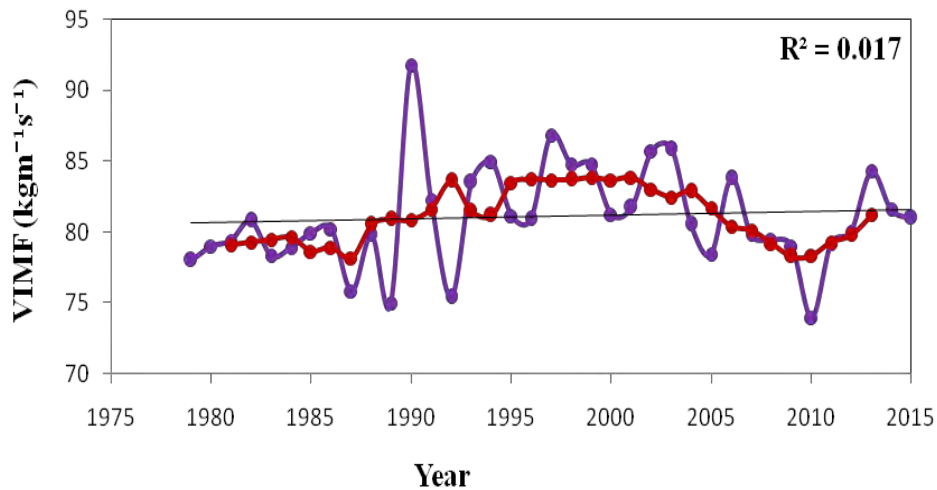


Fig. 4.17: Yearly variation of average VIMF and 5-year running mean (red line) for the North-West domain during 1979-2015.

Annual variation of seasonal average VIMF for the North-West domain is shown in Fig. 4.18. VIMF is not significantly increased over the North-West domain in the winter season with R^2 of 0.207. The value of VIMF in the pre-monsoon, monsoon and the post-monsoon season is remaining constant for 37 years over this domain. Maximum value of VIMF is observed to be $144.20 \text{ kg m}^{-1} \text{ s}^{-1}$ in the monsoon season and minimum value of VIMF is $34.89 \text{ kg m}^{-1} \text{ s}^{-1}$ in the winter season. The pre-monsoon season has higher flux ($61.62 \text{ kg m}^{-1} \text{ s}^{-1}$) than the moisture flux ($43.39 \text{ kg m}^{-1} \text{ s}^{-1}$) of the post-monsoon season.

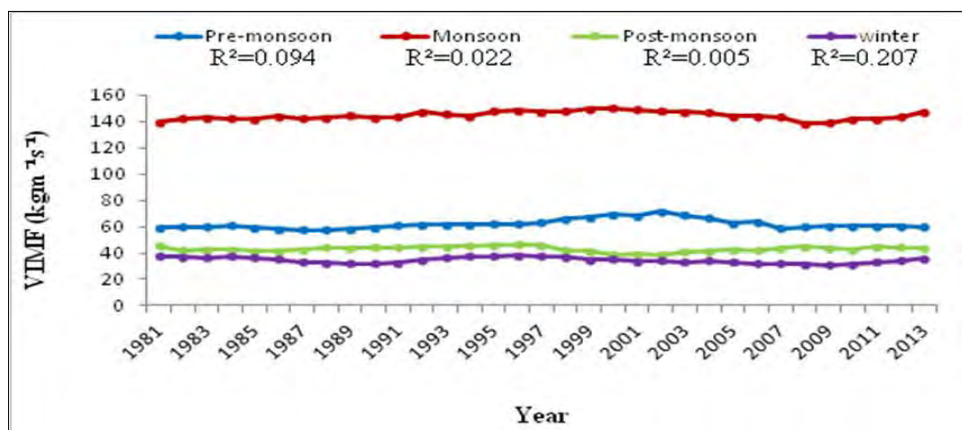


Fig. 4.18: 5-year running mean value of seasonal average VIMF for the North-West domain during 1979-2015.

4.3.5 Bangladesh and surrounding (BAN)

Yearly variation of low-level average VIMF for 1000 hPa to 850 hPa for Bangladesh and surrounding is shown in Fig. 4.19. Maximum value of moisture flux is observed to be $91.26 \text{ kg m}^{-1} \text{ s}^{-1}$ in 1998 and minimum value is observed to be $79.10 \text{ kg m}^{-1} \text{ s}^{-1}$ in 1992. Here, dark red line indicates 5-year running mean value. The coefficient of determination (R^2 value) shows the value of 0.0919.

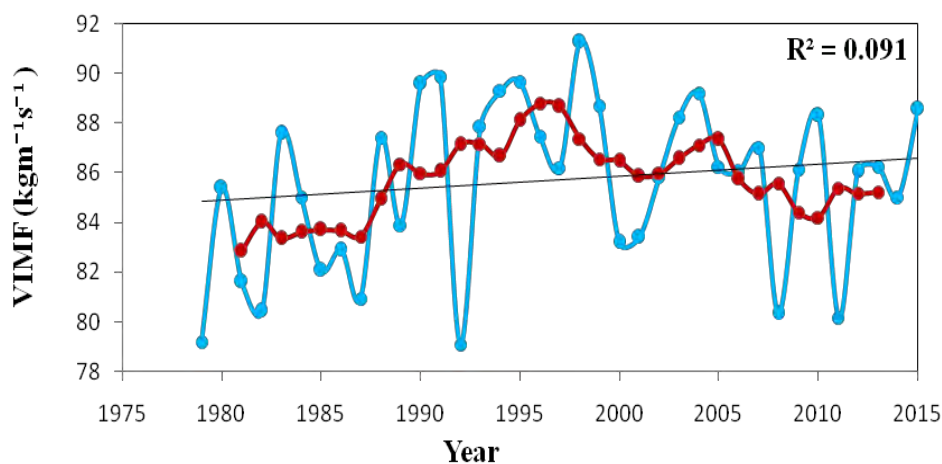


Fig. 4.19: Yearly variation of average VIMF and 5-year running mean (red line) for the Bangladesh and surrounding domain during 1979-2015.

That's mean the annual variation of VIMF is not significant over the Bangladesh and surrounding region for the study period.

Annual variation of seasonal average VIMF for the Bangladesh and surrounding domain is shown in Fig. 4.20. The value of VIMF in the monsoon, pre-monsoon, post-monsoon and the winter season is remaining constant for 37 years over the Bangladesh and surrounding domain. Maximum value of VIMF is observed to be $138.19 \text{ kg m}^{-1} \text{ s}^{-1}$ in the monsoon season and minimum value of VIMF is $39.08 \text{ kg m}^{-1} \text{ s}^{-1}$ in the winter season. The pre-monsoon season has higher flux ($78.97 \text{ kg m}^{-1} \text{ s}^{-1}$) than the moisture flux ($51.85 \text{ kg m}^{-1} \text{ s}^{-1}$) of the post-monsoon season.

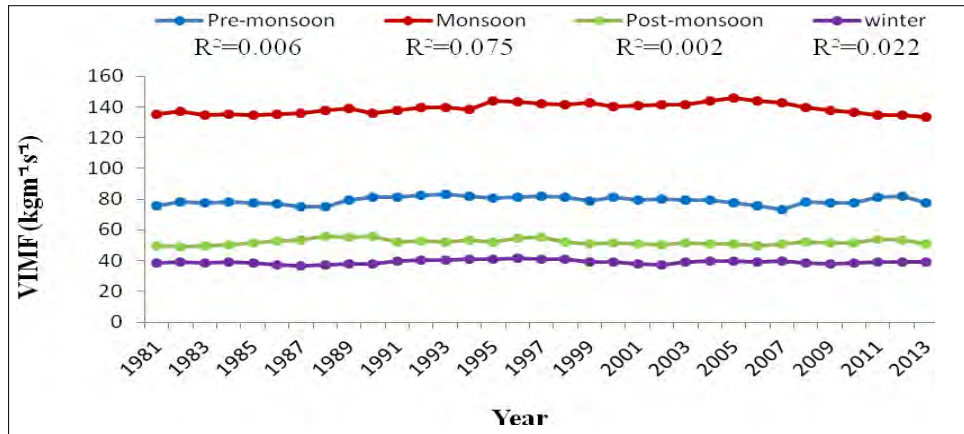


Fig. 4.20: 5-year running mean value of seasonal average VIMF for the Bangladesh and surrounding domain during 1979-2015.

4.3.6 North-East domain (NE)

Yearly variation of low-level average VIMF for 1000 hPa to 850 hPa for the North-East region is analyzed here. Fig. 4.21 shows the 37-year averaged VIMF for the North-East domain. Maximum value of moisture flux is observed $37.51 \text{ kg m}^{-1} \text{ s}^{-1}$ in 2005 and minimum value is observed $32.70 \text{ kg m}^{-1} \text{ s}^{-1}$ in 1989. Here, dark red line indicates 5-years running mean value. The co-efficient of determination (R^2 value) shows the value of 0.5444 which is significant. That's mean the annual variation of VIMF is found increase over the North-East domain for this period.

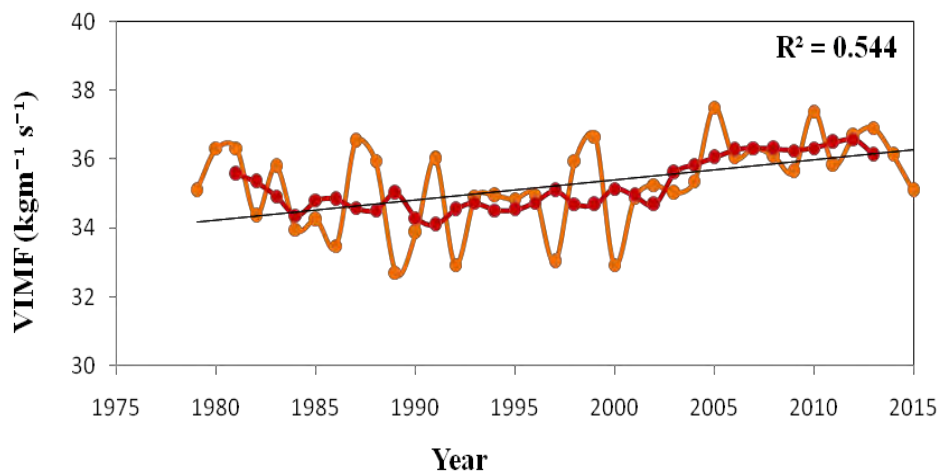


Fig. 4.21: Yearly variation of average VIMF and 5-year running mean (red line) for the North-East domain during 1979 to 2015.

Annual variation of seasonal average VIMF for the North-East domain is shown in Fig. 4.22. VIMF is increased over the North-East domain in the pre-monsoon with R^2 of 0.653 which is significant. Annual increasing rate is found 0.62% in the pre-monsoon season. The little increasing tendency of VIMF in the monsoon season is also observed. VIMF is remaining constant for 37 years in the post-monsoon and the winter season. Maximum value of VIMF is observed to be $51.18 \text{ kg m}^{-1} \text{ s}^{-1}$ in the monsoon season and minimum value of VIMF is $19.67 \text{ kg m}^{-1} \text{ s}^{-1}$ in the winter season. The pre-monsoon season has higher flux ($32.46 \text{ kg m}^{-1} \text{ s}^{-1}$) than the moisture flux ($27.50 \text{ kg m}^{-1} \text{ s}^{-1}$) of the post-monsoon season which is similar to the North-West and the Bangladesh and surrounding domains.

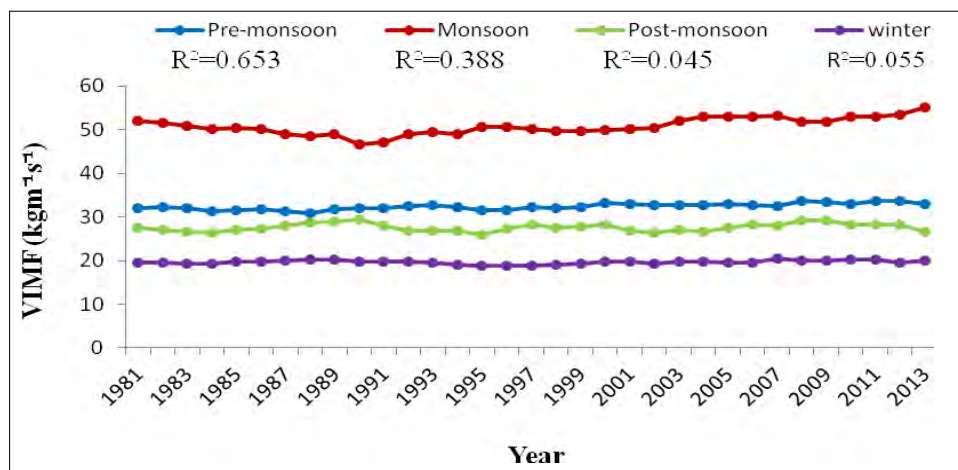


Fig. 4.22: 5-year running mean value of seasonal average VIMF for the North-East domain during 1979-2015.

Within all domains, the amount of VIMF over the North-East domain is found to increase annually. The pre-monsoon season of the North-East region contributes to the total annual increase, though the North-East region has lowest amount of VIMF over the study period.

4.4 Seasonal variation of VIMF for six domains

Seasonal variation of average VIMF for six domains in the pre-monsoon, monsoon, post-monsoon and the winter seasons are calculated and shown in Figs. 4.23 and 4.24.

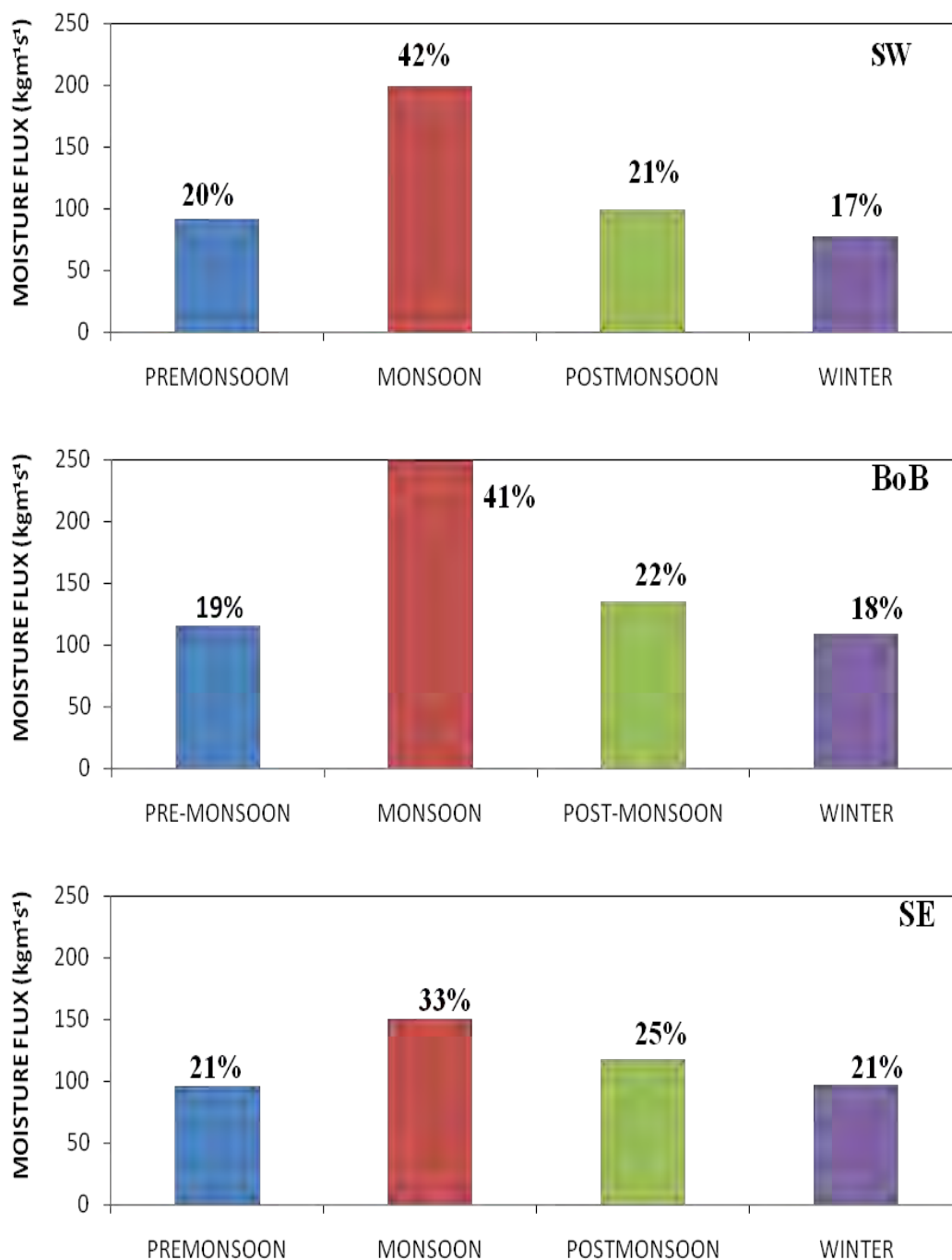


Fig. 4.23: Seasonal variation of average VIMF for the South-West, Bay of Bengal and the South-East domains during 1979-2015.

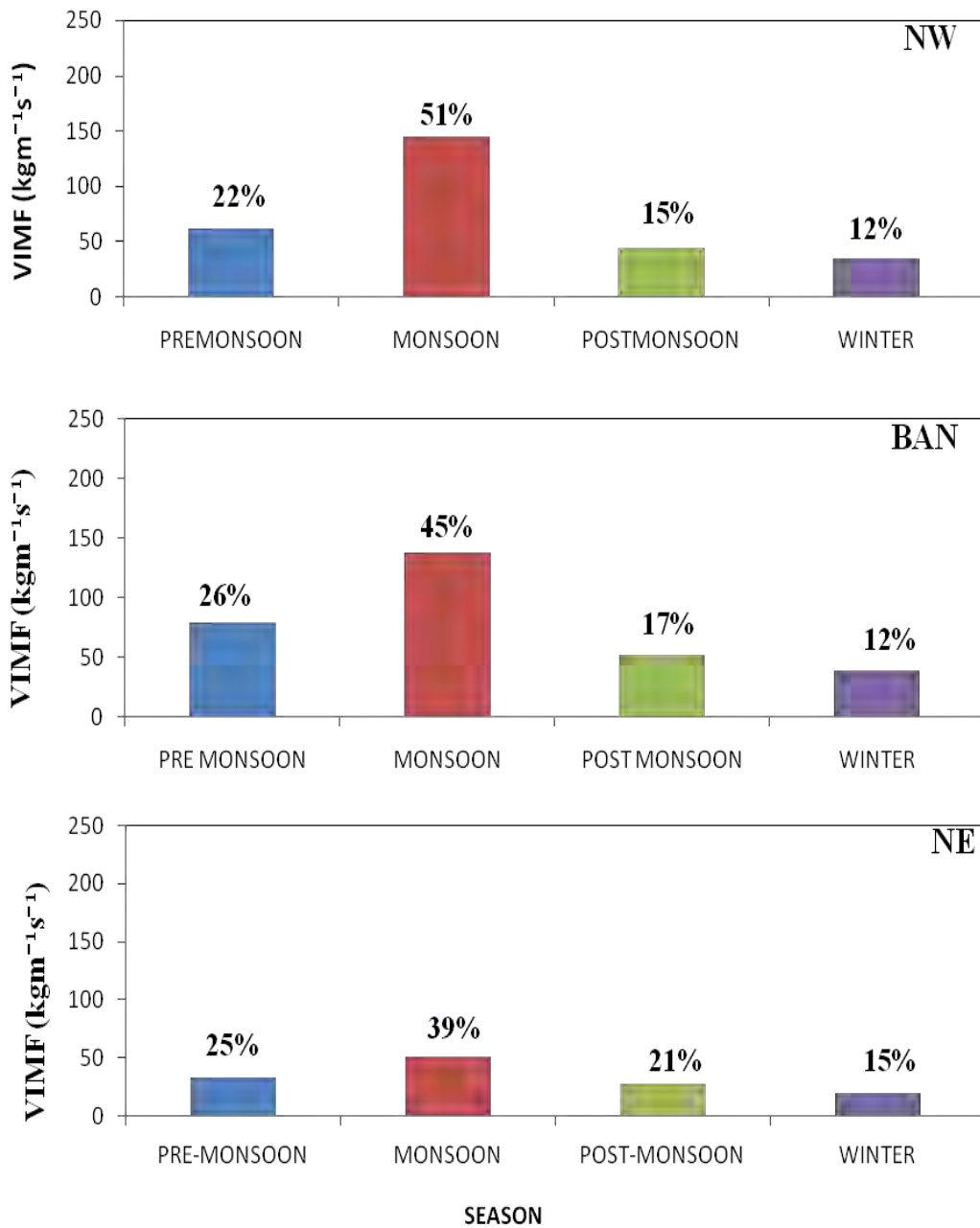


Fig. 4.24: Seasonal variation of average VIMF for the North-West, Bangladesh and surrounding and the North-East domains during 1979-2015.

Fig. 4.23 and 4.24 show that for all domains the highest moisture flux is observed in the monsoon season and lowest value in the winter season. VIMF is observed about 42%, 41%, 33%, 51%, 45% and 39% in the monsoon season for SW, BoB, SE, NW, BAN and NE domains, respectively whereas in the winter season amount of moisture flux are 17%, 18%, 21%, 12%, 12% and 15%. The post-monsoon season has higher moisture flux than the pre-monsoon season for the SW, BoB and SE domains but opposite for the NW, BAN and NE domains. Maximum and

minimum values of VIMF for all domains in the pre-monsoon, monsoon, post-monsoon and the winter seasons are given below.

Table-2: Seasonal variation of VIMF for six domains (1979-2015).

Pre-monsoon				
Domain	Maximum VIMF (kg m ⁻¹ s ⁻¹)		Minimum VIMF (kg m ⁻¹ s ⁻¹)	
	Year	Value	Year	Value
SW	1999	113.41	1987	73.07
<u>BoB</u>	1999	142.98	1987	92.59
SE	1986	112.94	2014	81.01
NW	2004	80.39	1987	51.54
BAN	2010	101.77	2008	64.59
NE	2010	37.05	1997	27.90

Monsoon				
Domain	Maximum VIMF (kg m ⁻¹ s ⁻¹)		Minimum VIMF (kg m ⁻¹ s ⁻¹)	
	Year	Value	Year	Value
SW	2013	217.26	2008	184.17
<u>BoB</u>	1982	274.15	2010	222.01
SE	1994	172.70	2010	119.43
NW	1994	156.91	2010	119.84
BAN	1997	118.33	2015	118.33
NE	2015	58.12	1989	42.97

Post-monsoon				
Domain	Maximum VIMF (kg m ⁻¹ s ⁻¹)		Minimum VIMF (kg m ⁻¹ s ⁻¹)	
	Year	Value	Year	Value
SW	1998	111.95	1997	82.53
BoB	1990	159.08	1997	112.06
SE	1998	145.18	2012	97.37
NW	1979	52.00	2000	30.56
BAN	1990	65.18	2011	42.39
NE	2010	33.90	1982	22.24

Winter				
Domain	Maximum VIMF (kg m ⁻¹ s ⁻¹)		Minimum VIMF (kg m ⁻¹ s ⁻¹)	
	Year	Value	Year	Value
SW	1984	91.80	1997	67.65
BoB	1984	125.79	2001	90.01
SE	2010	129.35	1997	82.45
NW	1998	40.44	2008	28.32
BAN	2005	48.01	1985	34.62
NE	2009	22.49	1997	17.15

4.5 Monthly variation of VIMF for six domains

Monthly variation of low-level 37-year averaged VIMF for sub-domains are shown in Fig. 4.25. For all domains, highest value of VIMF is observed in the months of June, July, August and September. The value of VIMF is found second highest in May, November and December for all domains. VIMF is higher over the BoB for all months except March. In March, the South-East domain shows higher value of VIMF than the BoB. The South-West domain has higher flux than the South-East domain in

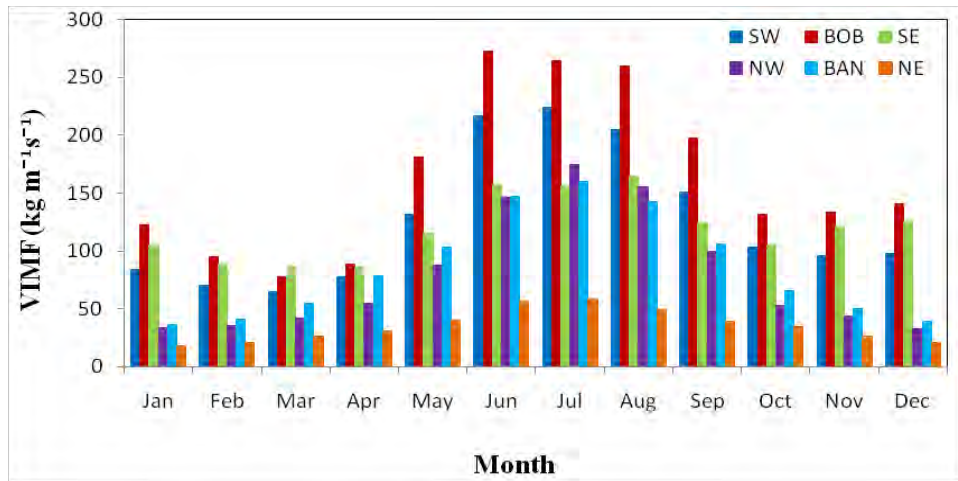


Fig. 4.25: Monthly variation of average VIMF for six domains during 1979-2015.

the months of May, June, July, August and September. In July and August, VIMF is higher over the North-West region than over Bangladesh and surrounding but for other months the Bangladesh and surrounding domain has higher flux than the North-West domain. The North-East region shows lowest VIMF over all domains for all months. Southern part has higher flux than Northern region for all months over the study area.

4.5.1 South-West domain (SW)

Monthly variation of low-level 37-year averaged VIMF for the South-West region is

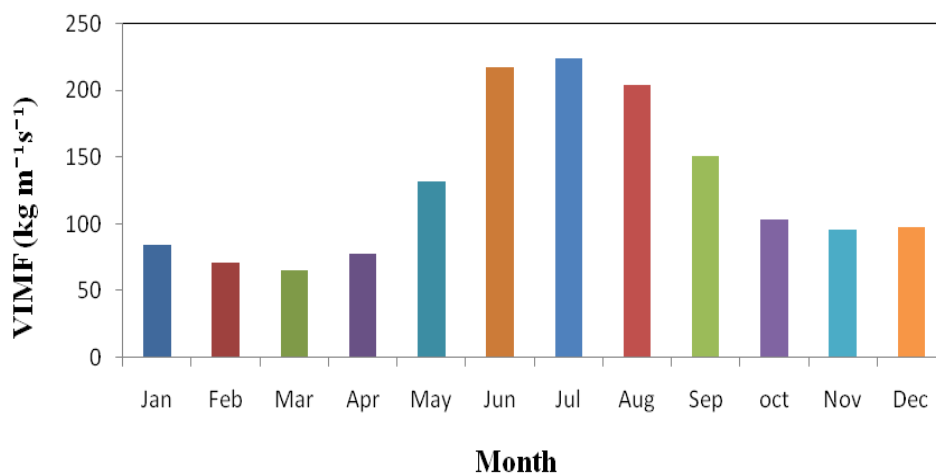


Fig. 4.26: Monthly variation of average VIMF for the South-West domain during 1979-2015.

shown in Fig. 4.26. Maximum value of VIMF is observed to be $224.24 \text{ kg m}^{-1} \text{ s}^{-1}$ in July and minimum value is $65.22 \text{ kg m}^{-1} \text{ s}^{-1}$ in March. Moisture is increasing from April to June, peak in July and then decreasing gradually. Mainly 52% of the total moisture flux is found in June, July, August and September over the South-West domain.

4.5.2 Bay of Bengal (BoB)

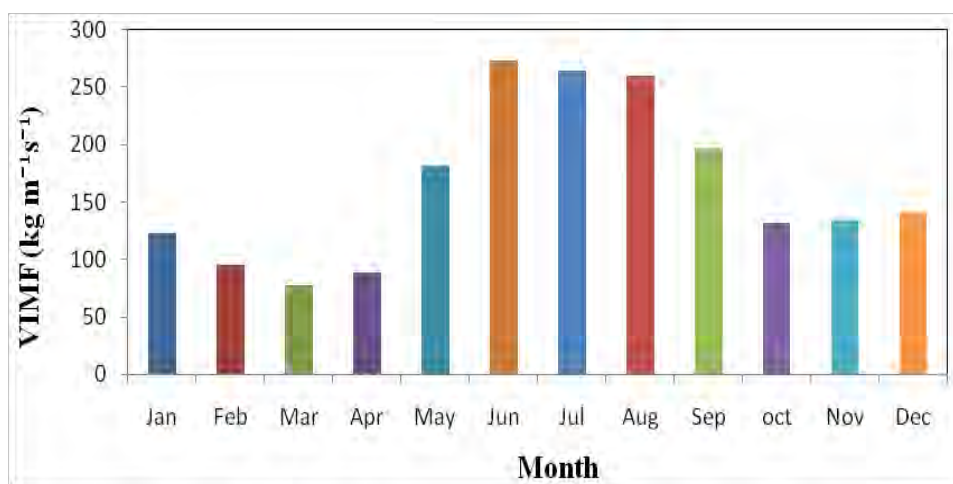


Fig. 4.27: Monthly variation of average VIMF for the Bay of Bengal domain during 1979- 2015.

Monthly variation of low-level 37-years averaged VIMF from 1000 hPa to 850 hPa for the Bay of Bengal region is shown in Fig. 4.27. It indicates that the maximum value of VIMF is observed to be $272.86 \text{ kg m}^{-1} \text{ s}^{-1}$ in June and minimum value is $77.67 \text{ kg m}^{-1} \text{ s}^{-1}$ in March. January shows higher value than February and March. Moisture flux is gradually increasing from April to June, peak in June and then decreasing at the beginning of October. Mainly 51% of the total moisture flux is found in June, July, August and September over the Bay of Bengal region.

4.5.3 South-East domain (SE)

Monthly variation of low-level 37-year averaged VIMF from 1000 hPa to 850 hPa for the South-East region is shown in Fig. 4.28. It shows that maximum value of VIMF is observed $156.03 \text{ kg m}^{-1} \text{ s}^{-1}$ in August and minimum value is $85.55 \text{ kg m}^{-1} \text{ s}^{-1}$ in April. Here in June, moisture flux is higher than July but lower than August.

Mainly 42% of the total moisture flux is found in June, July, August and September over the South-East region.

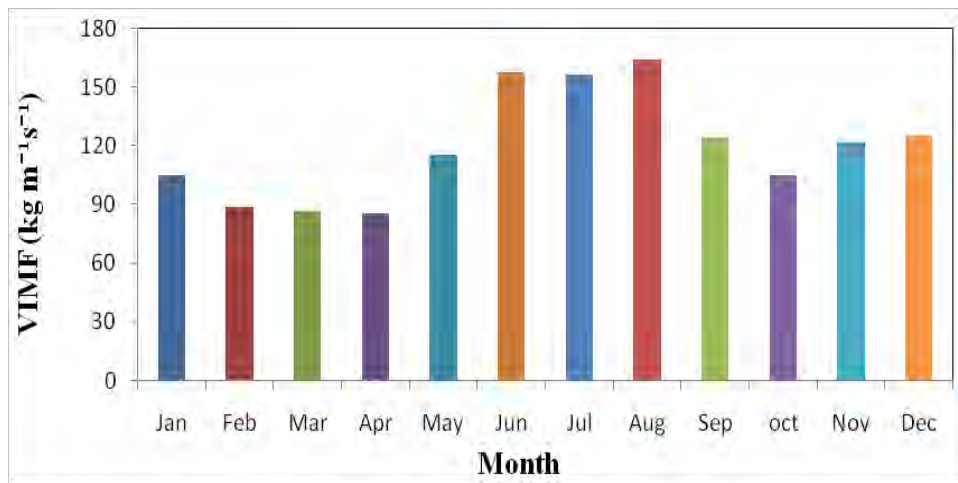


Fig. 4.28: Monthly variation of average VIMF for the South-East domain during 1979-2015.

4.5.4 North-West domain (NW)

Fig. 4.29 shows the monthly variation of low-level 37-year averaged VIMF from for the North-West region. Here, monthly trend shows the periodic nature.

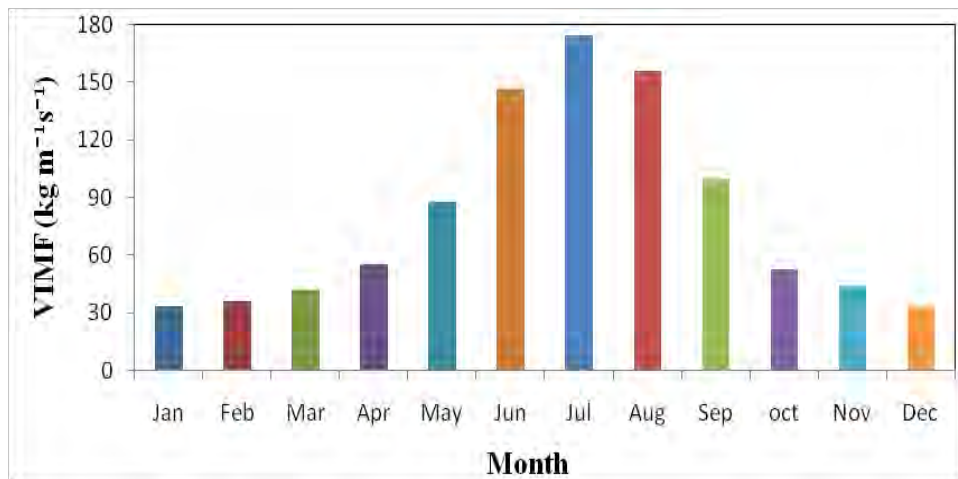


Fig. 4.29: Monthly variation of average VIMF for the North-West domain during 1979-2015.

Maximum value of VIMF is observed $174.82 \text{ kg m}^{-1} \text{ s}^{-1}$ in July and minimum value is $33.37 \text{ kg m}^{-1} \text{ s}^{-1}$ in December. Mainly 60% of the total moisture flux is found in June, July, August and September over the North-West region.

4.5.5 Bangladesh and surrounding (BAN)

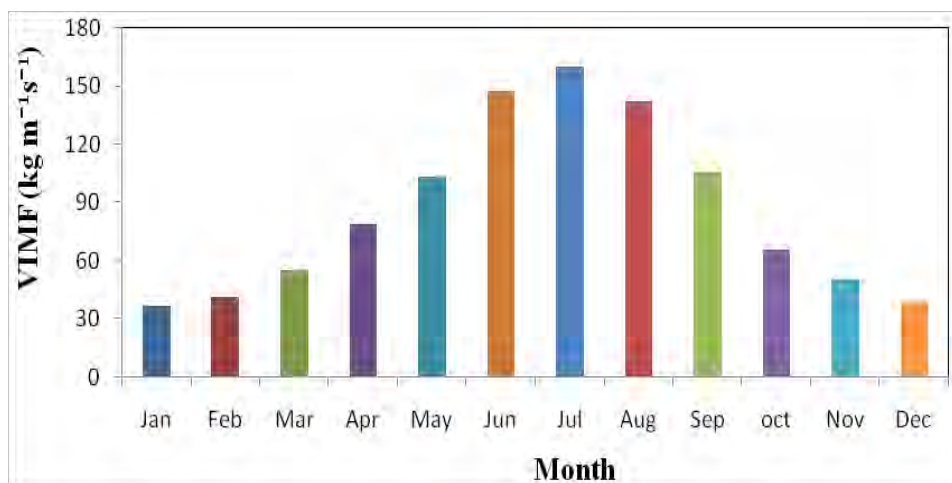


Fig. 4.30: Monthly variation of average VIMF for the Bangladesh and surrounding domain during 1979-2015.

Monthly variation of low-level 37-year averaged VIMF from 1000 hPa to 850 hPa for the Bangladesh and surrounding region is shown in Fig. 4.30. It shows that maximum value of vertically integrated moisture flux is observed $159.79 \text{ kg m}^{-1} \text{ s}^{-1}$ in July and minimum value is $36.86 \text{ kg m}^{-1} \text{ s}^{-1}$ in January. Moisture flux is increasing from March to July, peak in July and then decreasing gradually. Mainly 54% of the total moisture flux is found in June, July, August and September over the Bangladesh and surrounding region.

4.5.6 North-East domain (NE)

Monthly variation of low-level 37-year averaged VIMF from 1000 hPa to 850 hPa for the North-East region is shown in Fig. 4.31. Fig. 4.31 shows that maximum value of VIMF is observed $58.75 \text{ kg m}^{-1} \text{ s}^{-1}$ in July and minimum value is $18.62 \text{ kg m}^{-1} \text{ s}^{-1}$ in January same as Bangladesh and surrounding. Mainly 48% of the total moisture flux is found in June, July, August and September over the North-East region.

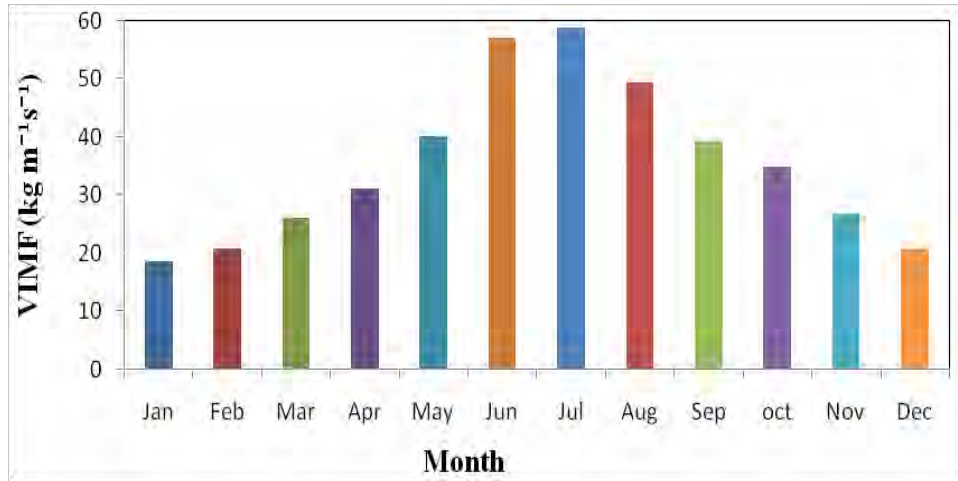


Fig. 4.31: Monthly variation of average VIMF for the North-East domain during 1979-2015.

All domain shows maximum VIMF in the month of July except the BoB and the South-East domain which have maximum value in the month of June and August respectively. But the value difference between the maximum value and the value in July is very little.

4.6 Region to Region variation

Region to region variation of 37-year averaged low-level VIMF during 1979-2015 for six domains are analyzed and compared in the following sections.

4.6.1 Annual variation of VIMF for six domains

Yearly variation of five years running mean value of low-level 37-year averaged VIMF for six domains are shown in Fig. 4.32. VIMF is increased in the North-East domain with R^2 of 0.54 which is moderately significant. Little variation is found for the Bay of Bengal in the years of 1991-1995. The South-East domain shows variation in the years of 1995-2002. Others domains have constant moisture flux for 37 years. Maximum value of VIMF is found over the Bay of Bengal and lowest amount of VIMF is observed over the North-East domain. About 27% of the total moisture flux is found over the Bay of Bengal. 21% of the total moisture flux is found over the South-West domain, 19% of the total flux over the South-East domain and 13% of the total flux over the North-West domain and 14% of the total

over Bangladesh & surrounding. Only 6% of the total moisture flux is observed over the North-East domain.

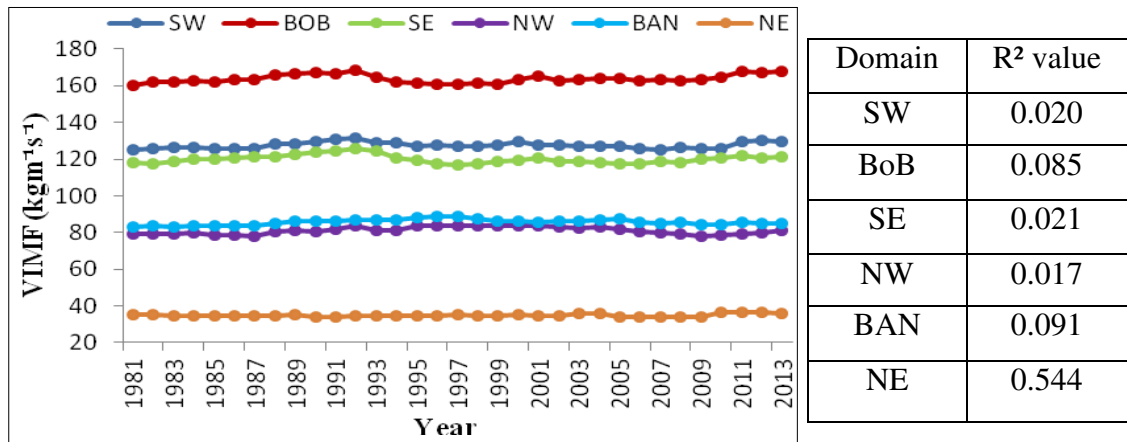


Fig. 4.32: 5-year running mean value of average VIMF for six domains during 1979-2015.

Average increasing rate of VIMF per year for all domains is not significant that as shown in Table 3. Increasing rate of VIMF is over the Bangladesh and surrounding domain is 0.44% which is not significant and over the South-East domain it shows only 0.10%. The North-West and the BoB domains have little higher increasing rate than the North-East and the South-West domains.

Table-3: Average increase of VIMF for six domains (1979-2015).

Domain	Averages increases in moisture flux (%) per year
SW	0.17
BoB	0.24
SE	0.10
NW	0.27
BAN	0.44
NE	0.11

4.6.2 Seasonal variation of VIMF for six domains

Fig. 4.33 shows the seasonal variation of 37-year averaged low-level VIMF for six domains. It indicates that the monsoon season transports the highest amount of VIMF for all domains and carries moisture from the Bay of Bengal towards the Southern regions than that in the Northern regions. That's why lowest amount of moisture flux is found over the Northern region in the monsoon season. The South-West, Bay of Bengal and the South-East part have higher moisture flux than the Northern part and Bangladesh in the pre-monsoon, post-monsoon and the winter season. Bangladesh and surrounding has higher flux than the North-West and the North-East part for all seasons but in the monsoon season the North-West part has higher moisture flux than Bangladesh and surrounding.

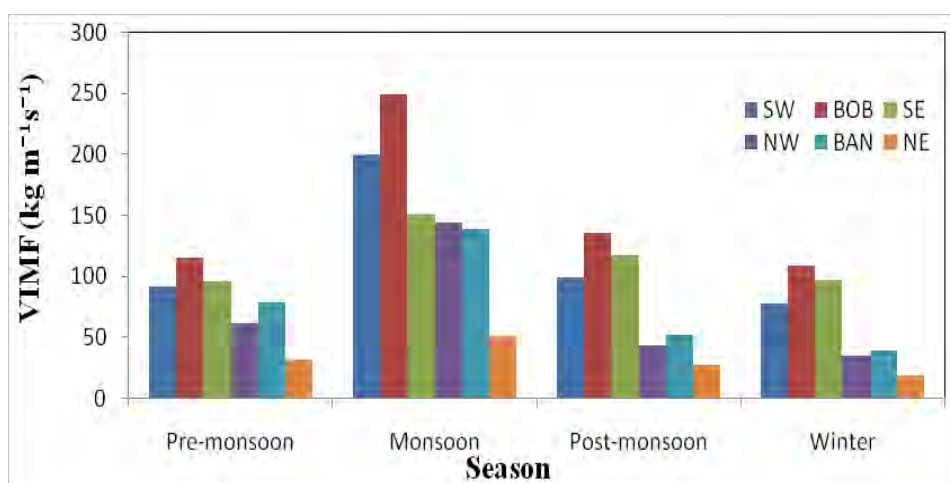


Fig 4.33: Seasonal variation of average VIMF for six domains during 1979-2015.

Table-4: Percentage of seasonal VIMF for six domains (1979-2015).

Domain	Pre-monsoon (% of total flux)	Monsoon (% of total flux)	Post-monsoon (% of total flux)	Winter (% of total flux)
SW	20	42	21	17
BoB	19	41	22	18
SE	21	33	25	21
NW	22	51	15	12
BAN	26	45	17	12
NE	25	39	21	15

4.6.3 Monthly variation of VIMF for six domains

Monthly variation of low-level average VIMF for 37 years from 1979 to 2015 for six domains is discussed in this section. Fig. 4.34 indicates that highest amount of VIMF is found the Bay of Bengal in June and lowest amount of VIMF is found over the North-East region. Southern region has higher flux than the Northern region. Moisture transport is highest in July for all study areas, however, in BoB it is little higher in June and for the South-East domain, VIMF is high in the month of August. For all domains lowest amount of VIMF is found in the month of January for Northern region and March for the Southern region.

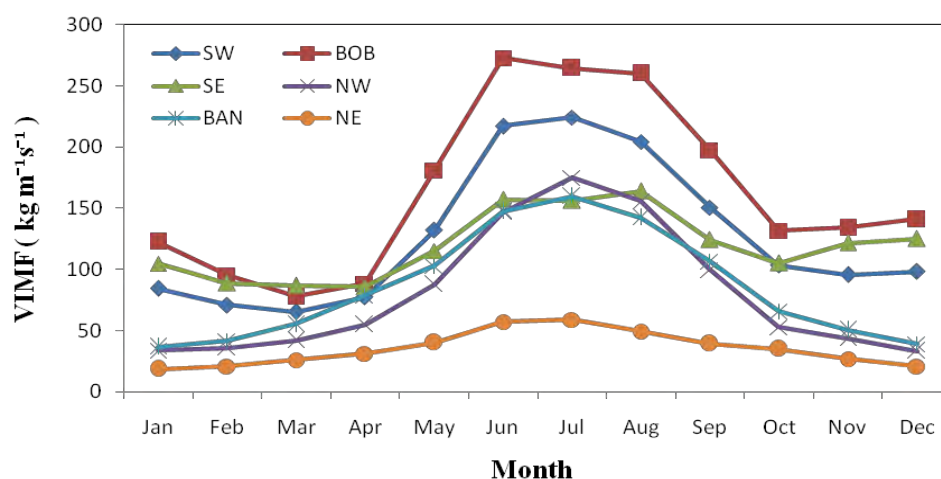


Fig. 4.34: Monthly variation of average VIMF for six domains during 1979-2015.

Table 5: Monthly variation of VIMF for six domains (1979-2015).

Domain	Maximum VIMF ($\text{kg m}^{-1} \text{s}^{-1}$)		Minimum VIMF ($\text{kg m}^{-1} \text{s}^{-1}$)	
	Month	Value	Month	Value
SW	July	224.24	March	65.22
BoB	June	272.86	March	77.67
SE	August	164.19	April	85.55
NW	July	174.82	December	33.73
BAN	July	159.79	January	36.86
NE	July	58.75	January	18.62

4.7 Variability of Precipitation

4.7.1 Spatial distribution of precipitation for study area

Spatial distribution of average 37-year precipitation (1979-2015) over SA is shown in Fig. 4.35. South Asian geographical features are very favorable for the development of intense convection due to the interaction between moist and dry air masses coming from the Bay of Bengal and India. Average of 37 years' precipitation is higher in the North-East domain. The rainfall is a result of the convergence of wind flow from the Bay of Bengal and reverse winds from the South China Sea.

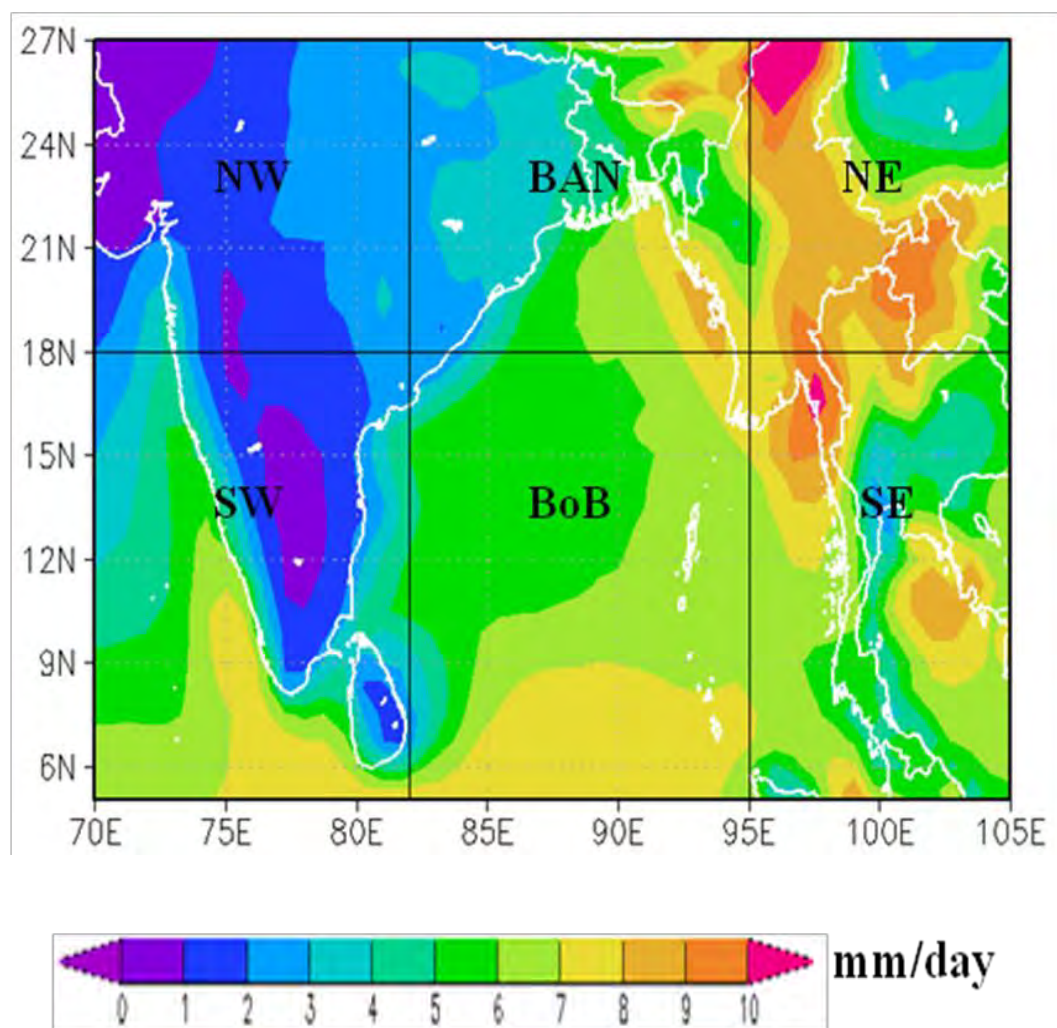


Fig. 4.35: Spatial distribution of average precipitation (shading; mm/day) during 1979-2015.

About 7.06 mm/day precipitation is observed over the North-East area, while lowest amount of precipitation is observed in the North-West domain and its value is only 1.77 mm/day. Precipitation is 4.96 mm/day over the Bangladesh and surrounding domain, 6.36 mm/day for the South-East domain, 6.34mm/day for the Bay of Bengal and 4.03 mm/day for the South-West domain are observed.

4.7.2 Seasonal variation of precipitation for six domains

Seasonal variation of 37-year averaged precipitation (1979-2015) for six domains is discussed in this section. Highest amount of precipitation for six domains is found in

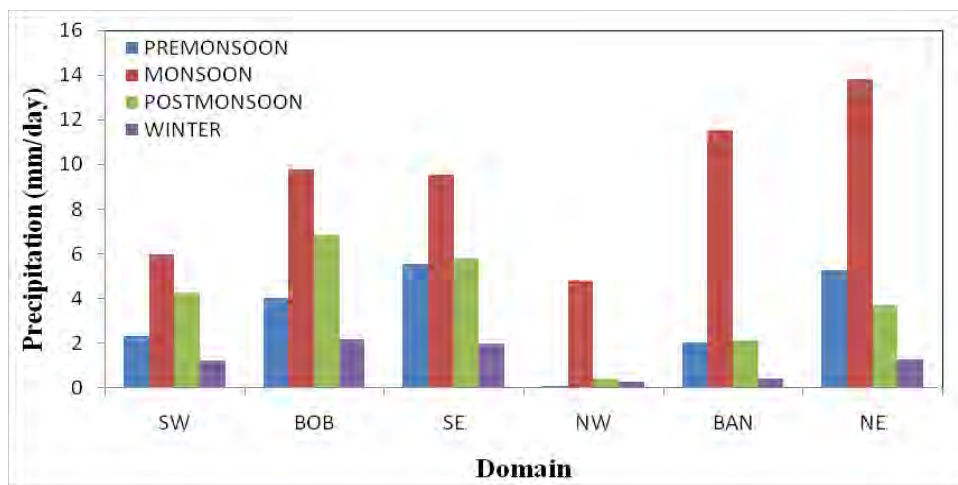


Fig. 4.36: Seasonal variation of 37-year averaged precipitation (mm/day) for six domains during 1979-2015.

the monsoon season and lowest amount of precipitation is observed in the winter season. In summer, moist air is carried northwards from the Indian Ocean over the Indian subcontinent, bringing rains. North-east monsoon affects the south-east coastal states of India, due to winds bringing moisture from the Bay of Bengal. For all domains, precipitation rate is higher in the post-monsoon season than that of the pre-monsoon season except the North-East domain. Precipitation rate is very low in the pre-monsoon, post-monsoon and winter season for North-West domain that shown in Table 6.

Table 6: Seasonal variation of precipitation for six domains (1979-2015).

Domain	Pre-monsoon	Monsoon	Post-monsoon	Winter
SW	2.32	5.97	4.26	1.22
BoB	4.01	9.78	6.48	2.18
SE	5.53	9.53	5.81	2.01
NW	0.09	4.81	0.40	0.28
BAN	2.05	11.53	2.15	0.43
NE	5.26	13.80	3.72	1.29

4.7.3 Monthly variation of precipitation for six domains

Monthly variations of average 37-year precipitation (1979-2015) for six domains are shown in Fig. 4.37. Highest amount of precipitation is observed in June, July, August and September for all domains. Precipitation is high in the North-East domain (7.07 mm/day) because of orographic precipitation. The North-West part receives lowest amount of precipitation (1.77 mm/day). It is drought-prone, as it tends to have less reliable rainfall due to sporadic lateness or failure of the southwest monsoon and the transport of dry air from arid region during pre-monsoon season [43].

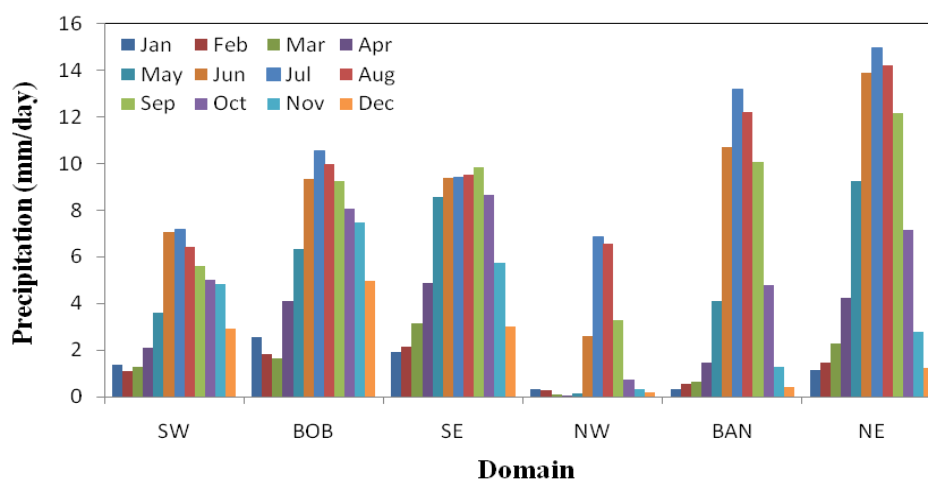


Fig. 4.37: Monthly variation of 37-year averaged precipitation (mm/day) for six domains during 1979-2015.

For all considerable domains, highest amount of precipitation is found in the month of July except the South-East domain. The South-East domain shows highest amount of precipitation (9.82 mm/day) in the month of September. Lowest amount of precipitation is found in January for the South-East, Bangladesh and surrounding and the North-East domain. Other domains show the lowest amount of precipitation in February for South-West domain, March for the BoB and April for the North-West domain.

Table 7: Monthly variation of precipitation for six domains (1979-2015).

Domain	Maximum value of precipitation (mm/day)		Minimum value of precipitation (mm/day)	
	Month	Value	Month	Value
SW	July	7.16	February	1.10
BoB	July	10.56	March	1.64
SE	September	9.82	January	1.89
NW	July	6.85	April	0.05
BAN	July	13.14	January	0.31
NE	July	14.95	January	1.14

4.8 Variability of Evaporation

4.8.1 Spatial distribution of evaporation for study area

Evaporation is the reverse of rainfall. It is a measurement that can be related to the loss of moisture from the soil and from plants. The annual average of evaporation during, 1979-2015, as calculated from the ERA-Interim data set, is shown in Fig. 4.38. It has been seen that the Northern part of SA has less evaporation rate and it is increasing toward the Southern part of SA. The 37-year averaged evaporation is highest over the South-East domain and second highest over the BoB. About 4.92 mm/day evaporation is found over the South-East domain and 4.75 mm/day evaporation is found over the Bay of Bengal, while lowest amount of evaporation is observed in the North-West domain and its value is only 1.28 mm/day. Evaporation is

2.90 mm/day over the Bangladesh and surrounding region, 3.71mm/day for the North-East domain and 3.33 mm/day for the South-West domain are observed.

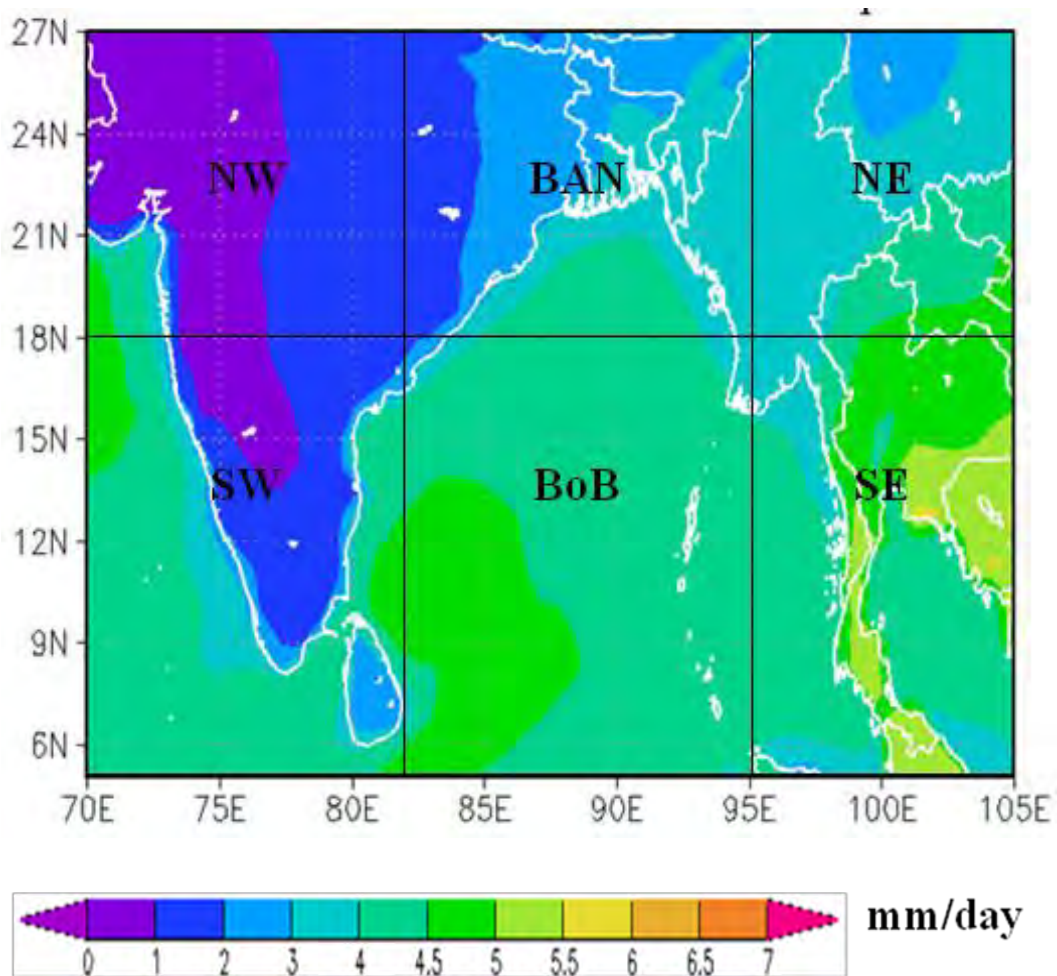


Fig. 4.38: Spatial distribution of averaged evaporation (shading; mm/day) during 1979-2015.

4.8.2 Seasonal variation of evaporation for six domains

Seasonal variation of 37-year averaged evaporation during 1979-2015 for six domains is shown in Fig. 4.39. All domains show the highest amount of evaporation in the monsoon season because temperature is high in the monsoon season. In the pre-monsoon season, the rate of evaporation is higher than the post-monsoon season for all domains except the Bay of Bengal. Evaporation rate is lower in the winter season for all study areas except the Bay of Bengal. For the BoB, evaporation rate is higher in the winter season than the pre-monsoon and post-monsoon season. About 30% of the total evaporation is observed in the monsoon season and 20% of the total

evaporation is found in the winter season. 50% of the total evaporation is observed in the pre-monsoon and the post-monsoon season.

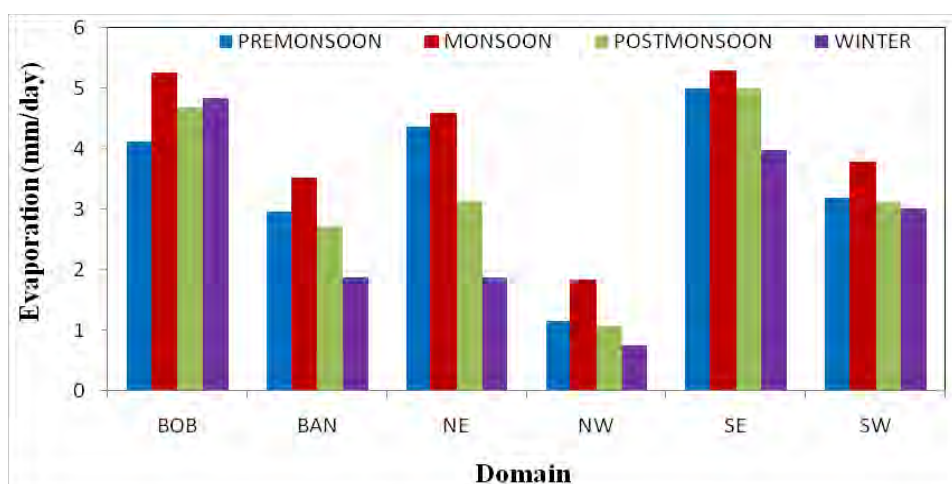


Fig 4.39: Seasonal variation of 37-year averaged evaporation (mm/day) for six domains during 1979-2015.

Table 8: Seasonal variation of evaporation for six domains (1979-2015)

Domain	Pre-monsoon	Monsoon	Post-monsoon	Winter
SW	3.18	3.77	3.12	3.01
BoB	4.11	5.25	4.67	4.84
SE	5.00	5.28	5.00	3.98
NW	1.15	1.81	1.07	0.74
BAN	2.96	3.50	2.72	1.87
NE	4.37	4.57	3.13	1.88

4.8.3 Monthly variation of evaporation for six domains

Evaporation depends on temperature. Highest evaporation (range 4 to 6 mm/day) takes place in the month of May to June when temperature remains maximum and lowest value is found in the month of January-March when minimum temperature takes place except the BoB (Fig. 4.40). For the Bay of Bengal, high evaporation rate is found in the month of June, December and January which show quite similar figure with the South-West domain. For the BoB and South-West domains evaporation rate is lower in March and October.

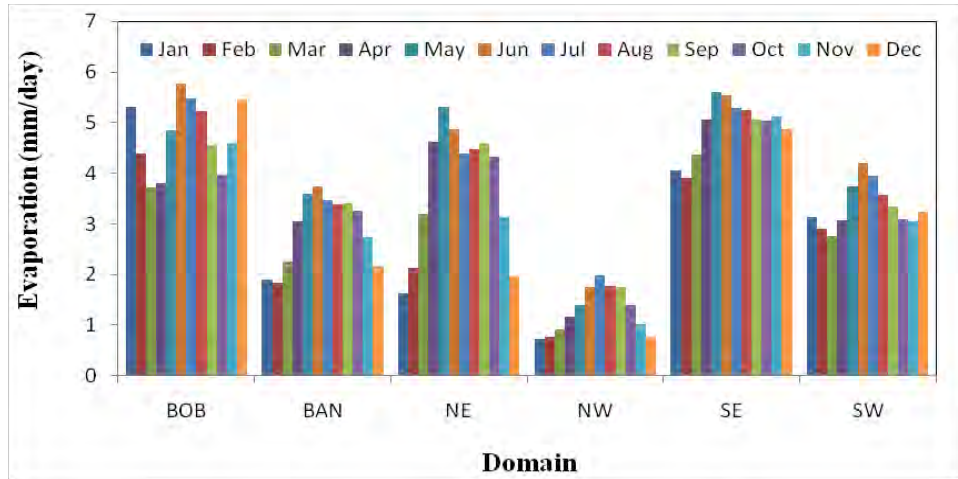


Fig 4.40: Monthly variation of 37-year averaged evaporation (mm/day) for six domains during 1979-2015.

Evaporation rate is high in May-October for the Bangladesh & surrounding region. For the South-East domain, high evaporation rate is observed in May-December. Evaporation is highest in May for the North-East domain and July for the North-West domain. January and December showed lower evaporation for the North-East and the North-West domains. Evaporation rate is higher in the South-East domain (24% of the total evaporation) than the other domains and only 6% of the total evaporation is found in the North-West domain.

Table 9: Monthly variation of evaporation for six domains (1979-2015).

Domain	Maximum value of evaporation (mm/day)		Minimum value of evaporation (mm/day)	
	Month	Value	Month	Value
SW	June	4.20	March	2.75
BoB	June	5.76	March	3.71
SE	May	5.59	February	3.91
NW	July	1.97	January	0.73
BAN	June	3.73	February	1.83
NE	May	5.30	January	1.63

4.9 Relation among precipitation, moisture flux and evaporation

Moisture flux and evaporation simultaneously contributes to the precipitation. Most of the precipitation comes from the moisture flux, even though exact amount of precipitation from moisture flux and evaporation are important to enrich the knowledge about precipitation over this area and also help to improve the parameters for accurate rainfall prediction by modifying physical processes associated with these parameters.

4.9.1 Relation between moisture flux and precipitation for study area

Fig. 4.41 shows the relation of monthly 37-year averaged moisture flux with precipitation during 1979 to 2015 for the study area. It indicates that how monthly averaged VIMF of the total area is correlated with the precipitation. When moisture flux rate is decreased in the month of January and February, precipitation of the area is also decreased. Conversely, precipitation rate is increased when the amount of moisture is getting increased and it happens from the month of April to August. In April, precipitation rate is increased with the increasing rate of moisture flux. Highest amount of moisture flux is found in the month of July ($191.74 \text{ kg m}^{-1} \text{ s}^{-1}$) and precipitation is also showed highest value in July (10 mm/day). Then in September to December, precipitation and moisture flux are both decreasing.

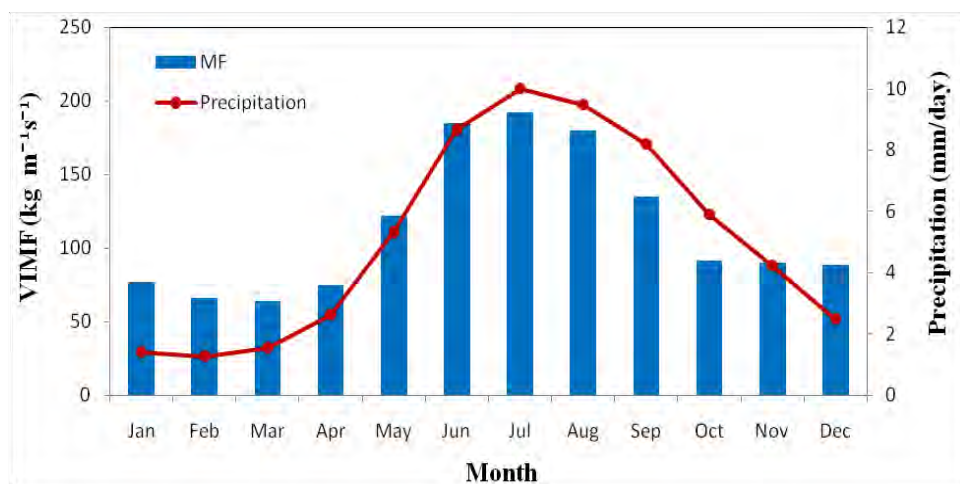


Fig. 4.41: Relation between moisture flux and precipitation for the study area.

Scatter plot of precipitation with VIMF is shown in Fig. 4.42. The co-efficient of determination (R^2 value) between precipitation and moisture flux for the study area

shows the value of 0.77. That means R^2 value is significant i.e 77% of the total variation in precipitation can be explained by the linear relationship between VIMF and precipitation. In this case moisture flux plays an important role to form precipitation over the study area.

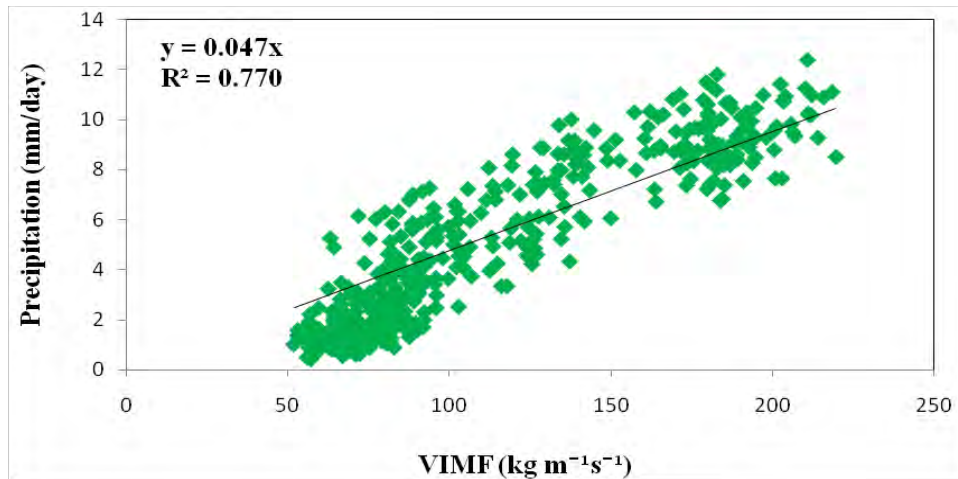


Fig. 4.42: Scatter plot between moisture flux and precipitation for the study area during 1979-2015.

4.9.2 Relation between evaporation and precipitation for study area

Fig. 4.43 shows the relation of monthly 37-year averaged evaporation with precipitation during 1979 to 2015 for the study area. It indicates how monthly averaged evaporation of the total area is correlated with the precipitation. In the month of February to June precipitation rate is increased with the increasing value of evaporation. But in July both are inversely related. And then, precipitation rate is decreased with the decreasing rate of evaporation from August to November. In December and January, evaporation rates are 3.27 mm/day and 3.10 mm/day where precipitation rates are 2.49 mm/day and 1.40 mm/day, respectively.

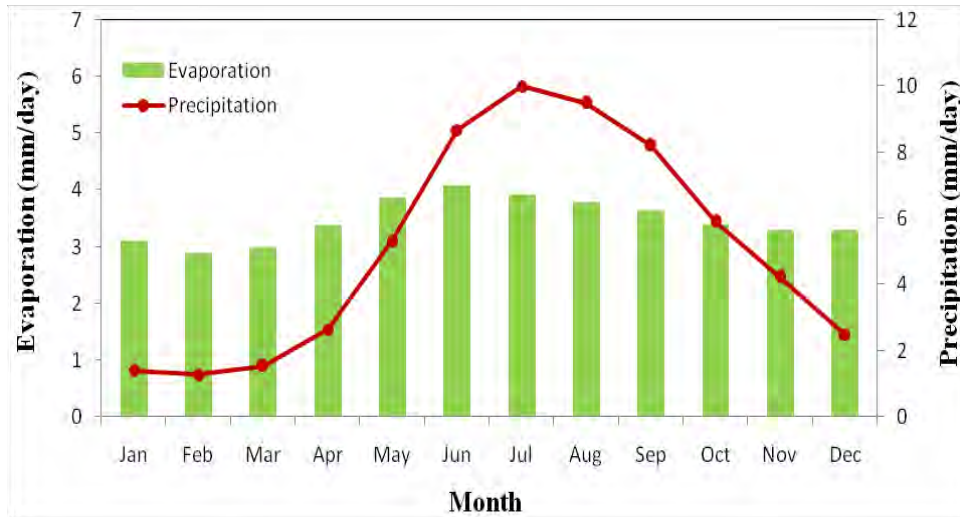


Fig. 4.43: Relation between evaporation and precipitation for the study area.

Scatter plot of precipitation and evaporation is shown in Fig. 4.44. The coefficient of determination (R^2 value) between evaporation and precipitation for the study area shows the value of 0.23. Here only 23% of the total variation of precipitation can be explained by the relationship between evaporation and precipitation over the study area.

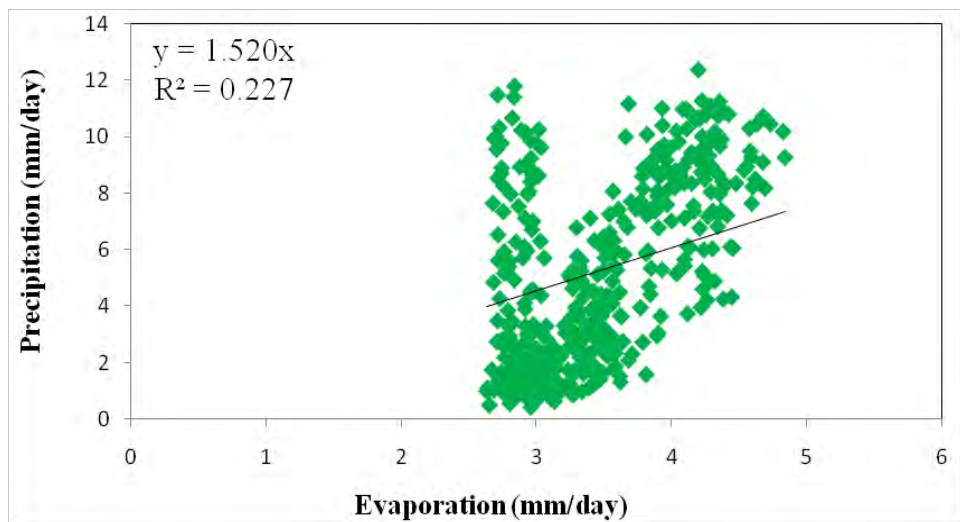


Fig. 4.44: Scatter plot between evaporation and precipitation and for the study area during 1979-2015.

4.9.3 Relation between moisture flux and precipitation for six domains

Fig. 4.45 shows the relation of monthly 37-year averaged VIMF with precipitation for all domains. Here 444 points are plotted in each figure. The relation between VIMF and precipitation for the South-West, Bay of Bengal and the South-East domain are shown in the left side and the North-West, Bangladesh and surrounding and the North-East domains are shown in the right side of the figure.

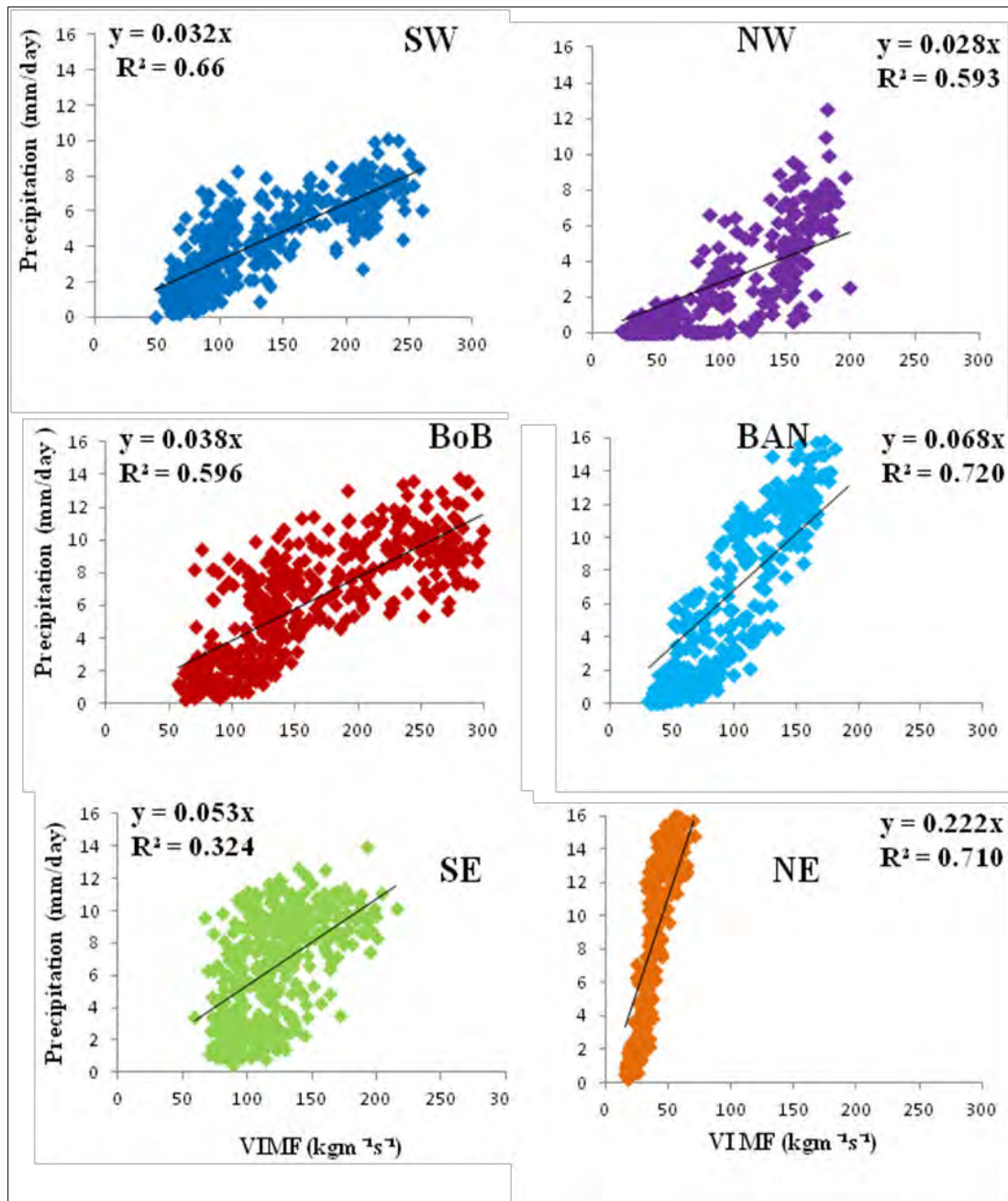


Fig. 4.45: Scatter plot between precipitation and moisture flux for six domains during 1979-2015.

The co-efficient of determination (R^2 value) is 0.66 between precipitation and moisture flux for the South-West domain, which is highly significant. That means that the moisture flux plays a significant role to form precipitation over the South-West domain whereas R^2 value between precipitation and moisture flux for the Bay of Bengal showed the value of 0.59. This value is similar to the value of R^2 for the North-West domain. So, it can say that precipitation is moderately to highly significant with moisture flux for the Bay of Bengal and the North-West domain. Precipitation has lower significant correlation with moisture flux for the South-East domain with R^2 value of 0.32. The co-efficient of determination (R^2 value) between precipitation and moisture flux for the Bangladesh and surrounding domain and the North-East domain are 0.72 and 0.71, which indicate that precipitation is highly significant with moisture flux.

4.9.4 Relation between evaporation and precipitation for six domains

Fig. 4.46 shows the relation of monthly average evaporation with precipitation for six domains during 1979 to 2015. The co-efficient of determination (R^2 value) between precipitation and evaporation is only 0.24, 0.12, 0.25, 0.32, 0.30, and 0.44 for the South-West, Bay of Bengal, South-East, North-West, Bangladesh and surrounding and the North-East, which are not significant. It indicates that evaporation does not play significant role to form precipitation over all domains. Table-10 shows the co-efficient of determination (R^2 value) between VIMF and evaporation with precipitation for six domains.

Table 10: R^2 value between VIMF and evaporation with precipitation for six domains.

Domain	The co-efficient of determinant (R^2 value)	
	Between VIMF and precipitation	Between evaporation and precipitation
SW	0.660	0.239
BoB	0.596	0.124
SE	0.324	0.254
NW	0.593	0.329
BAN	0.720	0.301
NE	0.710	0.443

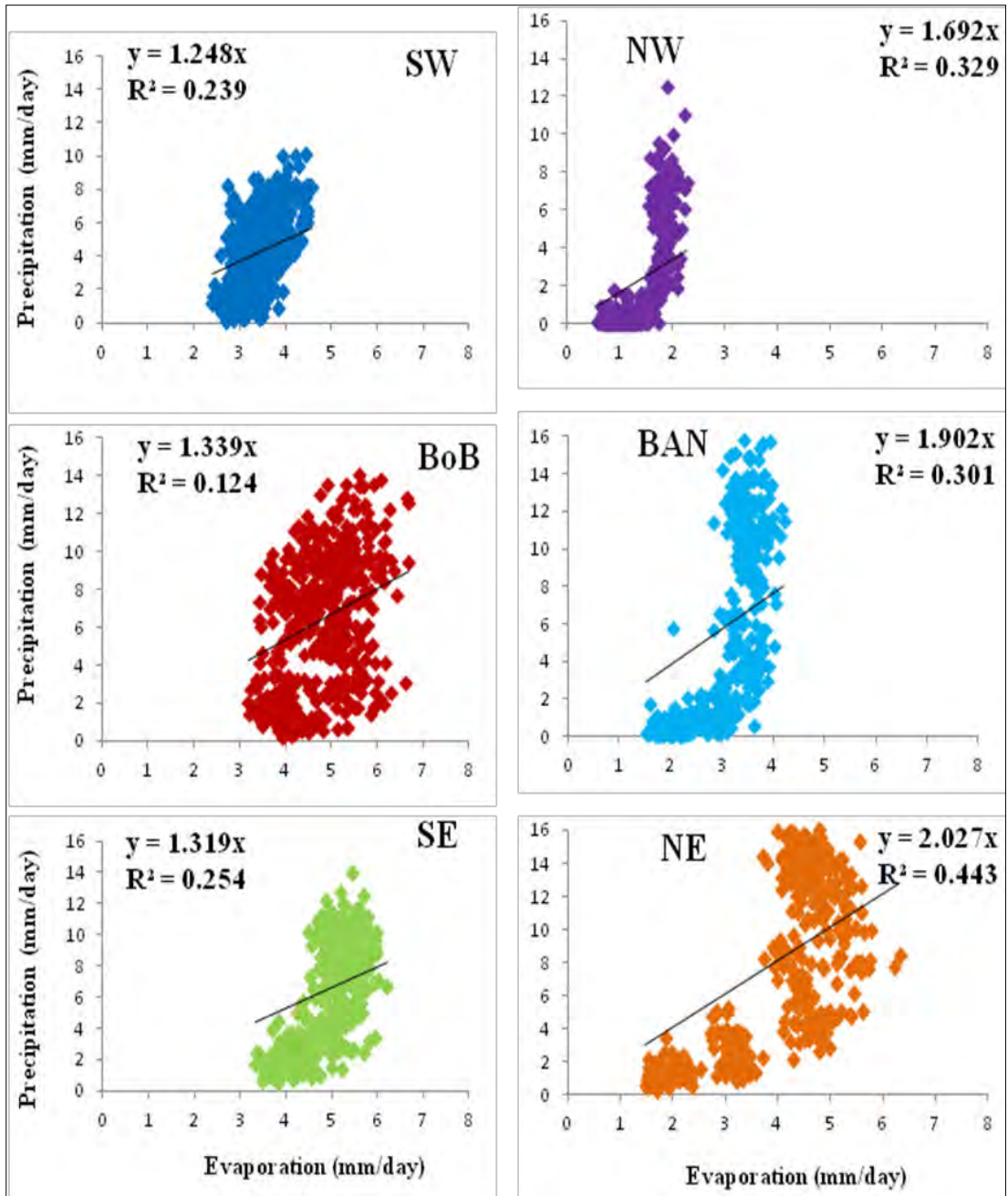


Fig. 4.46: Scatter plots between precipitation and evaporation for six domains during 1979-2015.

4.10 Components of precipitation

The amount of precipitation over any region depends on moisture flux that is advected from the ocean or local evaporation rate. Equations given in section 3.3.2 are used to find out the components of precipitation coming from the moisture flux and evaporation effect for six domains. The advective component P_a and the component of precipitation arising from local evaporation P_m by using equation (6) and (7) [section 3.3.2] in each domain are calculated individually for each month. The equation (6) and (7) are

$$P_m = \frac{EL}{EL + 2F_{in}} \times P \quad (6)$$

and
$$P_a = P - P_m = \left(1 - \frac{EL}{EL + 2F_{in}}\right)P \quad (7)$$

Here,

- P = total precipitation,
- P_a = advected component of precipitation,
- P_m = evaporation component of precipitation,
- L = domain length,
- F_{in} = moisture flux and
- E = evaporation.

The details calculation of P_a and P_m for one case is described below:

a) South-West domain (SW):

The Fig. 4.47 shows the South-West domain for the month of January averaged for the study period. Here, horizontal flux advected from easterly to westerly i.e in the zonal direction. So the length of the domain is aligned along east-west. Here, for average January,

$$F_{in} = 84.3469736 \text{ kg m}^{-1} \text{ s}^{-1}$$

$$\begin{aligned}
 P &= 1.345193087 \text{ mm day}^{-1} \\
 E &= 3.124658154 \text{ mm day}^{-1} \\
 &= 3.124658154 / (3600 * 24) \text{ kg m}^{-2} \text{ s}^{-1} \\
 &= 0.000036165 \text{ kg m}^{-2} \text{ s}^{-1} \\
 L &= (\text{zonal length in degree} * 110.574) \text{ km} \\
 &= (\text{zonal length in degree} * 110.574 * 1000) \text{ m} \\
 &= (13 * 110.574 * 1000) \text{ m} \\
 &= 1437462 \text{ m} \\
 EL &= 0.000036165 \text{ kg m}^{-2} \text{ s}^{-1} * 1437462 \text{ m} \\
 &= 51.98581323 \text{ kg m}^{-1} \text{ s}^{-1}
 \end{aligned}$$

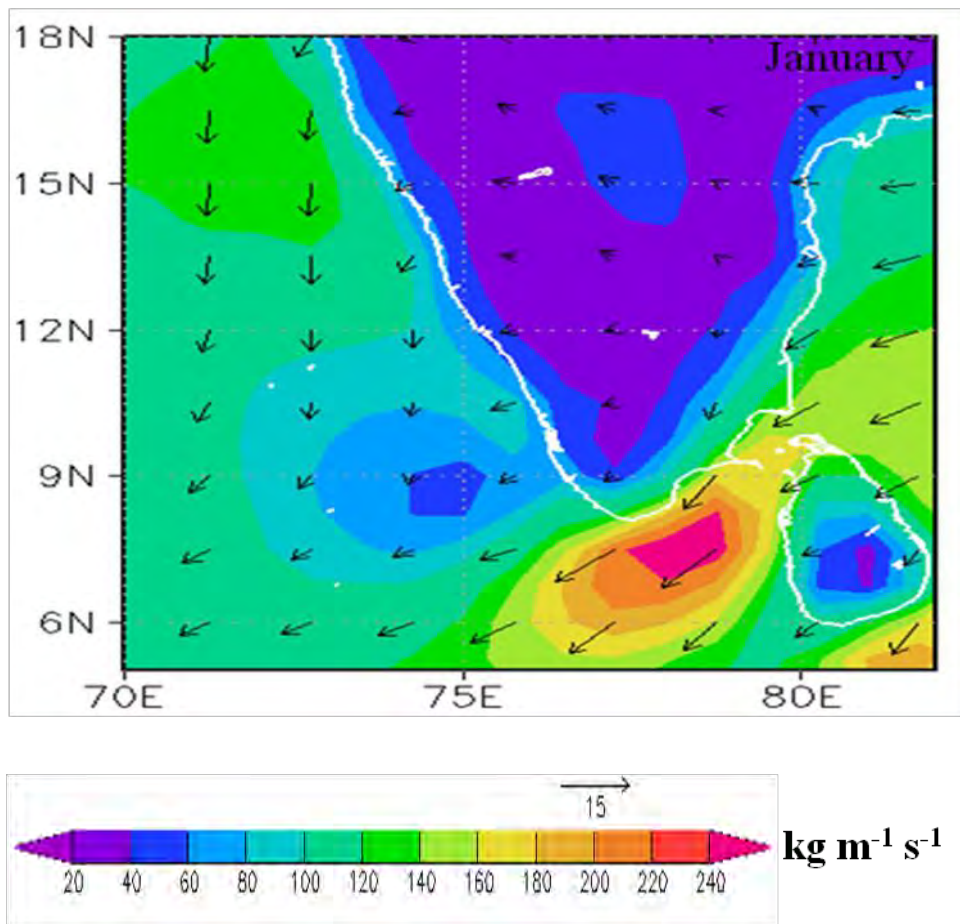


Fig. 4.47: The 37-year averaged VIMF (shading; $\text{kg m}^{-1} \text{ s}^{-1}$) and average wind velocity (m s^{-1}) in January for the South-West domain during 1979-2015.

So, substituting above value in equation (6) and we can write

$$\begin{aligned} P_m &= (51.98581323/ 51.98581323+2*84.3469736) *1.345193087 \text{ mm day}^{-1} \\ &= 0.316889 \text{ mm day}^{-1} \end{aligned}$$

Now substituting the value of P_m in equation (7), we get

$$\begin{aligned} P_a &= P - P_m \\ \text{or, } P_a &= 1.345193087 - 0.316889 \text{ mm day}^{-1} \\ &= 1.028304065 \text{ mm day}^{-1} \end{aligned}$$

According to this equation, P_a and P_m are calculated for all months separately and averaged the values in the SW domain.

b) Bay of Bengal (BoB):

Fig. 4.48 shows the BoB area for month January. Here, L is also considered along zonal direction. Using above calculation the following values are found. Here, for average January,

$$\begin{aligned} F_{in} &= 122.544098 \text{ kg m}^{-1} \text{ s}^{-1} \\ P &= 2.57345405 \text{ mm day}^{-1} \\ E &= 5.31145448 \text{ mm day}^{-1} \\ &= 5.31145448/ (3600*24) \text{ kg m}^{-2} \text{ s}^{-1} \\ &= 0.000061475 \text{ kg m}^{-2} \text{ s}^{-1} \\ L &= (\text{zonal length in degree} * 110.574) \text{ km} \\ &= (\text{zonal length in degree} * 110.574 * 1000) \text{ m} \\ &= (13 * 110.574 * 1000) \text{ m} \\ &= 1437462 \text{ m} \\ EL &= 0.000061475 \text{ kg m}^{-2} \text{ s}^{-1} * 1437462 \text{ m} \\ &= 88.36821736 \text{ kg m}^{-1} \text{ s}^{-1} \end{aligned}$$

So, substituting above value in equation (6) and we can write

$$P_m = (88.36821736 / 88.36821736 + 2 * 122.544098) * 2.57345405 \text{ mm day}^{-1}$$

$$= 0.681969346 \text{ mm day}^{-1}$$

Now substituting the value of P_m in equation (7), we get

$$P_a = P - P_m$$

or, $P_a = 2.57345405 - 0.681969346 \text{ mm day}^{-1}$

$$= 1.891484704 \text{ mm day}^{-1}$$

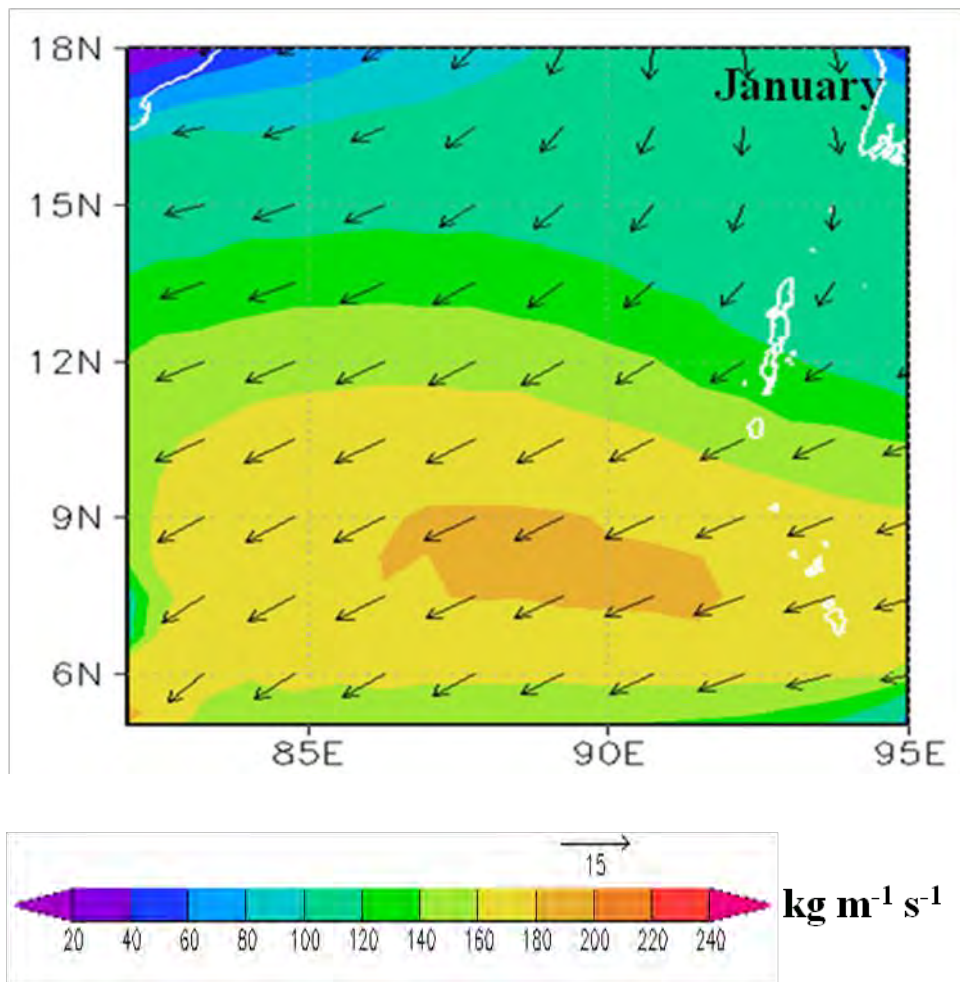


Fig. 4.48: The 37-year averaged VIMF (shading; $\text{kg m}^{-1} \text{s}^{-1}$) and average wind velocity (m s^{-1}) in January for the BoB domain during 1979-2015.

According to this equation, P_a and P_m are calculated for all months separately and averaged the values in the BoB domain.

c) South-East domain (SE):

Fig. 4.49 shows the South-East domain for month January. Here, L is also considered along zonal direction. Using (6) and (7) calculation the following values are found.

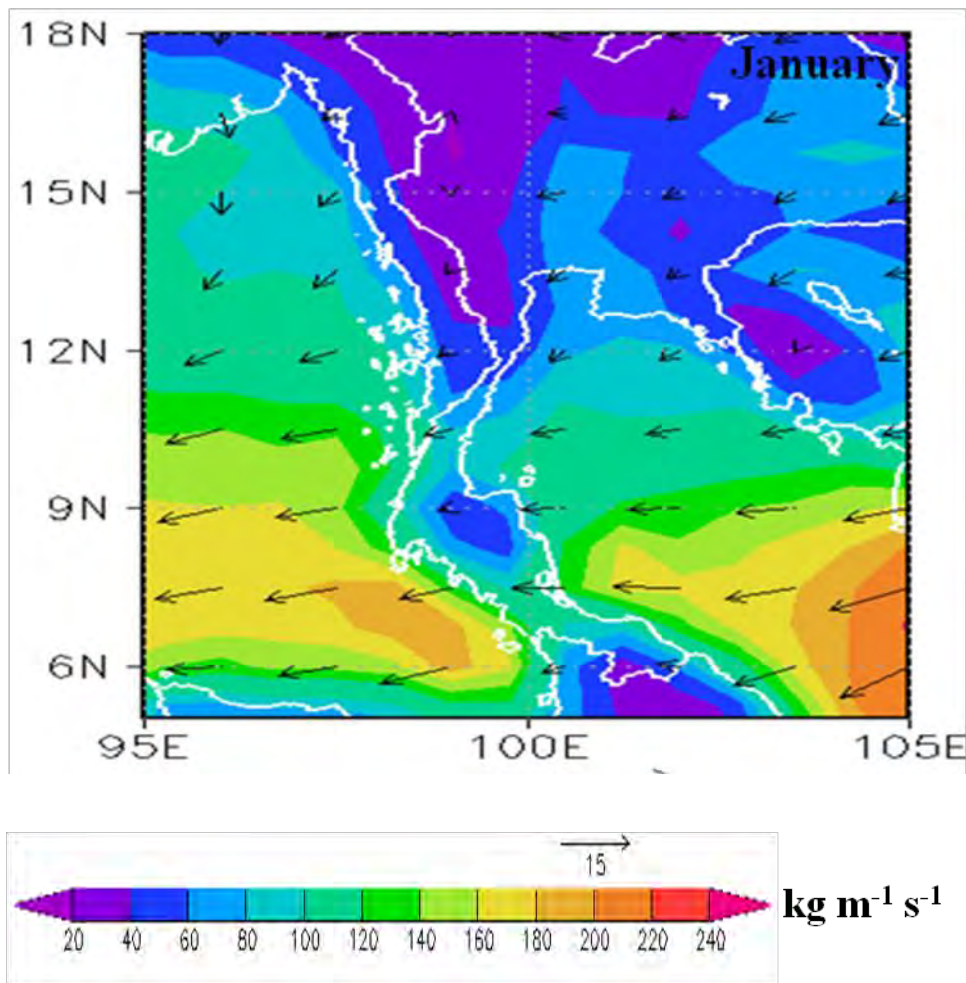


Fig. 4.49: The 37-year averaged VIMF (shading; $\text{kg m}^{-1} \text{s}^{-1}$) and average wind velocity (m s^{-1}) in January for the South-East domain during 1979-2015.

Here, for average January,

$$F_{in} = 104.938189 \text{ kg m}^{-1} \text{ s}^{-1}$$

$$\begin{aligned}
P &= 1.89539942 \text{ mm day}^{-1} \\
E &= 4.05537381 \text{ mm day}^{-1} \\
&= 4.05537381 / (3600*24) \text{ kg m}^{-2} \text{ s}^{-1} \\
&= 0.000046937 \text{ kg m}^{-2} \text{ s}^{-1} \\
L &= (\text{zonal length in degree} * 110.574) \text{ km} \\
&= (\text{zonal length in degree} * 110.574 * 1000) \text{ m} \\
&= (13 * 110.574 * 1000) \text{ m} \\
&= 1437462 \text{ m} \\
EL &= 0.000046937 \text{ kg m}^{-2} \text{ s}^{-1} * 1437462 \text{ m} \\
&= 67.47043689 \text{ kg m}^{-1} \text{ s}^{-1}
\end{aligned}$$

So, substituting above value in equation (6) and we can write

$$\begin{aligned}
P_m &= (67.47043689/67.47043689 + 2*104.938189) * 1.89539942 \text{ mm day}^{-1} \\
&= 0.461095711 \text{ mm day}^{-1}
\end{aligned}$$

Now substituting the value of P_m in equation (7), we get

$$\begin{aligned}
P_a &= P - P_m \\
\text{or, } P_a &= 1.89539942 - 0.461095711 \text{ mm day}^{-1} \\
&= 1.434303709 \text{ mm day}^{-1}
\end{aligned}$$

According to this equation, P_a and P_m are calculated for all months separately and averaged the values in the SE domain.

d) North-West domain (NW):

Fig. 4.50 shows the North-West area for month January. Here, L is also considered along zonal direction. Using equation (6) and (7), the following values are found. Here, for average January,

$$F_{in} = 33.726159 \text{ kg m}^{-1} \text{ s}^{-1}$$

$$P = 0.307095 \text{ mm day}^{-1}$$

$$E = 0.731574 \text{ mm day}^{-1}$$

$$= 0.731574 / (3600 * 24) \text{ kg m}^{-2} \text{ s}^{-1}$$

$$= 0.000008467 \text{ kg m}^{-2} \text{ s}^{-1}$$

$$L = (\text{zonal length in degree} * 110.574) \text{ km}$$

$$= (\text{zonal length in degree} * 110.574 * 1000) \text{ m}$$

$$= (9 * 110.574 * 1000) \text{ m}$$

$$= 995166 \text{ m}$$

$$EL = 0.000008467 \text{ kg m}^{-2} \text{ s}^{-1} * 995166 \text{ m}$$

$$= 8.426070 \text{ kg m}^{-1} \text{ s}^{-1}$$

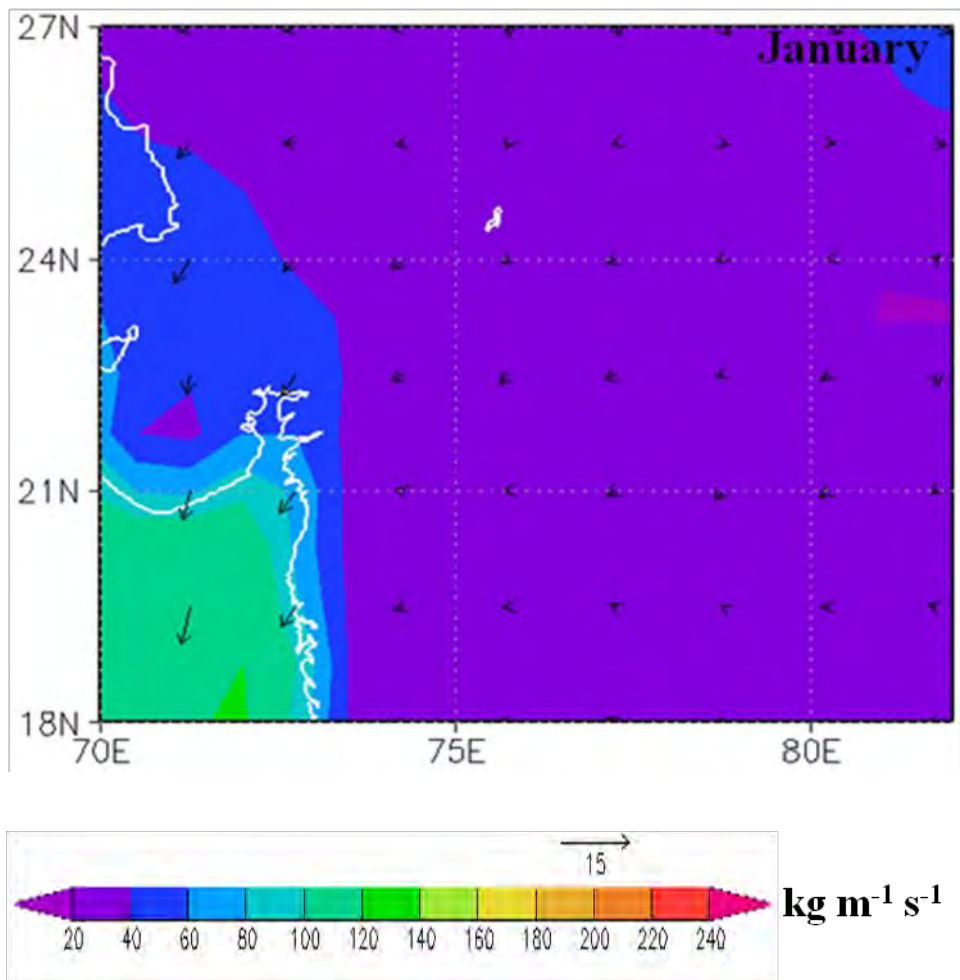


Fig. 4.50: The 37-year averaged VIMF (shading; $\text{kg m}^{-1} \text{ s}^{-1}$) and average wind velocity (m s^{-1}) in January for the North-West domain during 1979-2015.

So, substituting above value in equation (6) and we can write

$$\begin{aligned} P_m &= (8.426070 / 8.426070 + 2 * 33.726159) * 0.307095 \text{ mm day}^{-1} \\ &= 0.034101991 \text{ mm day}^{-1} \end{aligned}$$

Now substituting the value of P_m in equation (7), we get

$$\begin{aligned} P_a &= P - P_m \\ \text{or, } P_a &= 0.307095 - 0.034101991 \text{ mm day}^{-1} \\ &= 0.272993009 \text{ mm day}^{-1} \end{aligned}$$

According to this equation, P_a and P_m are calculated for all months separately and averaged the values in the NW domain.

e) Bangladesh and surrounding (BAN):

Fig. 4.51 shows the Bangladesh and surrounding area for month January. Here, L is also considered along zonal direction. Using above calculation the following values are found. Here, for average January,

$$F_{in} = 36.864036 \text{ kg m}^{-1} \text{ s}^{-1}$$

$$P = 0.3190041 \text{ mm day}^{-1}$$

$$\begin{aligned} E &= 1.905370 \text{ mm day}^{-1} \\ &= 1.905370 / (3600 * 24) \text{ kg m}^{-2} \text{ s}^{-1} \\ &= 0.000022052 \text{ kg m}^{-2} \text{ s}^{-1} \end{aligned}$$

$$\begin{aligned} L &= (\text{zonal length in degree} * 110.574) \text{ km} \\ &= (\text{zonal length in degree} * 110.574 * 1000) \text{ m} \\ &= (9 * 110.574 * 1000) \text{ m} \\ &= 995166 \text{ m} \end{aligned}$$

$$\begin{aligned} EL &= 0.000022052 \text{ kg m}^{-2} \text{ s}^{-1} * 995166 \text{ m} \\ &= 21.94540063 \text{ kg m}^{-1} \text{ s}^{-1} \end{aligned}$$

So, substituting above value in equation (6) and we can write

$$P_m = (21.94540063 / (21.94540063 + 2 * 36.864036)) * 0.3190041 \text{ mm day}^{-1}$$

$$= 0.0731728 \text{ mm day}^{-1}$$

Now substituting the value of P_m in equation (7), we get

$$P_a = P - P_m$$

or,

$$P_a = 0.3190041 - 0.0731728 \text{ mm day}^{-1}$$

$$= 0.24583132 \text{ mm day}^{-1}$$

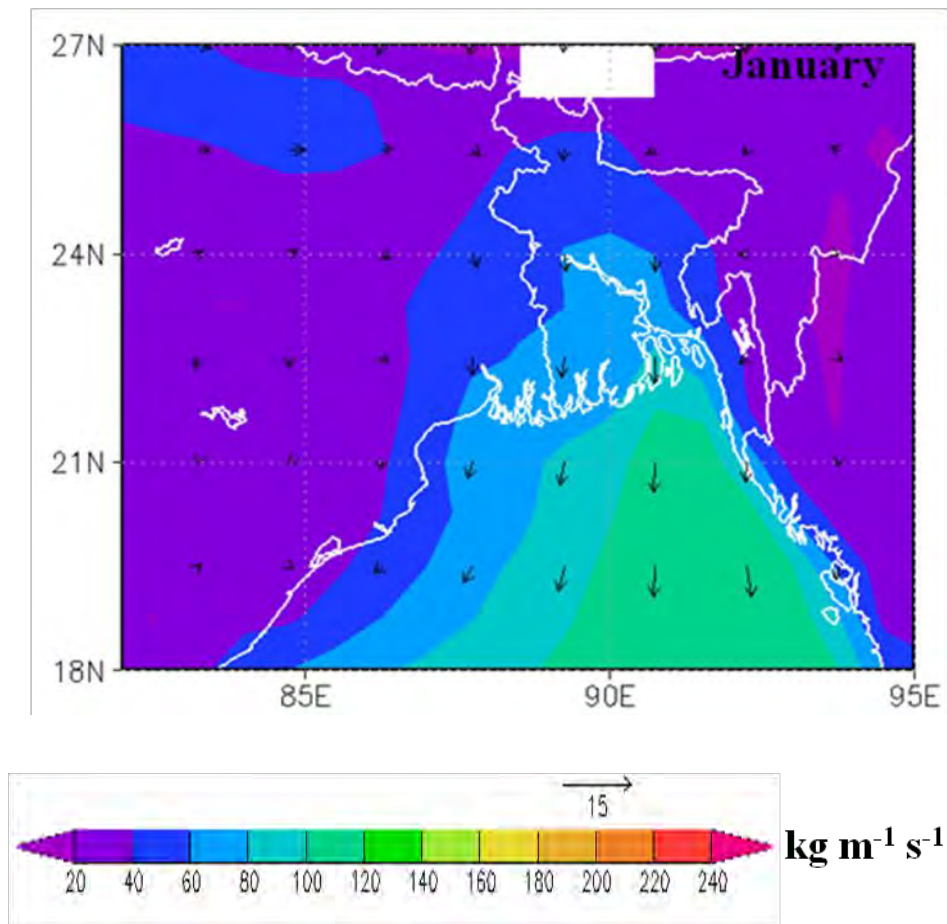


Fig. 4.51: The 37-year averaged VIMF (shading; $\text{kg m}^{-1} \text{s}^{-1}$) and average wind velocity (m s^{-1}) in January for Bangladesh and surrounding during 1979-2015.

According to this equation, P_a and P_m are calculated for all months separately and averaged the values in the BAN domain.

f) North-East domain (NE):

Fig. 4.52 shows the North-East area for month January. Here, L is also considered along zonal direction. Using above calculation the following values are found. Here, for average January,

$$F_{in} = 18.6236203 \text{ kg m}^{-1} \text{ s}^{-1}$$

$$P = 1.14793105 \text{ mm day}^{-1}$$

$$\begin{aligned} E &= 1.63488384 \text{ mm day}^{-1} \\ &= 1.63488384 / (3600*24) \text{ kg m}^{-2} \text{ s}^{-1} \\ &= 0.000018922 \text{ kg m}^{-2} \text{ s}^{-1} \end{aligned}$$

$$\begin{aligned} L &= (\text{zonal length in degree} * 110.574) \text{ km} \\ &= (\text{zonal length in degree} * 110.574 * 1000) \text{ m} \\ &= (9 * 110.574 * 1000) \text{ m} \\ &= 995166 \text{ m} \end{aligned}$$

$$\begin{aligned} EL &= 0.000018922 \text{ kg m}^{-2} \text{ s}^{-1} * 995166 \text{ m} \\ &= 18.83079643 \text{ kg m}^{-1} \text{ s}^{-1} \end{aligned}$$

So, substituting above value in equation (6) and we can write

$$\begin{aligned} P_m &= (18.83079643 / 18.83079643 + 2 * 18.6236203) * 1.14793105 \text{ mm day}^{-1} \\ &= 0.38547098 \text{ mm day}^{-1} \end{aligned}$$

Now substituting the value of P_m in equation (7), we get

$$\begin{aligned} P_a &= P - P_m \\ \text{or, } P_a &= 1.14793105 - 0.38547098 \text{ mm day}^{-1} \\ &= 0.76246007 \text{ mm day}^{-1} \end{aligned}$$

According to this equation, P_a and P_m are calculated for all months separately and averaged the values in the NE domain.

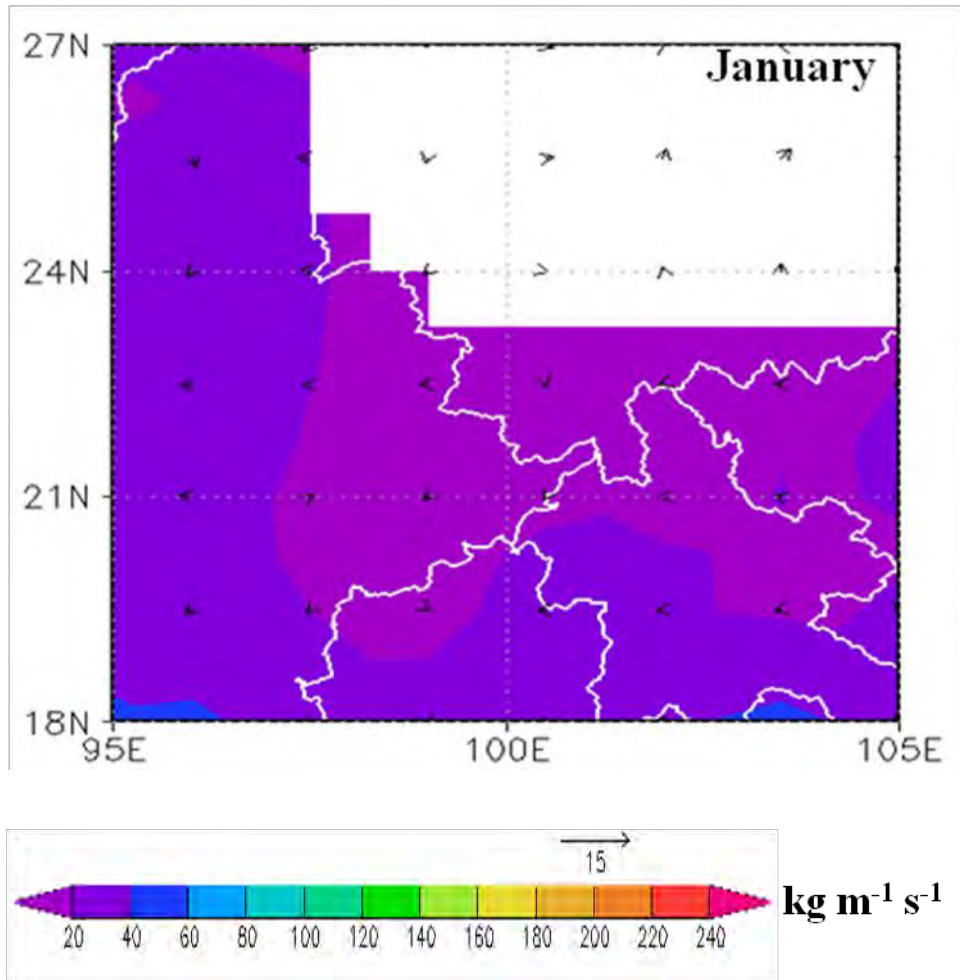


Fig. 4.52: The 37-year averaged VIMF (shading; $\text{kg m}^{-1} \text{s}^{-1}$) and average wind velocity (m s^{-1}) in January for the North-East domain during 1979-2015.

Table-11 shows the 37-year averaged VIMF, evaporation, precipitation, advective components of precipitation (P_a) and the precipitation arising from local evaporation (P_m) for six domains and total domain. Highest value of VIMF is found in the BoB domain and lowest value over the North-East domain. On the other hand evaporation is highest in the South-East domain and lowest value shows in the North-West domain. 37-years averaged precipitation is highest in the North-East domain and lowest over the North-West domain. For all domains, advective precipitation is higher than the precipitation arising from local evaporation. Advective component of precipitation over the BoB domain (5.16 mm/day) is higher than the other domains. The amount of precipitation arising from local evaporation is highest (2.6 mm/day) over the North-East domain. Advective precipitation (P_a) is five times greater than

Table-11: Value of VIMF, E, P, P_a and P_m for six domains.

Domain	VIMF ($\text{kg m}^{-1} \text{s}^{-1}$)	E (mm/day)	P (mm/day)	P_a (mm/day)	P_m (mm/day)
SW	127.48	3.33	4.03	3.34	0.69
BoB	164.28	4.75	6.34	5.16	1.18
SE	119.96	4.92	6.35	4.74	1.61
NW	81.00	1.28	1.77	1.64	0.13
BAN	85.46	2.90	4.96	4.25	0.71
NE	35.01	3.71	7.07	4.47	2.60
TOTAL	113.71	3.45	5.09	3.65	1.44

the precipitation arising from local evaporation for the South-West, Bay of Bengal and Bangladesh region. For the North-East domain, advective component of precipitation (4.47 mm/day) is 1.72 times greater than the precipitation arising from local evaporation (2.6 mm/day). Both moisture flux and evaporation play important role to form precipitation over the North-East domain and highest amount of precipitation (7.07 mm/day) is found over this region. Advective component of precipitation is about 72% of the total precipitation and 28% of the total precipitation arises from local evaporation (Fig. 4.53).

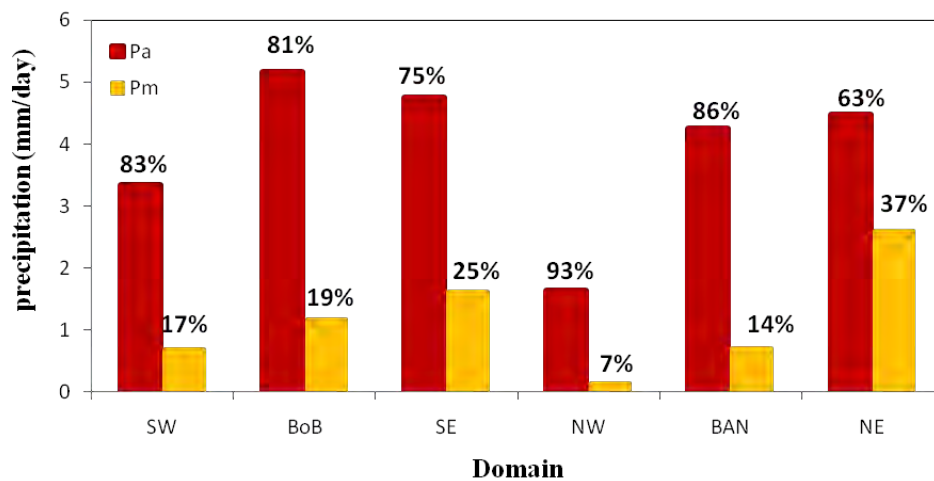


Fig. 4.53: Percentage of the advective component of precipitation (P_a) and precipitation arising from local evaporation (P_m) for six domains.

4.11 Verification of P_a and P_m

Fig. 4.54 and 4.55 shows the 37-year averaged monthly variation of moisture flux and the component of precipitation P_a advected from VIMF, evaporation and the component of precipitation arising from local evaporation P_m for the six domains.

a) South-West domain (SW)

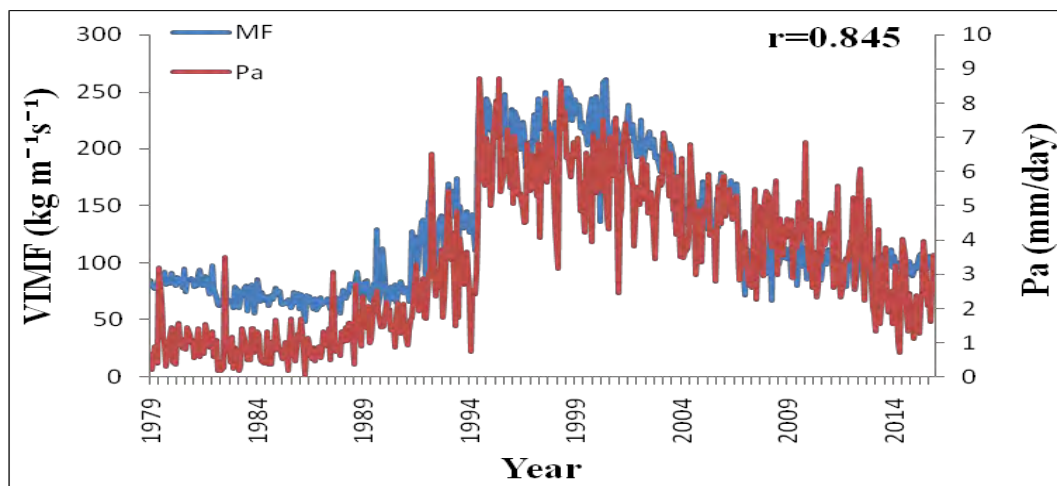


Fig. 4.54: Variation of monthly average VIMF and P_a for SW domain.

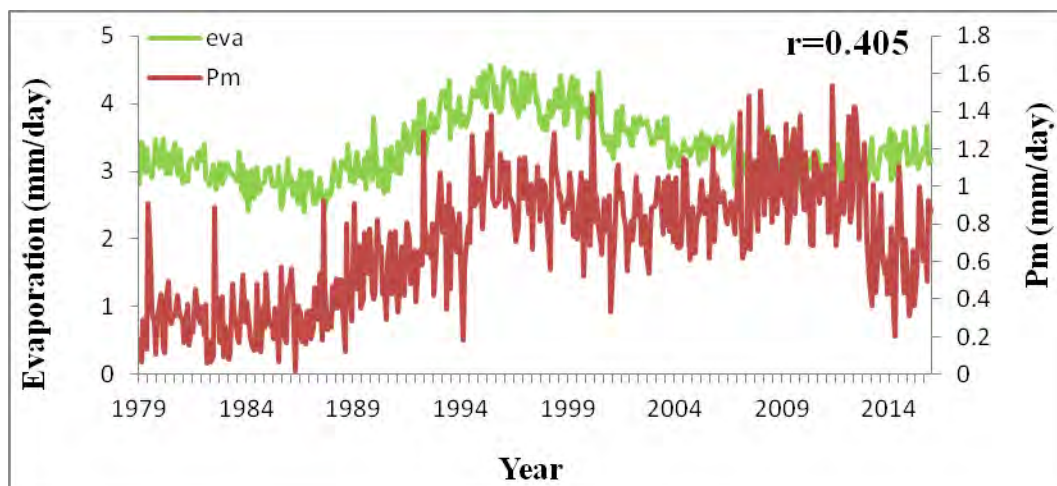


Fig. 4.55: Variation of monthly average evaporation and P_m for SW domain.

For the South-West domain, the 37-year averaged monthly variation between VIMF and the component of precipitation P_a advected from VIMF is shown in Fig. 4.54. Variation of evaporation and P_m is also shown in Fig. 4.55. The co-efficient

determination (R^2 value) between VIMF and P_a is 0.714 whereas the R^2 value between evaporation and P_m is 0.164. Here 71% VIMF has linear relation to form precipitation while evaporation has only 16%. Correlation between VIMF and advective component of precipitation is significant but correlation between evaporation and P_m is 0.405 which is not significant.

b) Bay of Bengal (BoB)

For the BoB domain, 65% VIMF has linear relation to form precipitation while evaporation has only 4%. Correlation between VIMF and advective component of precipitation is highly significant but correlation between evaporation and P_m is 0.213 which is not significant.

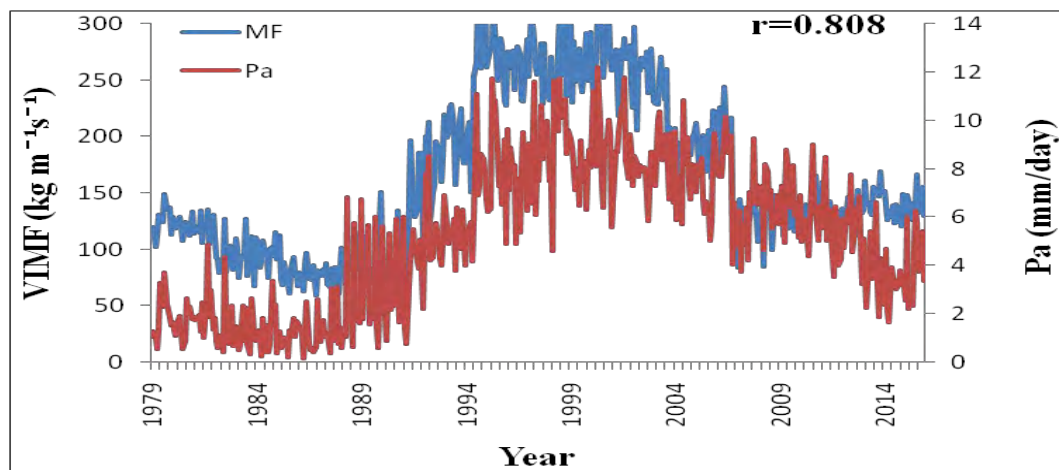


Fig. 4.56: Variation of monthly average VIMF and P_a for BoB domain.

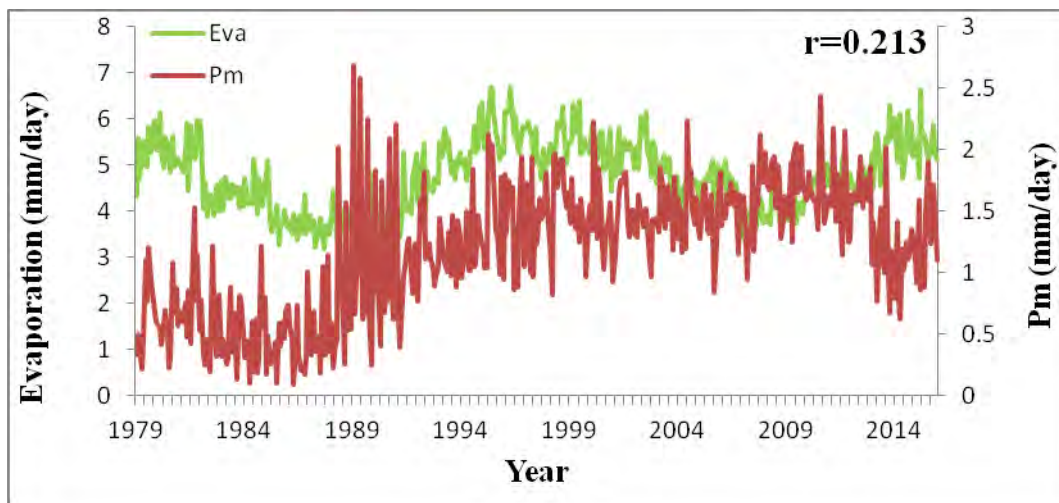


Fig. 4.57: Variation of monthly average evaporation and P_m for BoB domain.

c) South-East domain (SE)

The 37-year averaged monthly variation between VIMF and the component of precipitation P_a advected from VIMF is shown in Fig. 4.58. Variation of evaporation and P_m is also shown in Fig. 4.59. For the South-East domain, 40% VIMF has linear relation to form precipitation while evaporation has 42%. Correlation between VIMF and P_a and evaporation and P_m both are moderately significant.

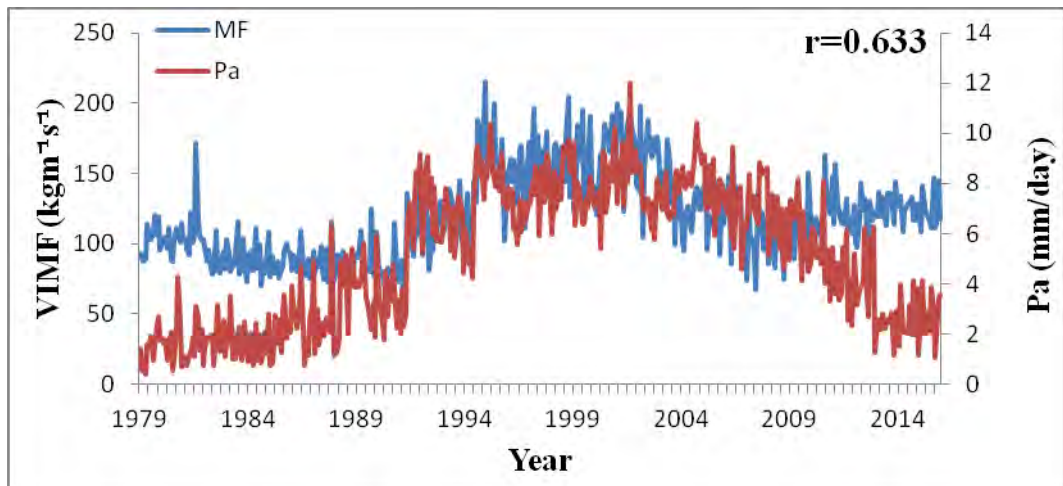


Fig. 4.58: Variation of monthly average VIMF and P_a for SE domain.

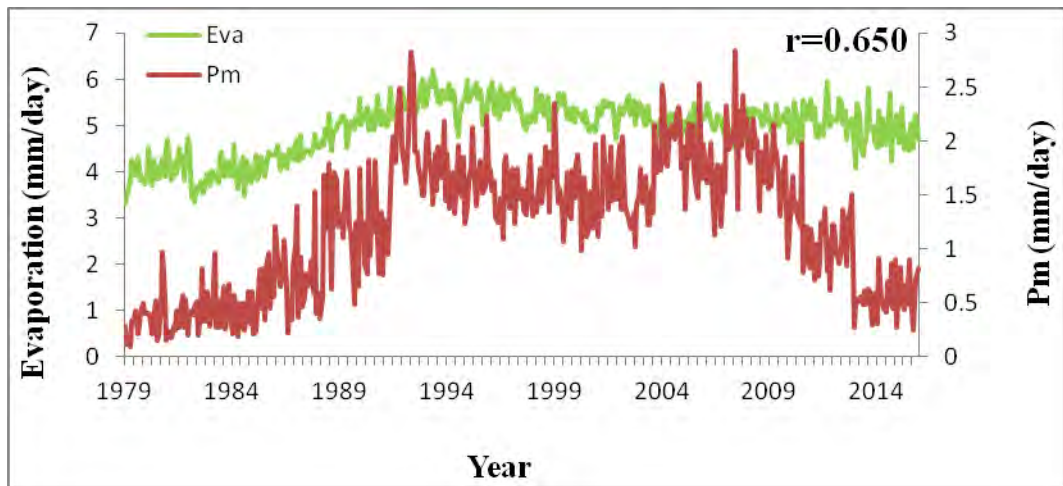


Fig. 4.59: Variation of monthly average evaporation and P_m for SE domain.

d) North-West domain (NW)

For the South-West domain, the 37-year averaged monthly variation between VIMF and the component of precipitation P_a advected from VIMF is shown in Fig. 4.60. Variation of evaporation and P_m is also shown in Fig.4.61. For the North-West domain, 71% VIMF has highly significant linear relation to form precipitation while evaporation has 60%. Correlation between VIMF and P_a and evaporation and P_m both are significant.

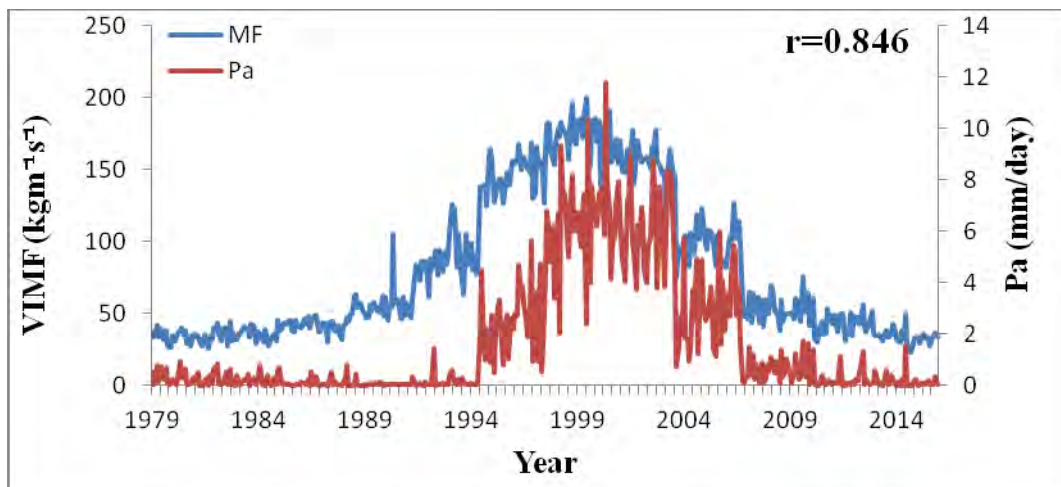


Fig. 4.60: Variation of monthly average VIMF and P_a for NW domain.

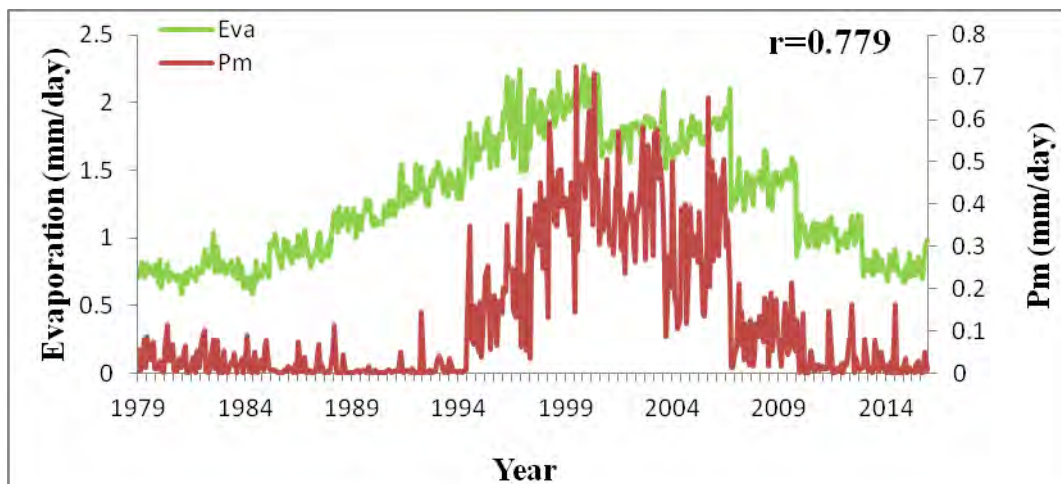


Fig. 4.61: Variation of monthly average evaporation and P_m for NW domain.

e) Bangladesh and surrounding (BAN)

For the Bangladesh and surrounding domain, the 37-year averaged monthly variation between VIMF and the component of precipitation P_a advected from VIMF is shown in Fig. 4.62. Variation of evaporation and P_m is also shown in Fig.4.63. The coefficient determination (R^2 value) between VIMF and P_a is 0.864 whereas the R^2 value between evaporation and P_m is 0.620. Here 86% VIMF has linear relation to form precipitation while evaporation has only 62%. Correlation between VIMF and advective component of precipitation is highly significant whereas correlation between evaporation and P_m is 0.787 which is also significant.

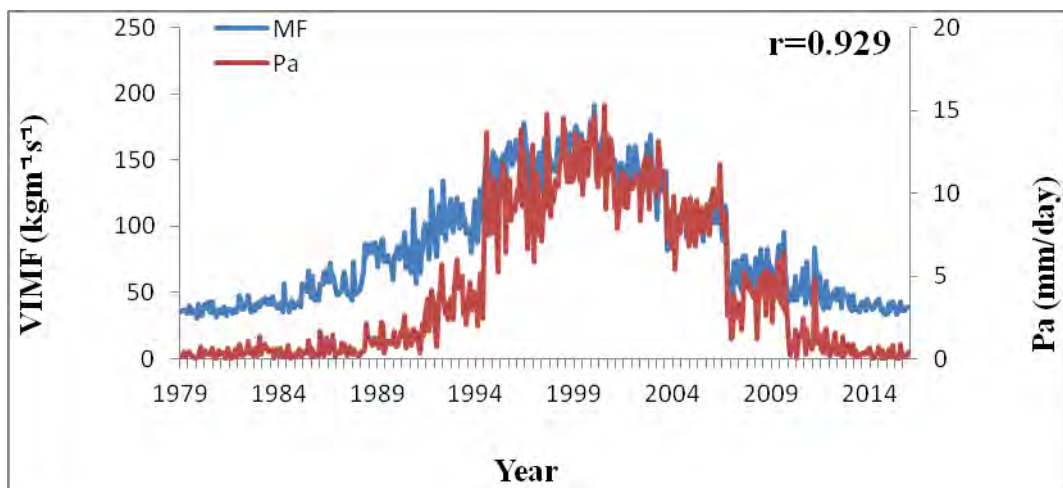


Fig. 4.62: Variation of monthly average VIMF and P_a for BAN domain.

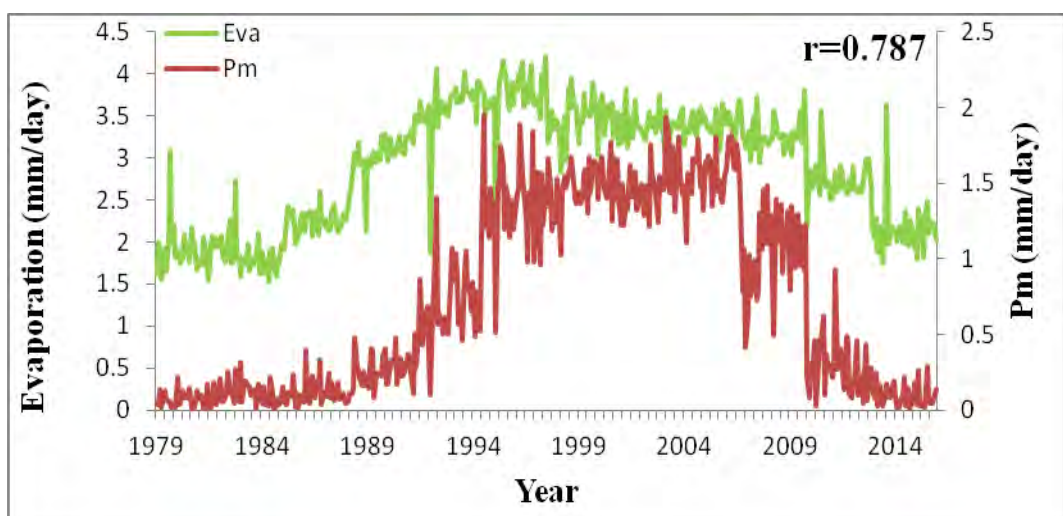


Fig. 4.63: Variation of monthly average evaporation and P_m for BAN domain.

e) North-East domain (NE)

The 37-year averaged monthly variation between VIMF and the component of precipitation P_a advected from VIMF is shown in Fig. 4.64. Variation of evaporation and P_m is also shown in Fig.4.65. The co-efficient determination (R^2 value) between VIMF and P_a is 0.896 whereas the R^2 value between evaporation and P_m is 0.668. Here, 89% VIMF has linear relation to form precipitation while evaporation has only 66%. Correlation between VIMF and advective component of precipitation is highly significant and correlation between evaporation and P_m is 0.817 which is also highly significant.

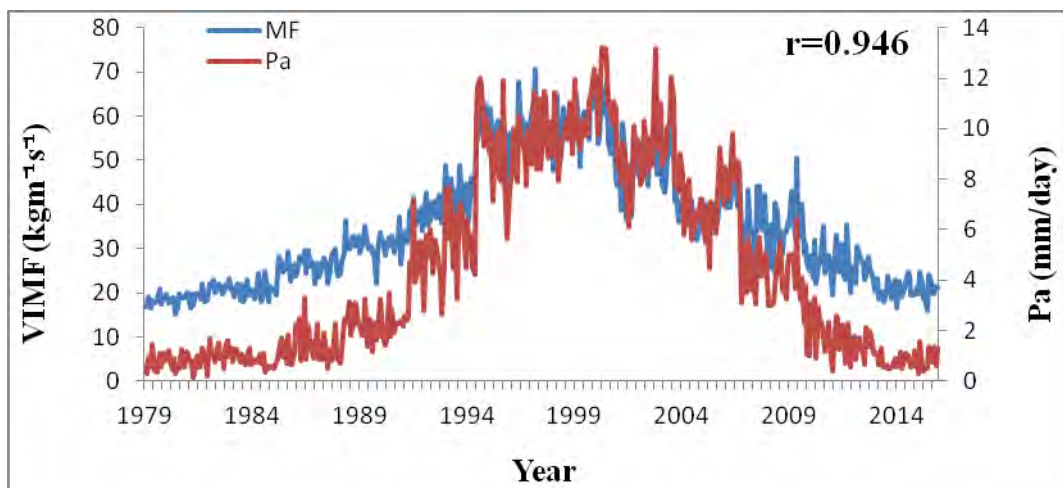


Fig. 4.64: Variation of monthly average VIMF and P_a for NE domain.

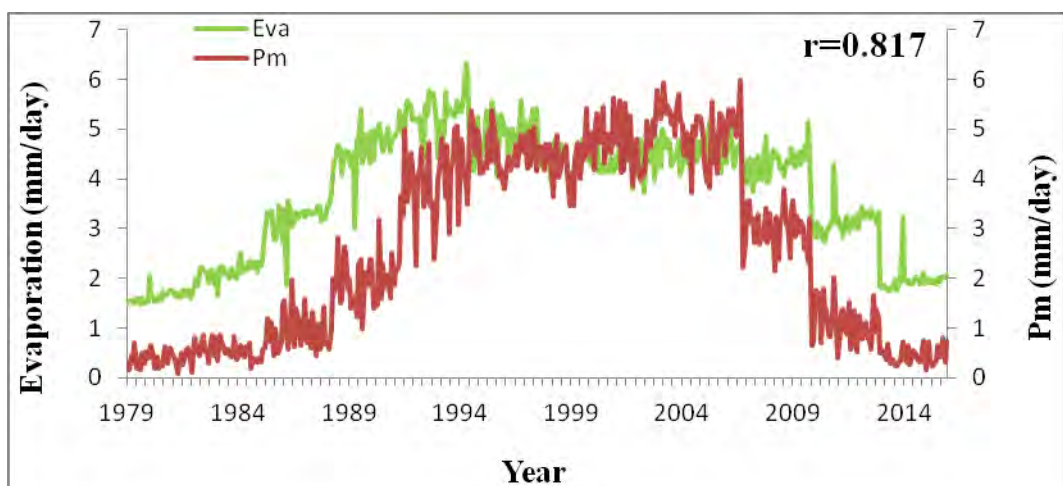


Fig. 4.65: Variation of monthly average evaporation and P_m for NE domain.

The co-efficient of determination (R^2 value) and correlation coefficient (r value) between VIMF and advective component of precipitation (P_a), Evaporation and precipitation arising from local evaporation (P_m) for six domains and total domain are given in Table-12.

Table-12: Monthly average R^2 value and r value for six domains (1979-2015).

Domain	R^2		r	
	VIMF and P_a	Eva. and P_m	VIMF and P_a	Eva. and P_m
SW	0.714	0.164	0.845	0.405
BoB	0.652	0.045	0.808	0.213
SE	0.401	0.423	0.633	0.650
NW	0.716	0.608	0.846	0.779
BAN	0.864	0.620	0.929	0.787
NE	0.896	0.668	0.946	0.817
Total Domain	0.871	0.456	0.933	0.675

CHAPTER-5

CONCLUSIONS

Precipitation is the most important atmospheric parameter. Precipitation that falls out of the atmosphere depends on one of the three moisture sources i.e. the moisture that already exists in the atmosphere, convergence of the moisture advected into the region by the wind and the evaporation of surface moisture into the atmosphere. Among them, advection plays the most significant role to form precipitation over South Asia, especially in the monsoon season. ERA-Interim reanalysis data generated by European Centre for Medium-Range Weather Forecasts (ECMWF) are used to analyze the transport of moisture from 1979 to 2015 over South Asia (SA) including the Bay of Bengal (BoB) and the eastern part of Arabian Sea (AS). For this purpose, low-level vertically integrated moisture flux (VIMF) from 1000 to 850 hPa is considered and calculated in this study. Long-term annual, seasonal and monthly variability of VIMF are measured over this region and find out their relations with precipitation.

The average value of VIMF over the study area is found $113.71 \text{ kg m}^{-1} \text{ s}^{-1}$. Highest amount of VIMF is estimated over the BoB and the eastern part of AS, mainly in the Ocean area, which contributes a significant amount of moisture to the South Asia. About 47% of the total moisture flux is found over the Ocean area. Southern part of the study area including ocean area acquires 67% of the total flux, whereas, 33% of the total moisture flux is found over the Northern part, mainly the land area.

The annual variation of VIMF from 1979 to 2015 in the study area shows almost constant value with very small fluctuations from year to year. The coefficient of determination (R^2) value is found 0.005 and the average increasing rate of VIMF is approximately 0.14% per year.

According to the season, the highest amount of VIMF is found $172.54 \text{ kg m}^{-1} \text{ s}^{-1}$ (41% of the total VIMF) in the monsoon season and the lowest amount of VIMF is $71.63 \text{ kg m}^{-1} \text{ s}^{-1}$ (17% of the total VIMF) in the winter season, whereas, other two seasons have the value of $88.10 \text{ kg m}^{-1} \text{ s}^{-1}$ (21% of the total VIMF) and

89.18 kg m⁻¹ s⁻¹ (21% of the total VIMF). Annual increasing of seasonal VIMF is also calculated for individual season which shows almost constant value. The average increasing rate of VIMF per year is approximately 0.5% in the pre-monsoon and winter seasons but the increasing rates are 0.31% and 0.33% for the monsoon and post-monsoon seasons, respectively.

The 37-year averaged VIMF over SA maintains a periodic pattern throughout the twelve months of the year with a maximum value of 191.74 kg m⁻¹ s⁻¹ in July. The minimum value of VIMF (63.74 kg m⁻¹ s⁻¹) is found in March which is 33% less than the maximum value.

For details distributions of moisture flux over the study region, six individual domains are considered and the variability of moisture flux is analyzed. The six domains are the South-West (SW), Bay of Bengal (BoB), South-East (SE), North-West (NW), Bangladesh and surrounding (BAN) and North-East (NE) domain. The individual average of VIMF over these domains is calculated for 37 year and the highest amount of VIMF (27% of the total VIMF) is found over the BoB domain. The SW and the SE regions obtain 21% and 19% of the total flux, respectively. About 13% and 14% of VIMF are observed over the NW and BAN domains, respectively. The lowest amount of VIMF is found to be advected over the NE domain which is only 6% of the total flux.

For all six domains, the highest VIMF is observed in the monsoon season and the lowest value is observed in the winter season. VIMF is measured about 42%, 41%, 33%, 51%, 45% and 39% of the total flux in the monsoon season, whereas, in the winter season the values are 17%, 18%, 21%, 12%, 12% and 15% of the total flux for the SW, BoB, SE, NW, BAN and NE domains, respectively. The intense southwesterly wind in the monsoon season transports the highest amount of moisture for all domains. Within the domains, the Southern regions (SW, BoB and SE) have two times higher VIMF than the Northern regions (NW, BAN and NE) in the monsoon season. In the Northern regions, BAN has more flux than the other domains for all seasons but in the monsoon season where the NW part has higher VIMF (144.31.kg m⁻¹ s⁻¹).

Annual variation of individual domain shows that VIMF is increased annually over the NE domain with R^2 value of 0.54, which is moderately significant. In others domains, VIMF are remained constant for 37 years. Also, the increasing rate of seasonal VIMF is not significant over the six domains except that in the pre-monsoon over the NE region. The pre-monsoon of the NE region mainly contributes to the total annual increase of VIMF over the NE region, though this region has lowest amount of VIMF ($35.01 \text{ kg m}^{-1} \text{ s}^{-1}$).

Monthly variation of 37-year averaged VIMF shows the maximum value in July for all domains except the BoB and SE domains which have maximum value in the month of June and August, respectively. But the values in June ($272.86 \text{ kg m}^{-1} \text{ s}^{-1}$) for the BoB and for SE in August ($164.19 \text{ kg m}^{-1} \text{ s}^{-1}$) are differs very little considering the corresponding values in July for each domain. The lowest amount of VIMF is observed approximately $29.73 \text{ kg m}^{-1} \text{ s}^{-1}$ in January for the Northern regions and that in March approximately $76.78 \text{ kg m}^{-1} \text{ s}^{-1}$ for the Southern regions of the study area.

To differentiate the amount of precipitation that comes out from VIMF and evaporation separately, 37 years (1979-2015) daily mean evaporation and precipitation data from ECMWF are also calculated for the study area. Average precipitation and evaporation of the total domain are estimated 5.09 mm/day and 3.45 mm/day, respectively. The R^2 value between VIMF and precipitation shows the value of 0.77, whereas, $R^2=0.22$ between evaporation and precipitation which indicates that only 22% of the total variation of precipitation can be explained by the relationship between evaporation and precipitation over the study area.

Therefore, according to the equation used by Trenberth (1999), the total precipitation over SA is separated into two components i.e. the advective component of precipitation (P_a) and the precipitation arising from local evaporation (P_m) and finally precipitation components are correlated with VIMF and evaporation values. The coefficient of determination (correlation coefficient) between VIMF and P_a is 0.871 (0.933) and that for evaporation and P_m is 0.456 (0.675). The estimated advective component of precipitation (P_a) is 3.65 mm/day which is more than two times greater than the precipitation arising from local evaporation (1.44 mm/day). So,

about 72% of the total precipitation comes from the advected part and 28% precipitation arises from local evaporation.

For all domains, advective component of precipitation (P_a) is higher than the precipitation arising from local evaporation (P_m). Advective component of precipitation (P_a) are 83%, 81%, 75%, 93%, 86%, 63% and precipitation arising from local evaporation (P_m) are 17%, 19%, 25%, 7%, 14%, 37% for the SW, BoB, SE, NW, BAN and NE domains, respectively. The value of P_a (5.16mm/day) is highest over the BoB and second highest is 4.74 mm/day over the SE domain, whereas, P_m is highest (2.6 mm/day) over the NE domain and second highest is 1.61 mm/day over the SE domain. P_a is approximately five times greater than the value of P_m for the SW, BoB and BAN regions. The value of P_a and P_m for the NW domain are 1.64 mm/day, 0.13 mm/day, respectively which are the lowest amount of P_a and P_m for the study area. For NE domain, P_a (4.47 mm/day) is about two times greater than P_m (2.6 mm/day). The highest amount of precipitation (7.07 mm/day) in this domain is also contributed by evaporation over this region. For all domains, the correlation and R^2 values between evaporation and P_m are found approximately 0.76 and 0.58 on average, respectively except the SW ($r=0.405$, $R^2=0.164$) and BoB ($r=0.213$, $R^2=0.045$) domains which have comparatively low values. Neglecting the contribution of the existing moisture in the above mention equation can cause the inconsistency in P_m over SA, especially over ocean. Therefore, further study by including the contribution of the existing moisture over SA will help us the Researchers to know the accurate contribution of precipitation. However, this study reveals that VIMF is the main contributor to the total precipitation over SA than the other contributors and on average, approximately 75% of the total precipitation comes from the advected moisture at low level, whereas, on average, approximately 25% precipitation arises from other sources.

REFERENCES

1. FAO (Food and Agriculture Organization), 2002. World agriculture: towards 2015/2030: summary report. Rome.
2. Li, X., Wen, Z., Zhou, W., and Wang, D., 2012: Atmospheric water vapor transport associated with two decadal rainfall shifts over east China, *Journal of the Meteorological Society of Japan*, vol. 90, pp. 587-602.
3. Trenberth, K. E., Dai, A., Rasmussen, R. M., and Parsons, D. B., 2003: The changing character of precipitation, *Bulletin American Meteorological Society*, vol. 84, pp. 1205-1217.
4. Brubaker K. L., Entekhabi D., and Eagleson P. S., 1993: Estimation of continental precipitation recycling, *Journal of Climate*, vol.6, pp. 1077-1089.
5. Lele, M. I., Leslie, L. M., and Lamb, P. J., 2015: Analysis of low-level atmospheric moisture transport associated with the west African monsoon, *Journal of Climate*, vol. 28, pp. 4414-4430.
6. Banacos, P.C., and Schultz, D. M., 2005: The use of moisture flux convergence in forecasting convective initiation: historical and operational perspectives, *Weather and Forecasting*, vol.20, pp. 351-366.
7. Salstein, D. A., Rosen, R. D., and Peixoto, J.P., 1982: Modes of variability in annual hemispheric water vapor and transport fields, *Journal of the atmospheric sciences*, vol. 40, pp. 788-803.
8. Benton, G. S., Estoque, M. A., 1954, Water-vapor transfer over the north American continent, *Journal of Meteorology*, vol. 11, pp. 462-477.
9. Rasmusson, E., M., 1968: Atmospheric water vapor transport and the water balance of North America, *Monthly weather review*, Vol. 96, pp. 720-734.
10. Rosen R.D., D.A. Salstein and J.P. Peixoto, 1979a. Variability in the Annual Fields of Large-Scale Atmospheric Water Vapor Transport *Monthly Weather Review.*, 107, 26-37.
11. Zhou, W., Li, C., and Chan, J. C. L., 2006: The inter-decadal variations of the summer monsoon rainfall over South China. *Meteorology and Atmospheric Physics*, vol. 93, pp. 165–175, doi: 10.1007/s00703-006-018-9.
12. Chan, J. C. L., and Zhou, W., 2005: PDO, ENSO and the early summer monsoon rainfall over south China. *Geophysical. Research. Letters.*, vol. 32, pp. 1-5.

13. Holman, K. D., and Vavrus, S. J., 2012: Understanding Simulated Extreme Precipitation Events in Madison, Wisconsin, and the Role of Moisture Flux Convergence during the Late Twentieth and Twenty-First Centuries. *Journal of Hydrometeorology*, vol.13, pp.877-894.
14. Webster, P. J., 1994: The role of hydrological processes in ocean-atmosphere interactions, *Reviews of Geophysics*, vol. 32, pp. 427–476,
15. Ding, Y., and Chan, J. C. L., 2005: The East Asian summer monsoon: An overview, *Meteorology and Atmospheric Physics.*, vol. 89, pp. 117–142.
16. Trenberth, K. E., 2006: Observed changes to the climate and their causes. Chapter 9 of *Confronting Climate Change: Critical Issues for New Zealand*. R. Chapman, J. Boston and M. Schwass (Eds.) Victoria University Press. pp. 93-102.
17. Wei, J., Su, H., and Yang, Z. L., 2015: Impact of moisture flux convergence and soil moisture on precipitation: a case study for the southern United States with implications for the globe, *Climate Dynamics*, DOI 10.1007/s00382-015-2593-2.
18. Min, W., and Schubert, S. D., 1997: The climate signal in regional moisture fluxes: a comparison of three global data assimilation products, *DAO Office Note* 97-10.
19. Trenberth, K. E., 1998: Atmospheric moisture recycling: Role of advection and local evaporation. *Journal of Climate*, vol. 12, pp. 1368–1381.
20. Cadet, D. L., and Nnoli, N. O., 1987: Water vapour transport over Africa and the Atlantic Ocean during summer 1979, *Quarterly Journal of the Royal Meteorological Society*, vol. 113, pp. 581–602.
21. Huang, Y., and Cui, X., 2015: Moisture sources of an extreme precipitation event in Sichuan, China, based on the Lagrangian method, *Atmospheric science letters*, vol. 16, pp. 177–183,
22. Ying J., Panmao, Z., and Qiyi, W., 2005: Variability of Summer Atmospheric Moisture Flux and Its Effect on Precipitation over East China, *Journal of Meteorological Research*, vol. 19, pp. 469-478.
23. Karmakar, S., 1998: Vertically-integrated tropospheric moisture, energy and their fluxes over Bangladesh during landfall of tropical cyclones, *Mausam*, vol. 49, pp 187-194.
24. http://ocw.usu.edu/Forest__Range__and_Wildlife_Sciences/Wildland_Fire_Management_and_Planning/Unit_4__Temperature-Moisture_Relationship_4.html, access time and date: 03.00 pm, 06 August 2016.

25. https://books.google.com.bd/books?id=6cRTp4enDxkC&printsec=frontcover&source=gbs_ge_summary_r&cad=0#v=onepage&q&f=false, access time and date: 03.00 pm, 06 August 2016.
26. <https://www.st-andrews.ac.uk/~dib2/climate/water.html>, access time and date: 11.00 am, 26 August 2016.
27. Wallace, John; Hobbs, Peter (2006). *Atmospheric Science* (2nd ed.). Elsevier. p. 80. ISBN 978-0-12-732951-2.
28. Rosen, R. D., Salstein D. A. and Peixoto, J. P., 1979: Variability in the annual fields of large-scale atmospheric water vapor transport. *Monthly Weather Review*, vol.114, pp. 2352-2362.
29. Palmén, E., and Holopainen E. O., 1962: Divergence, vertical velocity and conversion between potential and kinetic energy in an extratropical disturbance. *Geophysica*, vol. 8, pp. 89–113.
30. Johns, R H., 1993: Meteorological conditions associated with bow echo development in convective storms. *Weather Forecasting*, vol. 8, pp. 294–299.
31. Glickman, T. S., 2000: Glossary of Meteorology. 2nd edition, American Meteorological Society, pp. 855.
32. Xie, P., and Arkin, P. A., 1997: Global precipitation: A 17-year monthly analysis based on gauge observations, satellite estimates, and numerical model outputs. *Bulletin, American Meteorological Society*, vol. 78, pp. 2539–2558.
33. Huffman, G. J., and Coauthors, 1997: The Global Precipitation Climatology Project (GPCP) combined precipitation data set, *Bulletin, American Meteorological Society*, vol. 78, pp. 5–20.
34. Shenoi, S. S. C., Shankar, D. & Shetye, S. R., 2002: Differences in heat budgets of the near surface Arabian Sea and Bay of Bengal: Implications for the summer monsoon. *Journal of Geophysical Research*, vol. 107, 3052, DOI 10.1029/2000JC000679.
35. Gimeno, L. et al., 2012: Oceanic and terrestrial sources of continental precipitation. *Review of Geophysics*, vol. 50, pp. 1-41.
36. Caviedes, C. N., 2001: *El Niño in History: Storming Through the Ages* (1st edition.), University Press of Florida, ISBN 978-0-8130-2099-0.
37. Wildlife Conservation Society. Retrieved 1 December 2012.
38. P. Das, 2002: *The Monsoon*, Fourth Revised Editions, National Book Trust.

39. Gupta, A., 2005: *The Physical Geography of Southeast Asia*, Oxford University Press, ISBN 978-0-19-924802-5.
40. Berrisford P., Dee, D., Fielding, K., Fuentes, M., Kallberg, P., Kobayashi, S. and Uppala, S., 2009: *The ERA-Interim Archive*. ERA Report Series. 1. Technical Report. European Centre for Medium Range Weather Forecasts, pp. 16.
41. "Documentation of GrADS", 2015, Center for Ocean-Land-Atmosphere Studies, Institute of Global Environment and Society, George Mason University.
42. Akter, N., Tsuboki, K., 2012: Numerical Simulation of Cyclone Sidr Using a Cloud-Resolving Model: Characteristics and Formation Process of an Outer Rainband, *Monthly Weather Review*, vol. 140, pp. 789-810.
43. Akter, N, Tsuboki, K., 2014: Role of synoptic-scale forcing in cyclogenesis over the Bay of Bengal, *Climate Dynamics* ,Vol. 43, pp 2651–2662.